Electronic Supplementary Material (ESI) for New Journal of Chemistry.

NEW JOURNAL OF CHEMISTRY

ELECTRONIC SUPPLEMENTARY INFORMATION FOR

A Nitrogen Based Chiral Catenane for Enantioenriching Photocatalytic Aerobic Oxidation

Masoud Kazem-Rostami [a,b,*]

[a] *Department of Chemistry, Northwestern University, 2145 Sheridan Road, Evanston, Illinois 60208, USA*
[b] *Faculty of Science and Engineering, Macquarie University, North Ryde, NSW 2109, Australia*
** E-mail addresses: masoud.kr@northwestern.edu, masoud.kr@gmail.com*

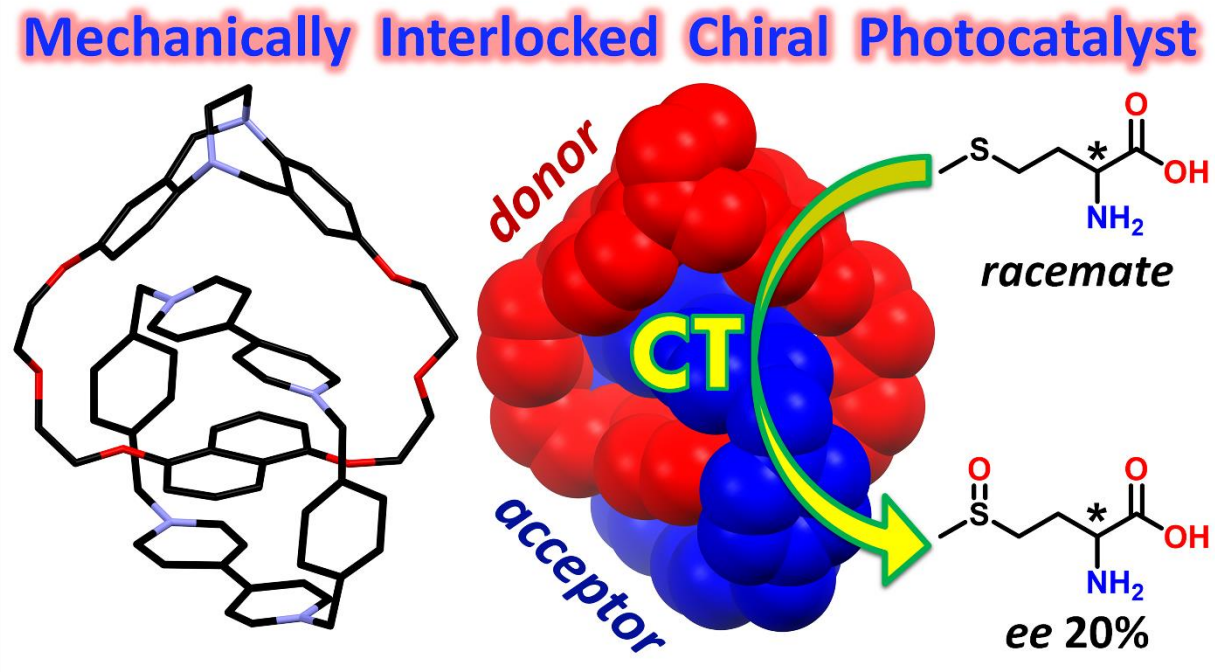

■ Table of Contents

■ Section A. Methods and Materials

Chiral Reversed-phase High-Performance Liquid Chromatography (HPLC)

Chiral HPLC chromatograms were recorded by multi-channel optical detection at 235, and 245 nm using Agilent's 1260 Infinity HPLC instrument equipped with a Phenomenex chiral analytical column (Chirex 3126 (D)-penicillamine, 150 × 4.6 mm, 5 µm) in tandem with a reverse-phase BEH C-18 (130 Å, 5 µm) guard column to prevent the entry and accumulation of hydrophobic species in the chiral stationary phase. The applied mobile phases included HPLC-grade H_2O, and acetonitrile (MeCN) purchased from Fisher Scientific. Copper (II) sulfate (2 mM) was added to the aqueous mobile phase (10% *v/v*) used for the chiral separation and quantification of (D)-methionine, (L)-methionine, and their sulfoxides.

Nuclear Magnetic Resonance (NMR) Spectroscopic Analysis

NMR spectra were recorded at 298 K, unless otherwise mentioned for variable temperature NMR experiments, using Bruker Avance III 600 MHz, Bruker Neo 600 MHz, and Bruker Avance III 500 MHz instruments running Topspin (version 4.0.8), and MestReNova (version 14) software programs for the analysis and plotting of the acquired spectra. Deuterated chloroform ($CDCl_3$), dimethyl sulfoxide (CD_3SOCD_3), acetonitrile (CD_3CN), and deuterium oxide (D_2O) were purchased from Cambridge Isotope Laboratories (CIL) and used for NMR spectroscopic analysis.

X-Ray Diffractometry

A Rigaku Cu-Synergy X-ray diffractometer was used to collect crystallographic data. This data was processed and refined with Olex V2-1.3 software before depositing the structures in the Cambridge Crystallographic Data Centre (CCDC).

Optical Activity and Circular Dichroism

Rudolph Autopol-IV optical polarimeter and Jasco J-815 were employed for measuring the optical activity and recording circular dichroism spectra, respectively.

Materials

Chromatography-grade solvents including methanol (MeOH), dimethylformamide (DMF), dichloromethane (CH_2Cl_2), acetone (CH_3COCH_3), and chloroform ($CHCl_3$) were purchased from Sigma and Fisher Scientific. The starting materials of reagent-grade purity were purchased from Combi-Blocks, Tokyo Chemical Industry (TCI), and Ambeed, and used without further purification.

Nomenclature for *R/S* stereocenters of Tröger's base analogs

The stereoisomers of Tröger's base analogs used throughout this supporting information and manuscript are assigned by Cahn–Ingold–Prelog priority rule as shown here. The counterclockwise arrow (drawn in red) is assigned to the *R* configuration and the clockwise arrow (drawn in blue) to the *S* configuration as the lone-pair electrons—the lowest priority group—stand toward the front.

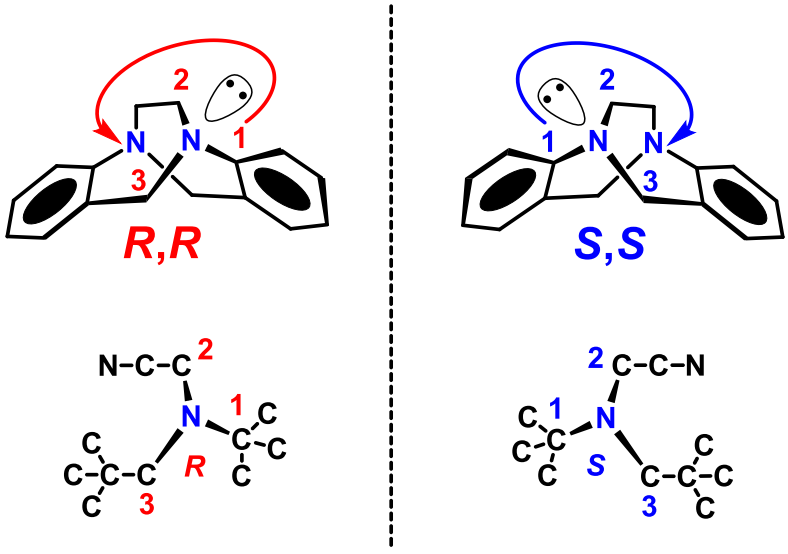

Stepwise synthesis of the chiral building blocks

Synthesis of Tröger's base analog (±)-1

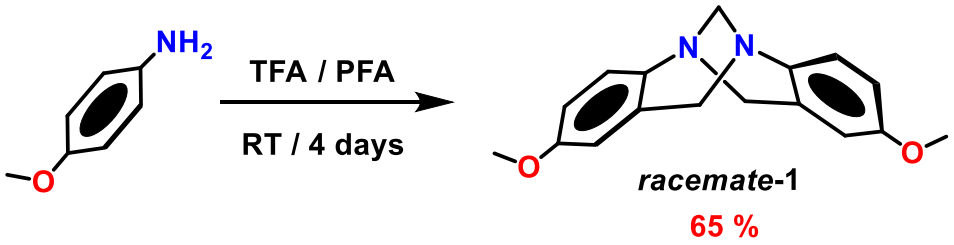

A synthetic procedure described[1] in the literature was repeated in order to obtain Tröger's base analog **(±)-1** from the condensation of *p*-anisidine with paraformaldehyde (PFA) in neat trifluoroacetic acid (TFA). R_f 0.22 (silica gel; isopropanol–hexanes, 10% *v/v*). ^{1}H NMR (500 MHz, $CDCl_3$): δ 7.06 (d, *J* = 8.8 Hz, 2H), 6.75 (dd, *J* = 8.8, 2.8 Hz, 2H), 6.43 (d, *J* = 2.8 Hz, 2H), 4.65 (d, *J* = 16.5 Hz, 2H), 4.30 (s, 2H), 4.08 (d, *J* = 16.5 Hz, 2H), 3.71 (s, 6H). MS (ESI +): *m/z* $[M + H]^+$ calcd for $[C_{17}H_{19}N_2O_2]^+$: 283.14; found: 283.1.

Synthesis of Tröger's base analog (±)-2

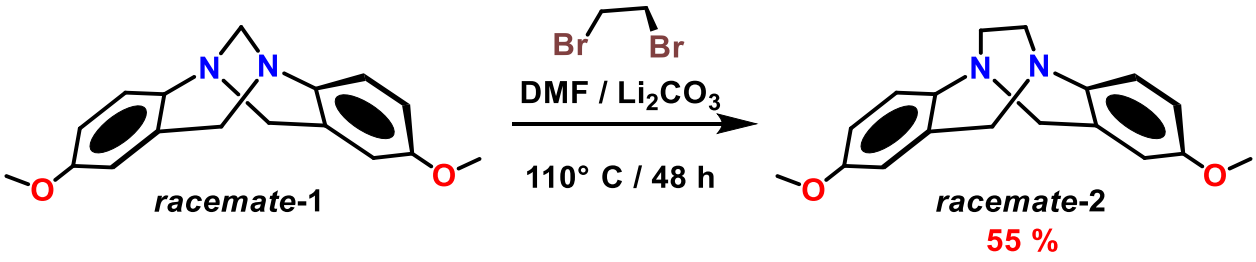

A synthetic procedure described[2] in the literature was adopted for this step in order to obtain Tröger's base analog **(±)-2** by subjecting **(±)-1** to 1,2-dibromoethane in hot dimethylformamide (DMF) in the presence of lithium carbonate. R_f 0.31 (silica gel;

isopropanol–hexanes, 10% *v/v*). ^{1}H NMR (500 MHz, $CDCl_3$): δ 7.06 (d, *J* = 8.6 Hz, 2H), 6.62 (dd, *J* = 8.6, 2.8 Hz, 2H), 6.43 (d, *J* = 2.8 Hz, 2H), 4.54 (d, *J* = 17.3 Hz, 2H), 4.37 (d, *J* = 17.3 Hz, 2H), 3.67 (s, 6H), 3.54–3.59 (m, 4H). MS (ESI +): *m/z* [M + H]$^{+}$ calcd for $[C_{18}H_{21}N_2O_2]^{+}$: 297.15; found: 297.1.

Chiral resolution of Tröger's base analog (±)-2

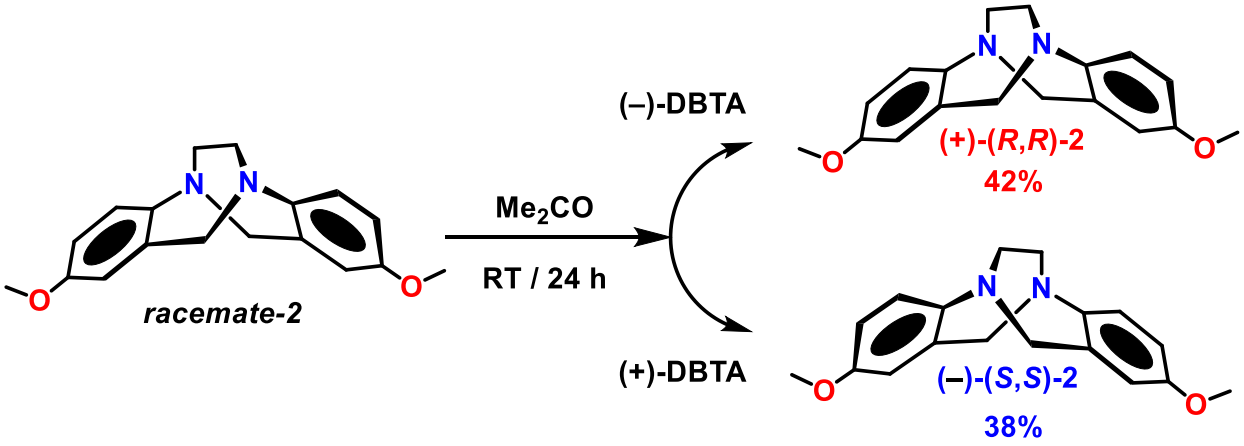

Repeated our procedure described[3] in the literature in order to coprecipitate the (+)-(*R*,*R*) enantiomer of Tröger's base analog **2** with (–)-*O*,*O*′-dibenzoyl-L-tartaric acid monohydrate—abbreviated (–)-DBTA—and separate it from the racemic mixture of **(±)-2**. Then coprecipitated (–)-(*S*,*S*) enantiomer of Tröger's base analog **2** with (+)-*O*,*O*′-dibenzoyl-D-tartaric acid monohydrate—abbreviated (+)-DBTA—repeating the exact same procedure. Enantiomer **(+)-(*R*,*R*)-2**: $[\alpha]_D^{22}$ +337 (*c* 0.100, CH_2Cl_2), Chiral HPLC ^{t}R 12.1 ± 0.2 min (major >99.8%, er >99.5:0.5), CCDC deposition number 1902226; Enantiomer **(–)-(*S*,*S*)-2**: $[\alpha]_D^{23}$ –332 (*c* 0.100, CH_2Cl_2), Chiral HPLC ^{t}R 14.1 ± 0.2 min (major >99.8%, er >99.5:0.5).[3a]

Synthesis of Tröger's base analogs (+)-(*R*,*R*)-3 and (–)-(*S*,*S*)-3

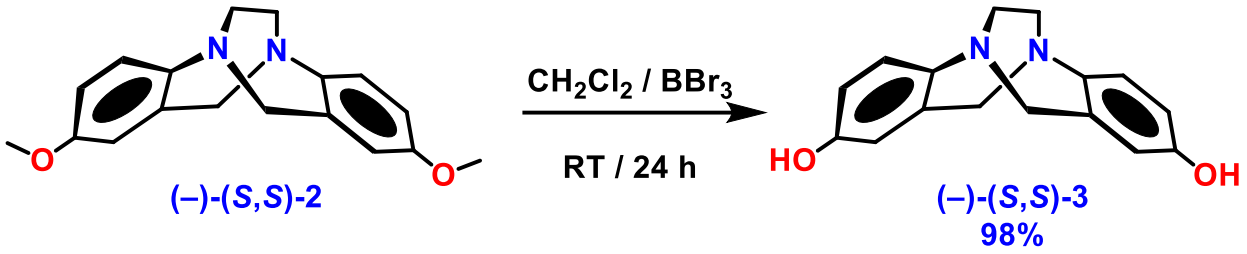

Repeated our procedure described[3a, 4] in the literature in order to obtain Tröger's base analog **(–)-(*S*,*S*)-3** from the demethylation of **(–)-(*S*,*S*)-2**. R_f 0.4 (silica gel; neat ethyl acetate). ^{1}H NMR (500 MHz, DMSO-d_6): δ 8.93 (s, 2H), 6.83 (d, J = 8.4 Hz, 2H), 6.40 (dd, J = 8.4, 2.7 Hz, 2H), 6.26 (d, J = 2.7 Hz, 2H), 4.41 (d, J = 17.2 Hz, 2H), 4.13 (d, J = 17.2 Hz, 2H), 3.37 (s, 4H). MS (ESI +): *m/z* $[M + H]^+$ calcd for $[C_{16}H_{17}N_2O_2]^+$: 269.12; found: 269.1. Enantiomer **(–)-(*S*,*S*)-3**: $[\alpha]_D^{24}$ –232 (*c* 0.100, ethyl acetate). CCDC deposition number 2122264.

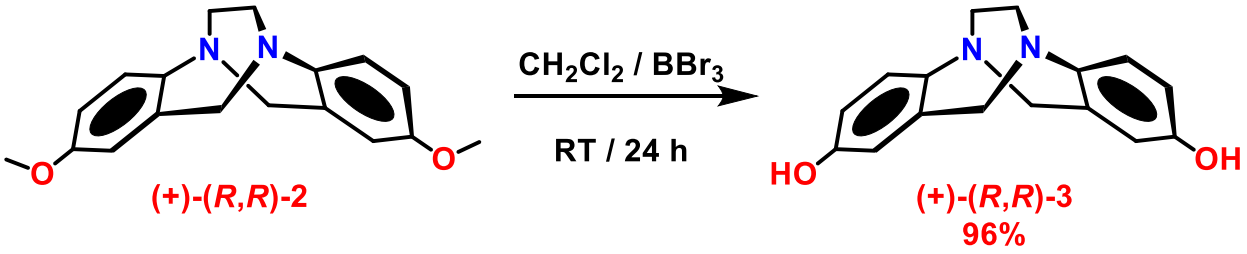

The same procedure was accordingly repeated using **(+)-(*R*,*R*)-2** instead of **(–)-(*S*,*S*)-2** to obtain **(+)-(*R*,*R*)-3** instead of **(–)-(*S*,*S*)-3**. Enantiomer **(+)-(*R*,*R*)-3**: $[\alpha]_D^{22}$ +261 (*c* 0.100, neat ethyl acetate).

Synthesis of 1,5-Bis[2-(2-chloroethoxy)ethoxy]naphthalene (4)

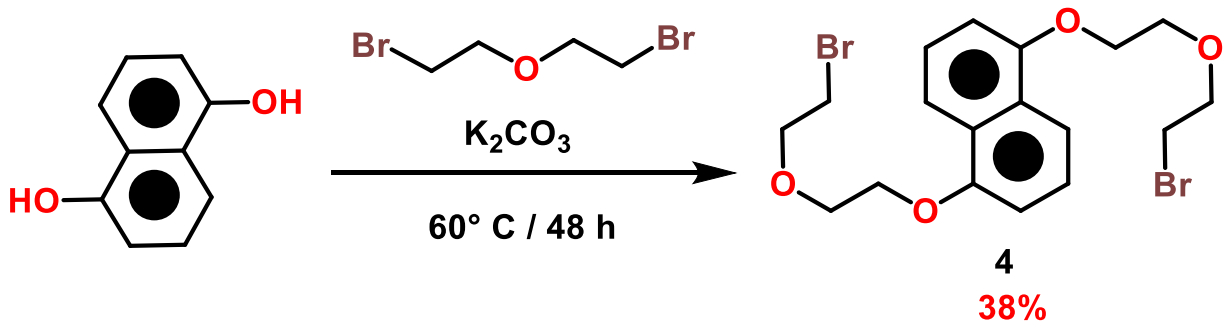

A synthetic procedure described[5] in the literature was adopted in order to obtain linker compound **4** from heating a suspension of K_2CO_3 and 1,5-dihydroxynaphthalene in acetone in the presence of an excess of bis(2-bromoethyl) ether. This yielded 38% of **4** as a semi-sticky white substance. R_f 0.45 (silica gel; ethyl acetate–hexanes, 20% *v*/*v*). ^{1}H NMR (500 MHz, $CDCl_3$): δ 7.86 (d, *J* = 8.4 Hz, 2H), 7.36 (t, *J* = 8.0 Hz, 2H), 6.85 (d, *J* = 7.7 Hz, 2H), 4.31 (t, *J* = 4.6 Hz, 4H), 4.02 (t, *J* = 4.7 Hz, 4H), 4.02 (t, *J* = 6.2 Hz, 4H), 3.52 (t, *J* = 6.1 Hz, 4H).

Synthesis of macrocycles (±)-5, (+)-(*R*,*R*)-5, and (–)-(*S*,*S*)-5

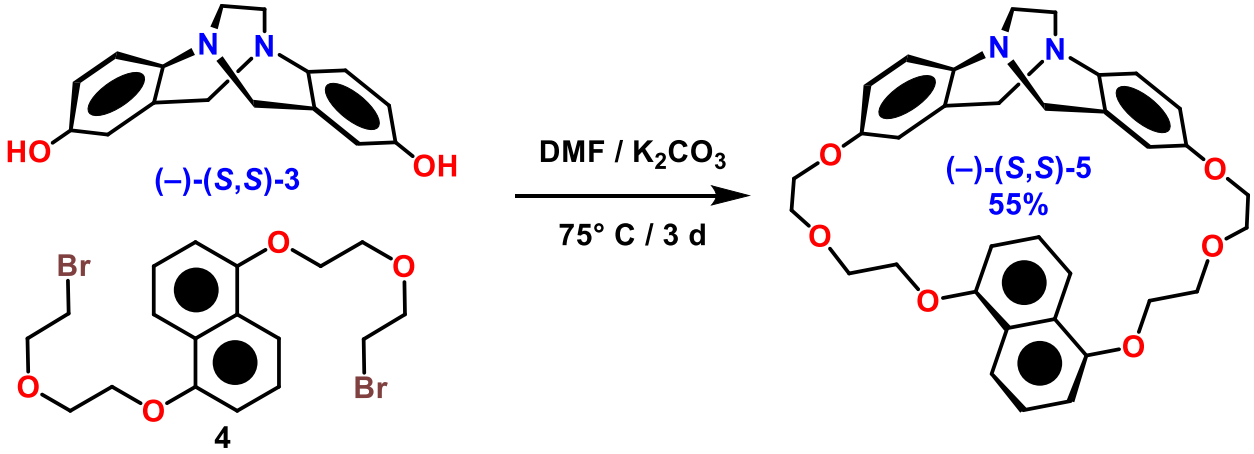

Two plastic syringes were separately loaded with solutions of Tröger's base analog **(–)-(*S*,*S*)-3** (1.0 mmol, 268 mg) in DMF (50 mL), and linker **4** (1.0 mmol, 462 mg) in DMF (50 mL), then mounted on a programmable syringe pump. These solutions were simultaneously injected slowly over 12 h into a stirring suspension of anhydrous K_2CO_3 (7 g) in DMF (200 mL) in a three-necked round bottom flask at 75° C under a slow stream of nitrogen gas (~50mL/min). Once the injections finished, the syringes were removed, stopped the flow of nitrogen, and the mixture was stirred continuously at 80° C for 72 h. The reaction mixture was then allowed to cool back to RT while being stirred continuously. The mixture was diluted with $CHCl_3$ (500 mL), allowed its K_2CO_3 contents to completely precipitate out, and filtered twice using sintered glass and then a paper filter until it became totally clear and pale yellow in color. The collected solution was reduced in volume by rotary evaporation at 60° C until dry. The remaining off-white organic residue was chromatographed to furnish **(–)-(*S*,*S*)-5** as a white solid (yield 55%). R_f 0.45 (silica gel; MeCN–CH_2Cl_2, 25% *v/v*). ^{1}H NMR (600 MHz, $CDCl_3$): δ 7.56 (d, *J* = 8.5 Hz, 2H), 7.06 (d, *J* = 8.4 Hz, 2H), 6.79 (d, *J* = 7.6 Hz, 2H), 6.65 (dd, *J* = 8.5 Hz, *J* = 2.7 Hz, 2H), 6.59 (d, *J* = 2.7 Hz, 2H), 6.53 (t, *J* = 8.0 Hz, 2H), 4.57 (d, *J* = 17.5 Hz, 2H), 4.44 (d, *J* = 17.5 Hz, 2H), 4.30–4.32 (m, 4H), 4.04–4.07 (m, 2H), 3.86–3.99 (m, 10H), 3.54–3.61 (m, 4H). ^{13}C NMR (150 MHz, $CDCl_3$): δ 156.1, 154.3, 129.0, 127.2, 124.9, 115.1, 113.9, 113.4, 108.0, 69.9, 69.7, 68.8, 67.6, 59.5, 55.2. UV-Vis: (MeCN) λ (log ε) = 325 nm (3.596), and 295 nm (4.073). HRMS-ESI (*m/z*): calcd. for $[C_{34}H_{37}N_2O_6]^+$ 569.26461, found 569.2652. $[\alpha]_D^{20}$ –841 (*c* 1.00, MeCN–$CHCl_3$, 10% *v/v*). CCDC deposition number: 2123650.

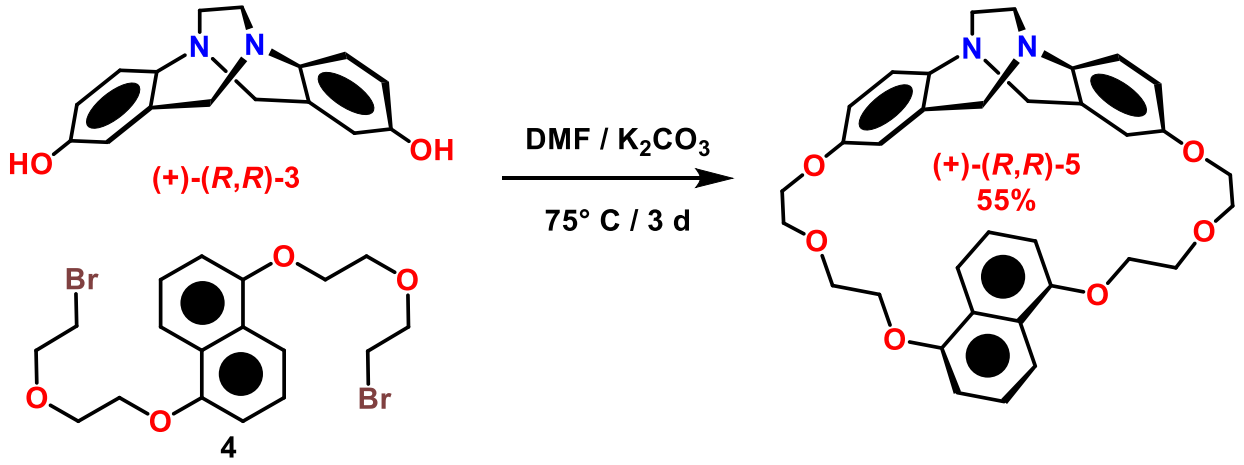

This procedure was repeated using **(+)-(*R*,*R*)-3** instead of **(–)-(*S*,*S*)-3** to obtain **(+)-(*R*,*R*)-5** instead of **(–)-(*S*,*S*)-5**. $[\alpha]_D^{20}$ +853 (*c* 1.00, MeCN–$CHCl_3$, 10% *v*/*v*).

Finally, the procedure was accordingly repeated again using ***racemate* (±)-3** in order to obtain ***racemate* (±)-5** which was then crystallized from MeCN. CCDC deposition number: 2087908.

Synthesis of 1,1''-(1,4-phenylenebis(methylene))bis(([4,4'-bipyridin]-1-ium))• bis(hexafluorophosphate) (6•2PF_6)

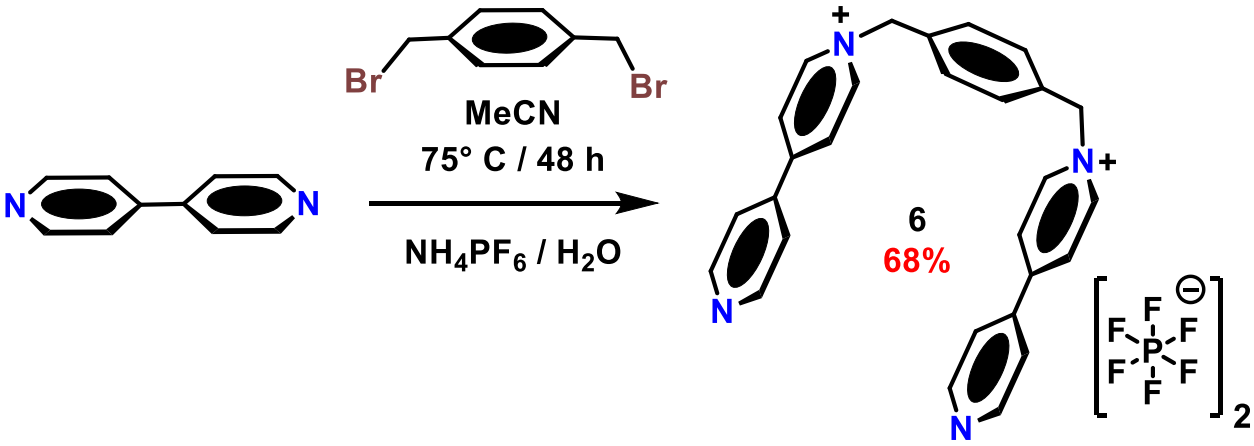

Applied a synthetic procedure described in the literature[6] to obtain compound **6**•2Br from heating 1,4-bis-bromomethyl-benzene with an excess of 4,4′-bipyridyl in MeCN. The crude was chromatographed using a reverse-phase C-18 column and H_2O–MeCN gradient (10–100% organic *v/v*). Br^- anion swapped for $PF6^-$ by the addition of NH_4PF_6 to the aqueous solution of **6**•2Br. This ion exchange precipitated **6**•2PF_6 out of the solution as a white powder in 68% yield. ^{1}H NMR (500 MHz, CD_3CN): δ 8.84 (m, 8H), 8.32 (d, *J* = 7.0 Hz, 4H), 7.78 (m, 4H), 7.55 (s, 4H), 5.77 (s, 4H). RP-HPLC ^{t}R 3.68 ± 0.1 min, >98% purity, C-18: 5µm 4.6×150mm, 20 °C.

Synthesis of catenanes (±)-7, (+)-(*R*,*R*)-7, and (–)-(*S*,*S*)-7

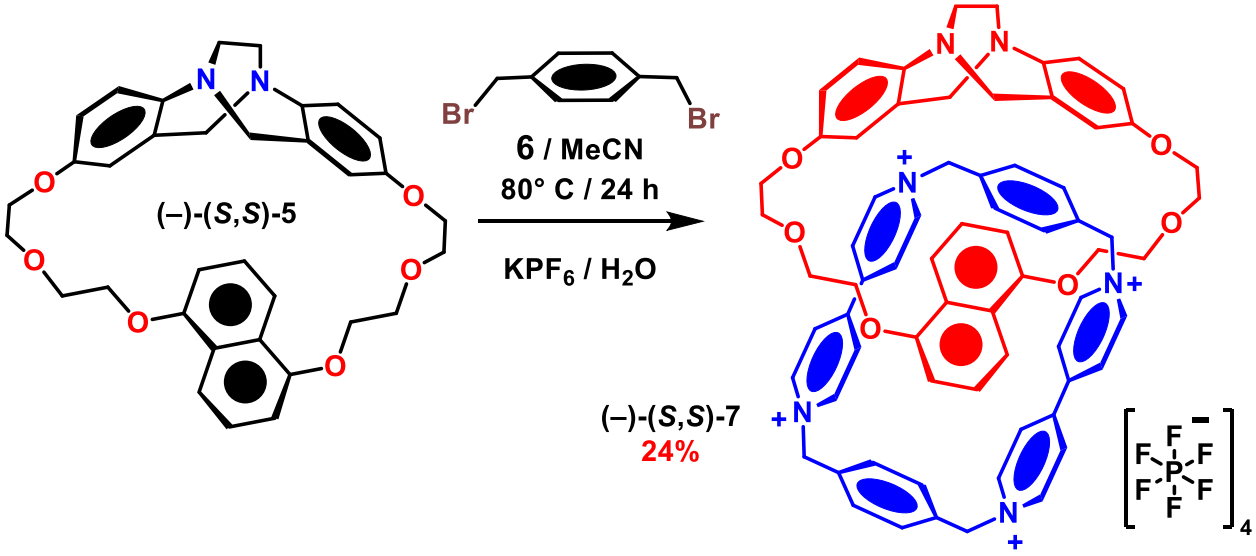

Solutions of compound **6**•2PF_6 (0.3 mmol, 212 mg) in MeCN (5 mL), and 1,4-bis-bromomethyl-benzene (0.3 mmol, 80 mg) in MeCN–$CHCl_3$ (5 mL, 1:1 *v/v*) were separately loaded in two plastic syringes. Then mounted these syringes on a programable syringe pump. These solutions were simultaneously injected slowly (10 µL.min^{-1}, over around 8 h) into a 100 mL three-necked round bottom flask

containing a solution of **(–)-(*S,S*)-5** (0.2 mmol, 114 mg) in MeCN (50 mL) stirring at 80° C under an slow stream of nitrogen gas. Once the injections finished, the syringes were removed, and stopped the flow of nitrogen gas when the total volume reached around 40 mL. Then allowed the mixture to stir continuously at 80° C overnight. The reaction mixture was then allowed to cool back to RT, sonicated for 10 min and transferred to a 50 mL Falcon tube along with KPF_6 (200 mg) and centrifuged at 5000 rpm for 5 min. The dark violet solution was decanted, transferred to a round bottom flask and rotavapped till dry. The remaining brownish-black residue chromatographed using a reversed-phase C-18 FC column and gradient mobile phase (H_2O–MeCN 10–100% organic *v/v*) to obtain pure catenane **(–)-(*S,S*)-7**•$4PF_6$ as a black-purple solid after removal of the solvents. The yellowish polymeric residue remaining in the Falcon tube was then digested with sonication in an aqueous NaOH solution (0.1 M, 20 mL) and extracted with $CHCl_3$ (20 mL × 3). The combined organic layers were dried over Na_2SO_4, filtered and rotavapped till dry. The remaining residue was chromatographed (silica gel, MeCN–CH_2Cl_2 3:7 *v/v*) to retrieve the remaining chiral macrocycle **(–)-(*S,S*)-5** as a white solid. This procedure yielded 24% of **(–)-(*S,S*)-7**•$4PF_6$, and recovered 67% of **(–)-(*S,S*)-5**. ^{1}H NMR (600 MHz, CD_3CN): δ 9.02 (d, *J* = 6.5 Hz, 2H, proton A), 8.72 (d, *J* = 6.5 Hz, 2H, proton B), 8.64 (d, *J* = 6.5 Hz, 2H, proton C), 8.33 (d, *J* = 6.5 Hz, 2H, proton D), 8.02 (dd, *J* = 8.2 and 1.3 Hz, 4H, proton E), 7.92 (dd, *J* = 8.2 and 1.3 Hz, 2H, proton F), 7.86 (dd, *J* = 8.2 and 1.3 Hz, 2H, proton G), 7.31 (m, 4H, proton H), 6.77 (d, *J* = 8.7 Hz, 2H, proton I), 6.69 (dd, *J* = 8.7 and 2.8 Hz, 2H, proton J), 6.37 (dd, *J* = 6.5 and 2.3 Hz, 2H, proton K), 6.28 (d, *J* = 7.9 Hz, 2H, proton L), 6.24 (dd, *J* = 6.5 and 2.3 Hz, 2H, proton M), 5.87 (t, *J* = 8.1 Hz, 2H, proton N), 5.82 (d, *J* = 13.5 Hz, 2H, proton P), 5.7 (s, 4H, proton O), 6.24 (dd, *J* = 6.5 and 2.3 Hz, 2H, proton M), 5.68 (d, *J* = 13.5 Hz, 2H, proton P'), 5.54 (d, *J* = 2.7 Hz, 2H, proton Q), 4.53–4.57 (m, 2H, proton R), 4.44–4.48 (m, 2H, proton R'), 4.30–4.39 (m, 4H, proton T), 4.14–

4.20 (m, 4H, proton U), 4.08 (d, J = 17.3 Hz, 2H, proton V), 4.00–4.04 (m, 4H, proton W), 3.62 (d, J = 17.4 Hz, 2H, proton X), 3.04–3.22 (m, 4H, proton Y), 2.21 (d, J = 8.2 Hz, 2H, proton Z). ^{13}C NMR (150 MHz, $CDCl_3$): δ 155.5, 151.8, 146.1, 146.0, 145.2, 145.0, 144.7, 144.2, 144.1, 141.3, 137.5, 137.5, 132.4, 132.3, 131.9, 131.7, 130.4, 128.3, 128.1, 126.7, 125.8, 125.2, 124.2, 116.0, 110.5, 109.4, 105.9, 71.7, 70.6, 68.6, 67.4, 66.1, 65.6, 58.7, 55.5. UV-Vis: (MeCN) λ (log ε) = 525 nm (2.8587), and 265 nm (5.2876). HRMS-ESI (m/z): calcd. for $[C_{70}H_{68}N_6O_6P_2F_{12}]^{2+}$ 689.22365, found 689.2242; calcd. for $[C_{70}H_{68}N_6O_6P_3F_{18}]^{+}$ 1523.41203, found 1524.4158. $[\alpha]_{633}^{20}$ –56 (c 0.10, MeCN). CCDC deposition number: 2127780.

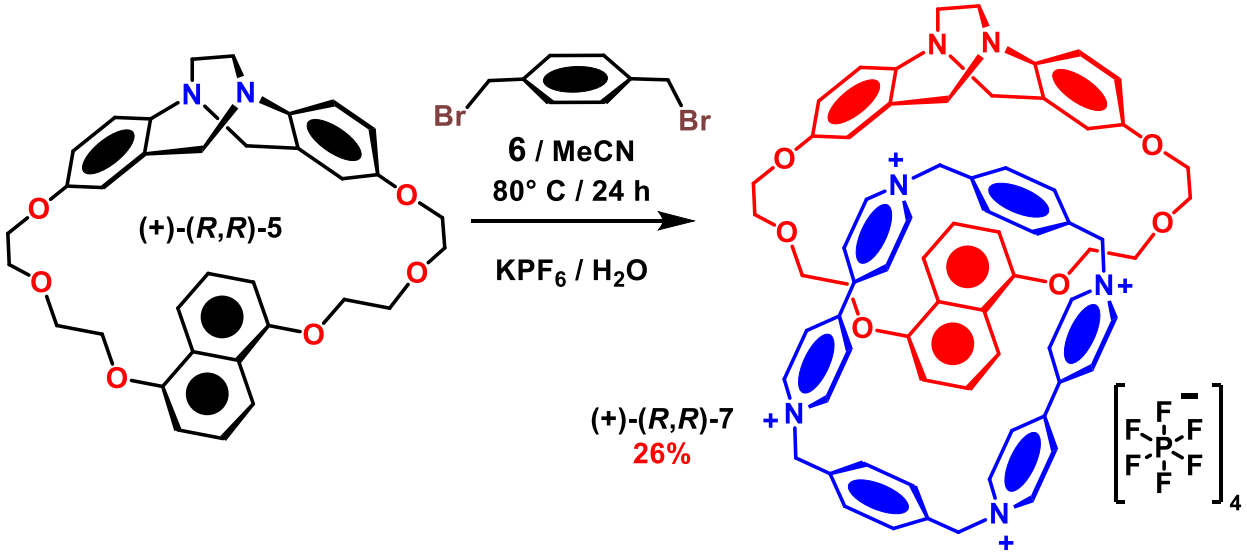

The same procedure was repeated using **(+)-(*R,R*)-5** instead of **(–)-(*S,S*)-5** to obtain **(+)-(*R,R*)-7**•4PF_6 instead of **(–)-(*S,S*)-7**•4PF_6 in 26% yield. $[\alpha]_{633}^{20}$ +48 (c 0.10, MeCN).

Finally, the same procedure was accordingly repeated using ***racemate* (±)-5** to obtain ***racemate* (±)-7**•4PF_6 in 23% yield which was then crystallized for comparison purposes. CCDC deposition number: 2131821.

Preparation of water-soluble catenanes (+)-(*R,R*)-7•4Cl and (–)-(*S,S*)-7•4Cl

Applied an anion exchange procedure described[7] in the literature to obtain **7**•4Cl from a solution of **7**•4PF6 in MeCN treated with tetrabutylammonium chloride. The generated precipitate was then collected by filtration, rinsed with dry Me_2CO thoroughly, and dried under high vacuum giving **7**•4Cl as a purple solid in 85% yield.

Photocatalytic Aerobic Oxidation of DL-Methionine

Adopted a procedure described in the literature[7] for the photocatalytic aerobic oxidation of methionine, except for using DL-methionine instead of L-methionine and wavelength of 235 nm for diode-array detection (DAD). These reactions performed in autosampler vials charged with a micro magnetic stir bar and stock solutions of the desired enantiomers of **7**•4Cl (500 μL, 1.0 mM, HPLC grade H_2O) and methionine (500 μL, 10 mM, HPLC grade H_2O) kept under pure O_2 (1 atm) while exposed to LED light irradiation. Kessil PR160L427nm-19V40W and Chirex-3126-(D)-penicillamine were employed as the source of light and chiral analytical HPLC column, respectively. The chiral HPLC settings and other related details are found in the HPLC method section. The peaks at around 4, 13, and 15 min are characteristic for methionine sulfoxide, L-methionine and D-methionine, respectively. The ratio of their integrals at 235 nm was used to determine the oxidation yield during the process. The isolated methionine sulfoxides were characterized by ^{1}H NMR and ESI-MS.

■ Section B. Single-Crystal X-Ray Diffraction

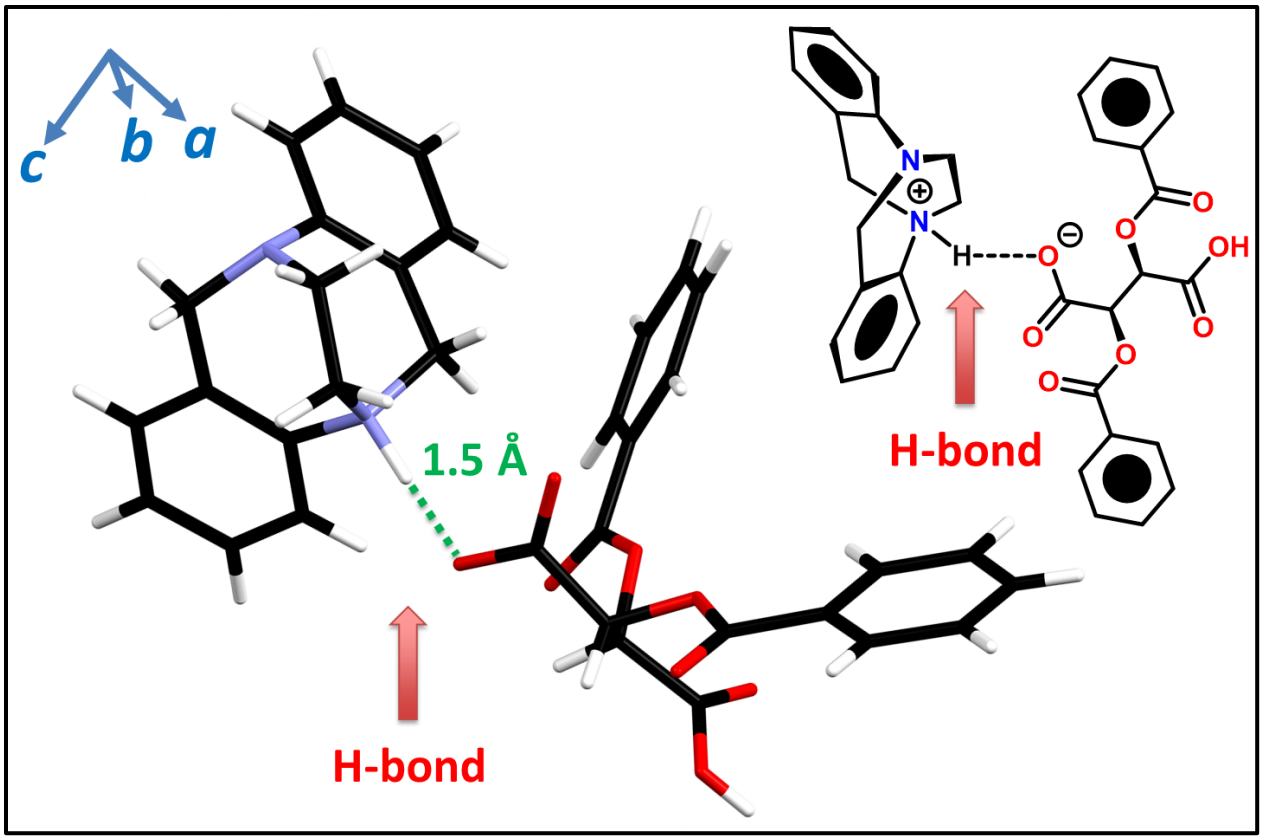

Figure S1. A glimpse of the structures of (*S*,*S*)-enantiomer of an unsubstituted Tröger's base analog cocrystallized with (–)-*O*,*O'*-dibenzoyl-L-tartaric acid solved by single-crystal X-ray diffraction. Red arrows indicate a proton exchange and intermolecular hydrogen bonding interactions. Blue arrows indicate the unit cell axis and carbons, oxygen, nitrogen, and hydrogen atoms are shown in black, red, blue, and white, respectively. CCDC deposition number 2042985, Space Group: $P2_12_12_1$, Cell: *a* 11.3 *b* 11.8 *c* 25.23 Å, α 90 β 90 γ 90°, Temperature: 200 K, Crystallized in acetone

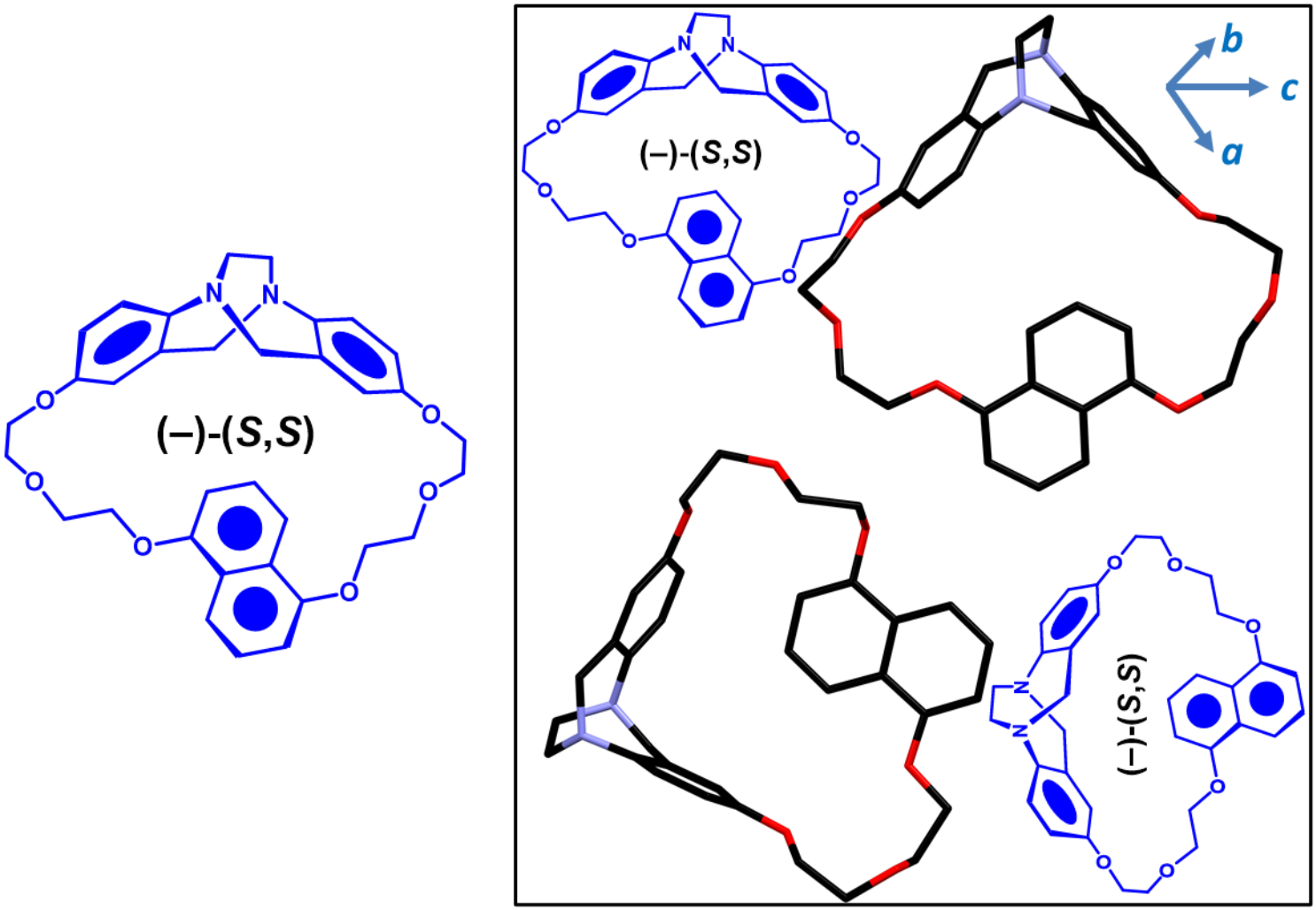

Figure S2. A glimpse of the unit cell structures of enantiopure **(–)-(*S*,*S*)-5** macrocycle solved by single-crystal X-ray diffraction excluding protons for clarity sake. CCDC deposition number 2123650, Space Group: $P2_1$, Cell: *a* 15.8 *b* 8.6 *c* 20.5 Å, α 90 β 95 γ 90°, Temperature: 100 K, Crystallized from MeCN

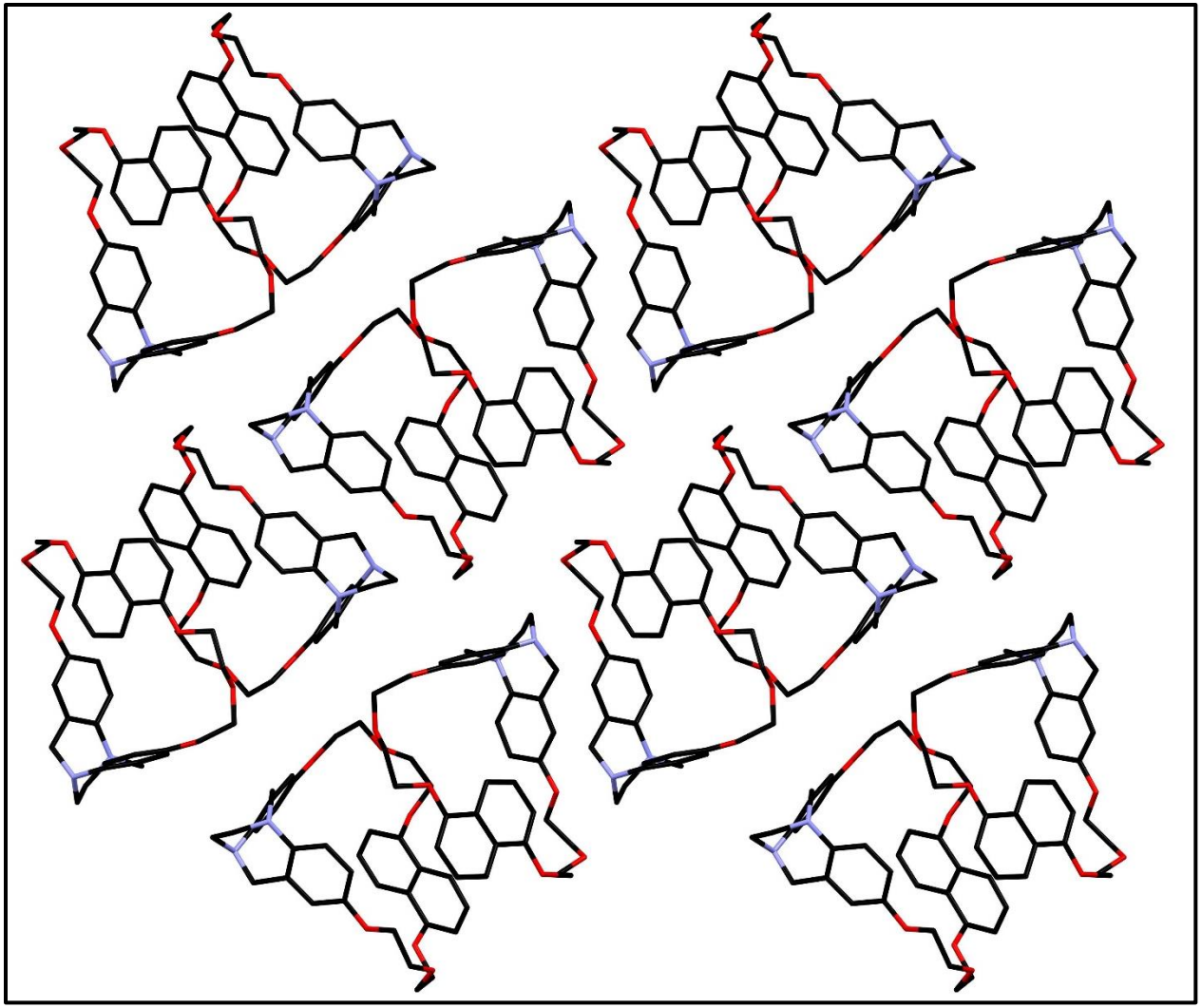

Figure S3. The packing order of enantiopure **(–)-(*S,S*)-5** macrocycle solved by single-crystal X-ray diffraction viewed along *b*-cell axis excluding protons for sake of clarity. CCDC deposition number 2123650, Space Group: $P2_1$, Cell: *a* 15.8 *b* 8.6 *c* 20.5 Å, α 90 β 95 γ 90°, Temperature: 100 K, Crystallized from MeCN

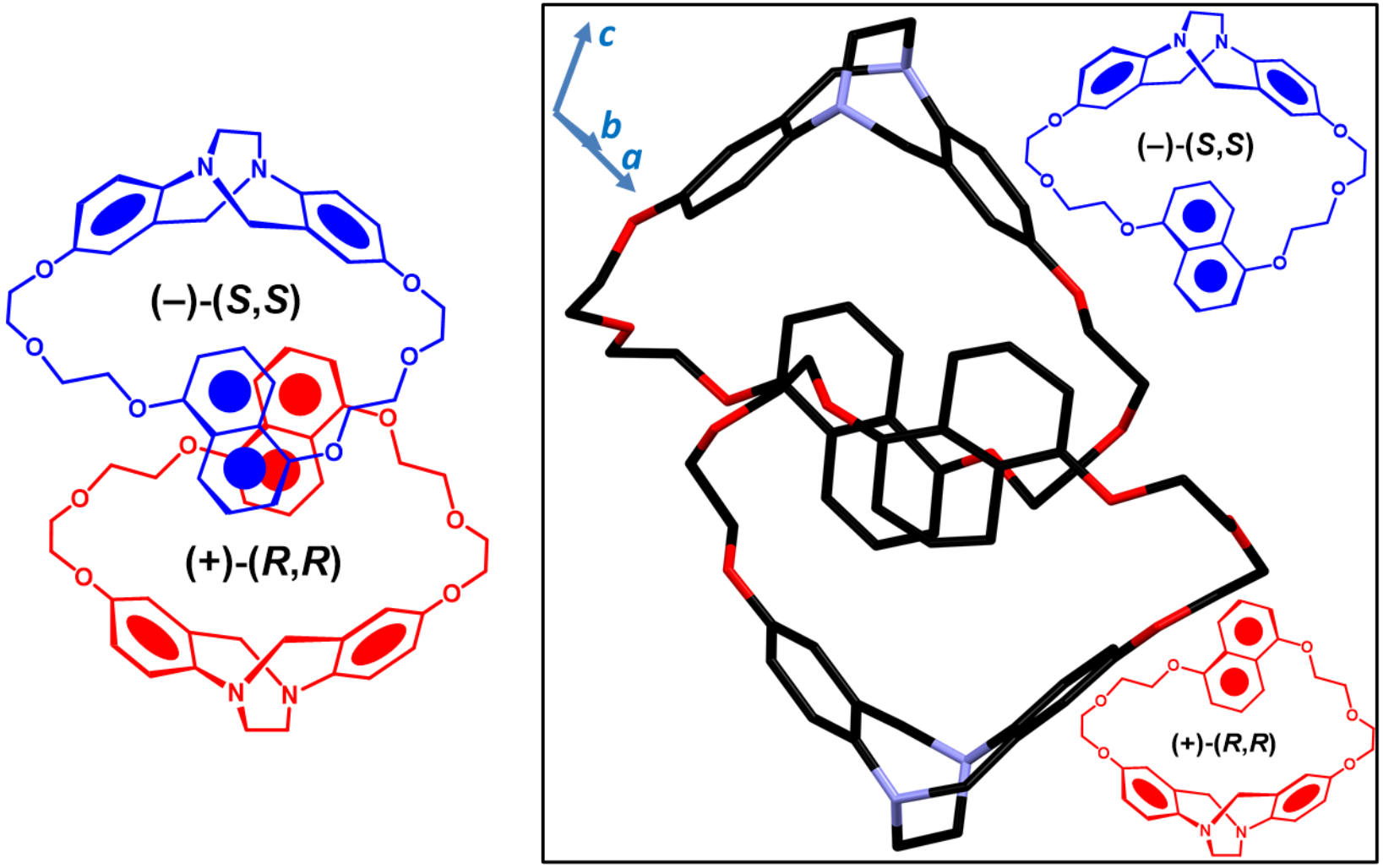

Figure S4. A glimpse of the unit cell structures of macrocycles **(+)-(*R*,*R*)-5** and **(–)-(*S*,*S*)-5** solved by single-crystal X-ray diffraction excluding protons for clarity. CCDC deposition number 2087908, Space Group: *C*2/c, Cell: *a* 34.8 *b* 9.1 *c* 36.0 Å, α 90 β 95 γ 90°, Temperature: 100 K, Crystallized from MeCN

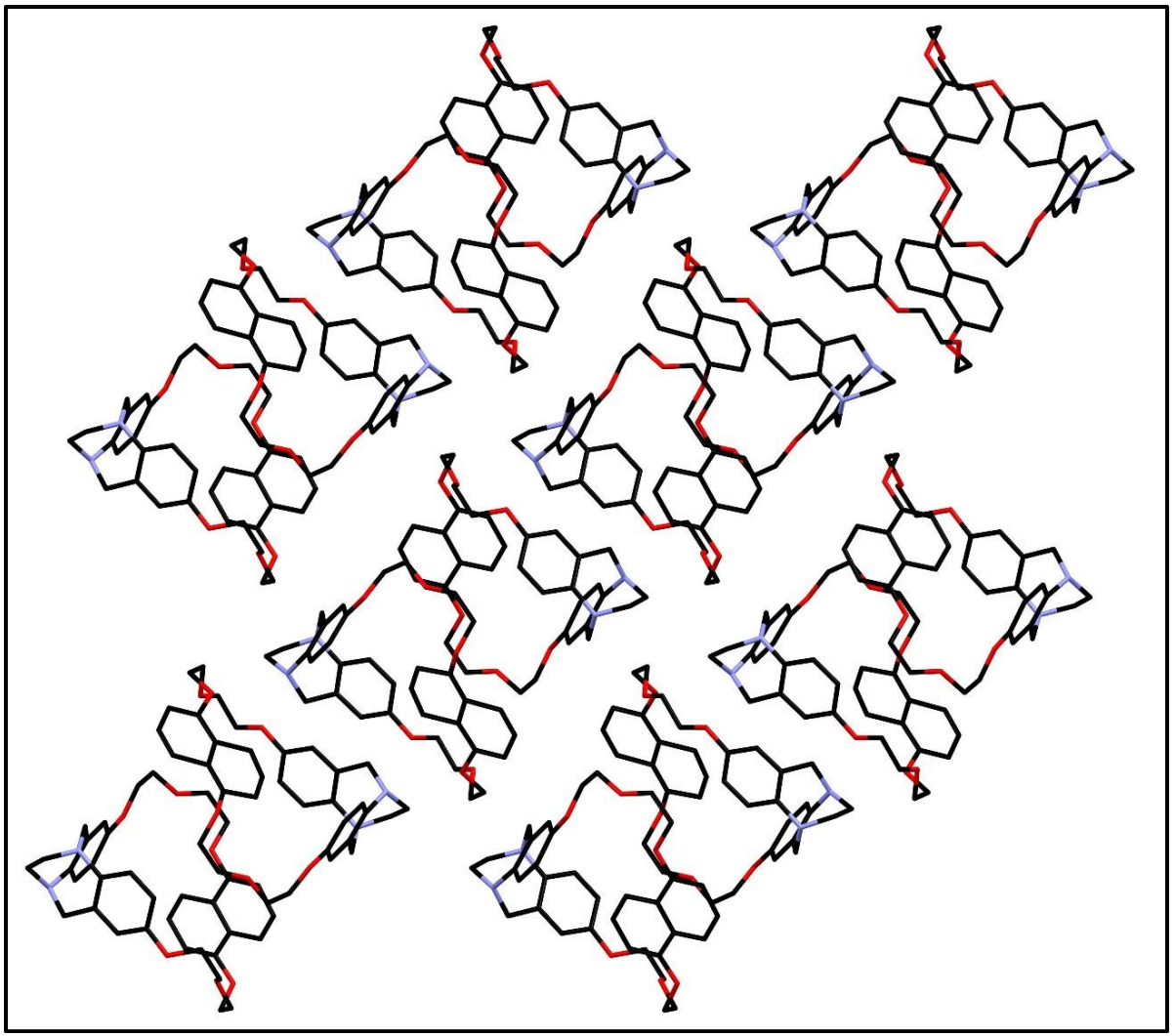

Figure S5. The packing order of macrocycles **(+)-(*R*,*R*)-5** and **(–)-(*S*,*S*)-5** solved by single-crystal X-ray diffraction viewed along *b*-cell axis excluding protons for clarity. CCDC deposition number 2087908, Space Group: *C*2/c, Cell: *a* 34.8 *b* 9.1 *c* 36.0 Å, α 90 β 95 γ 90°, Temperature: 100 K, Crystallized from MeCN

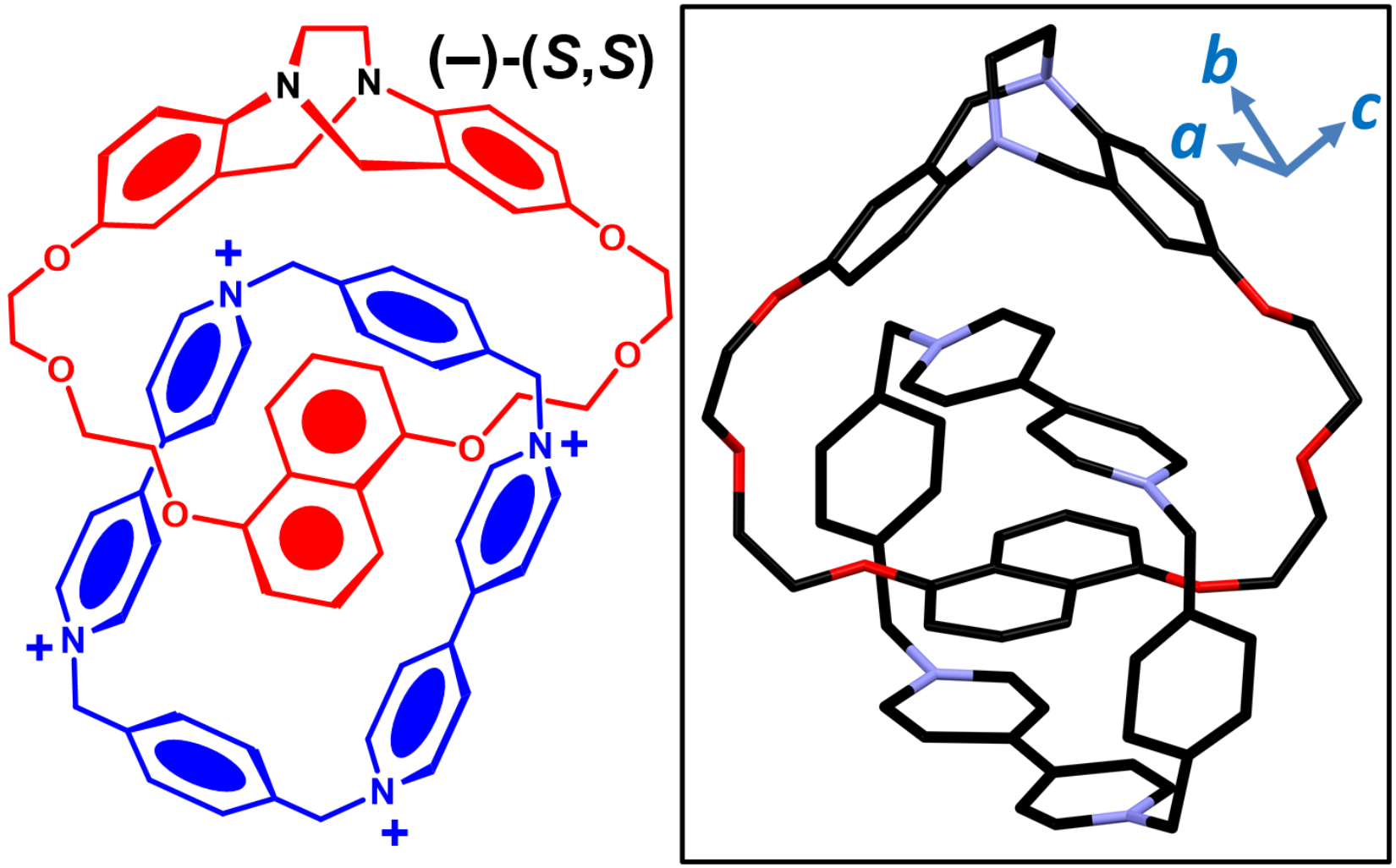

Figure S6. A glimpse of the structures of enantiopure catenane **(–)-(*S*,*S*)-7•4PF$_6$** solved by single-crystal X-ray diffraction excluding protons and PF_6^- counter ions for clarity. CCDC deposition number 2127780, Space Group: $P2_1$, Cell: *a* 14.1 *b* 25.2 *c* 24.5 Å, α 90 β 92 γ 90°, Temperature: 250 K, Crystallized from MeCN

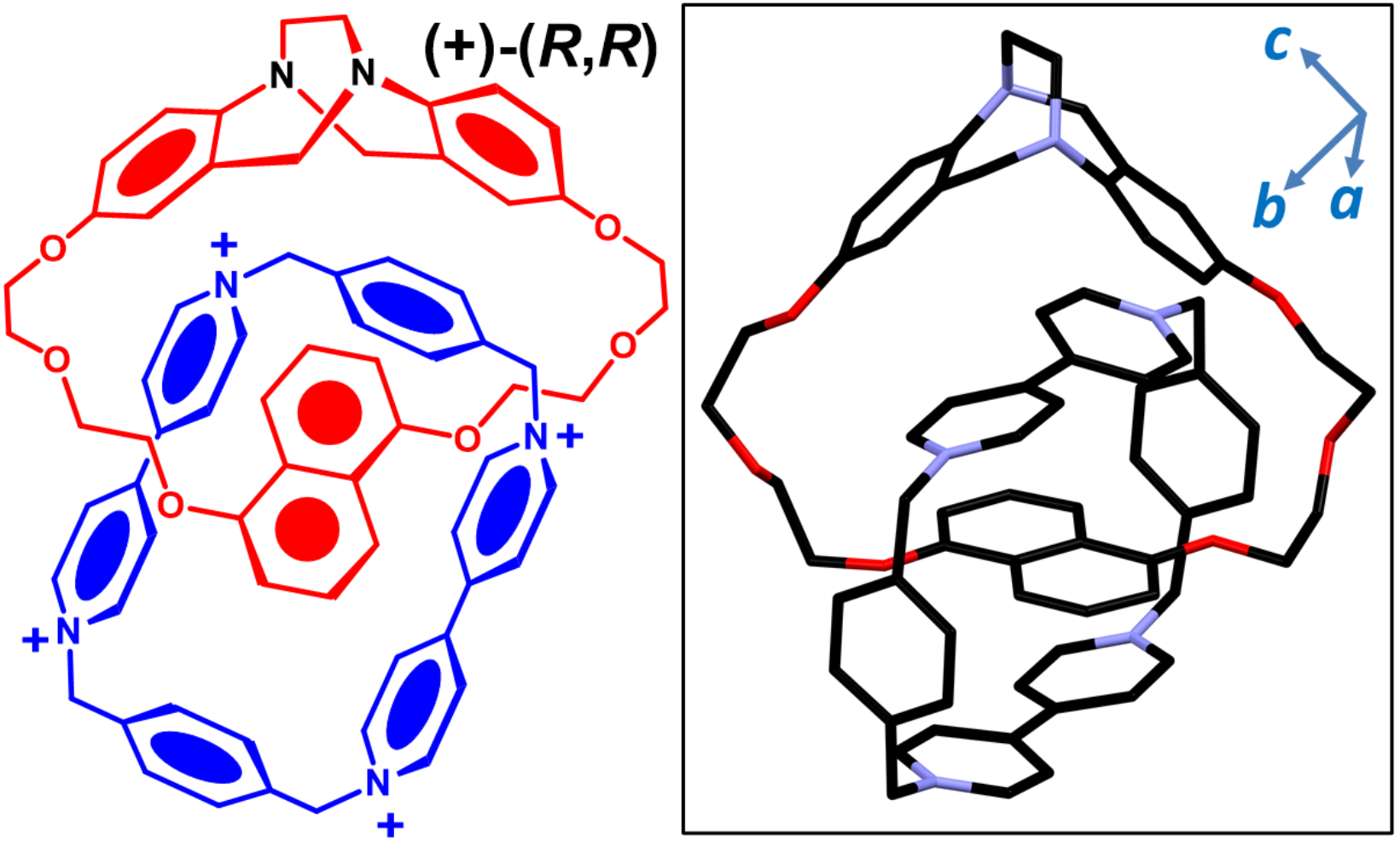

Figure S7. A glimpse of the structures of catenane **(–)-(*R*,*R*)-7•4PF$_6$** solved by single-crystal X-ray diffraction excluding protons, the opposite enantiomer and PF_6^- counter ions for clarity. CCDC deposition number 2131821, Space Group: $P2_1/c$, Cell: *a* 13.9 *b* 22.2 *c* 23.4 Å, α 90 β 94 γ 90°, Temperature: 100 K, Crystallized from MeCN

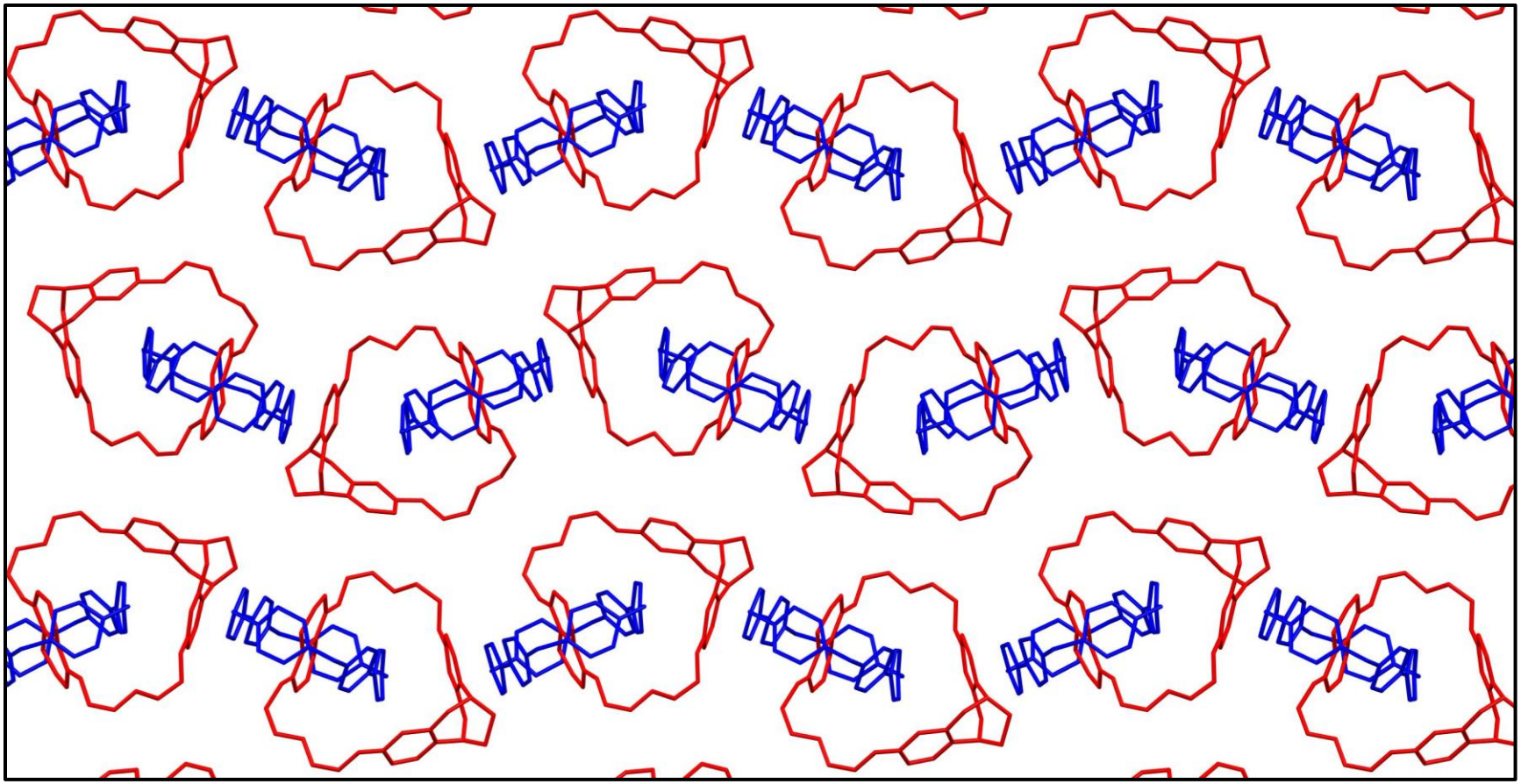

Figure S8. The packing order of enantiopure catenane **(–)-(*S*,*S*)-7•4PF$_6$** viewed along *a*-cell axis solved by single-crystal X-ray diffraction excluding protons and PF_6^- counter ions for clarity. CCDC deposition number 2127780, Space Group: $P2_1$, Cell: *a* 14.1 *b* 25.2 *c* 24.5 Å, α 90 β 92 γ 90°, Temperature: 250 K, Crystallized from MeCN. Chiral donor rings are shown in red and the acceptor rings in blue

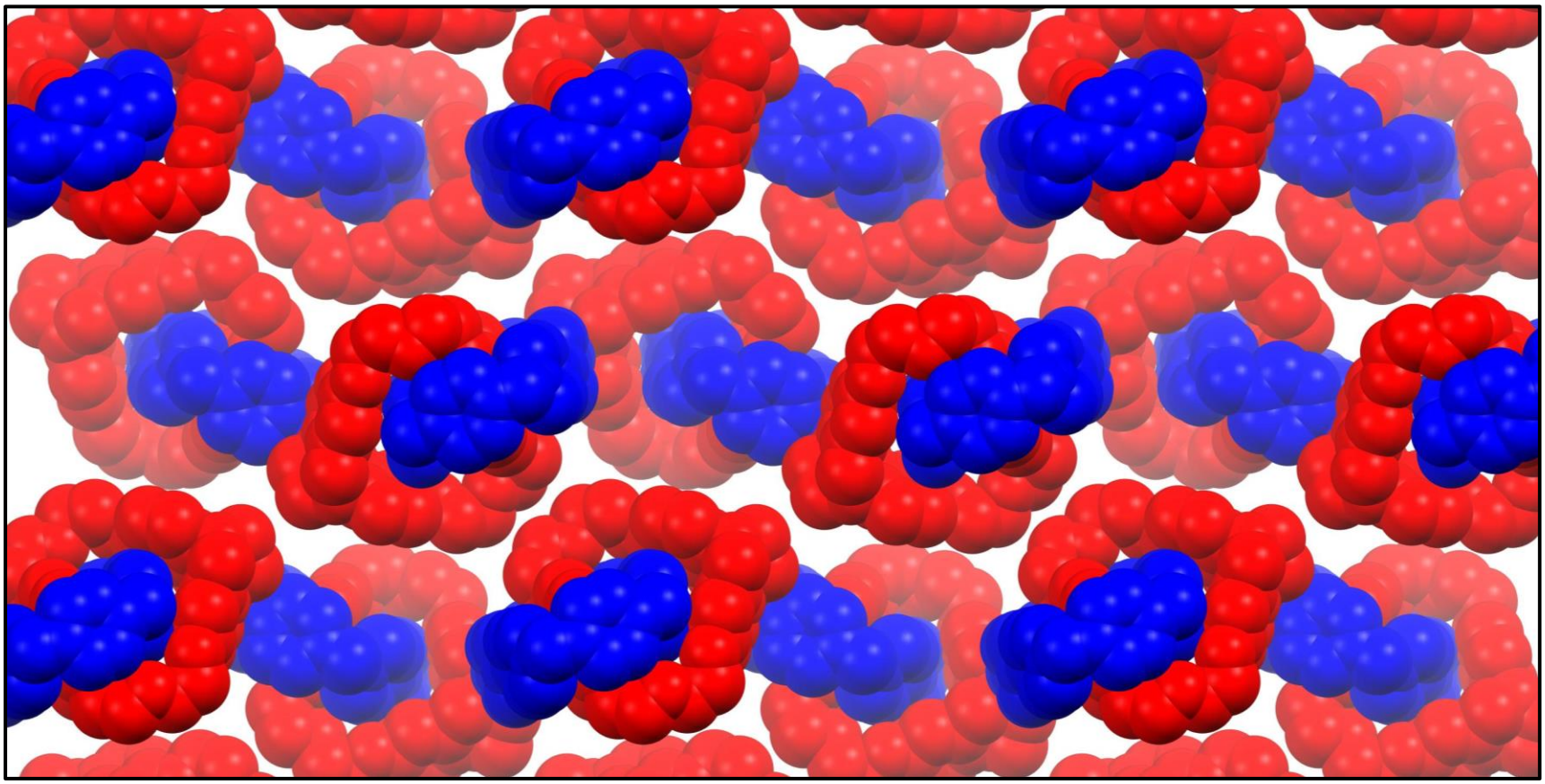

Figure S9. Depth cue spacefill presentation of the packing order of enantiopure catenane **(–)-(*S*,*S*)-7•4PF$_6$** viewed along *a*-cell axis solved by single-crystal X-ray diffraction excluding protons and PF_6^- counter ions for clarity. CCDC deposition number 2127780, Space Group: $P2_1$, Cell: *a* 14.1 *b* 25.2 *c* 24.5 Å, α 90 β 92 γ 90°, Temperature: 250 K, Crystallized from MeCN; Chiral donor rings are shown in red and the acceptor rings in blue

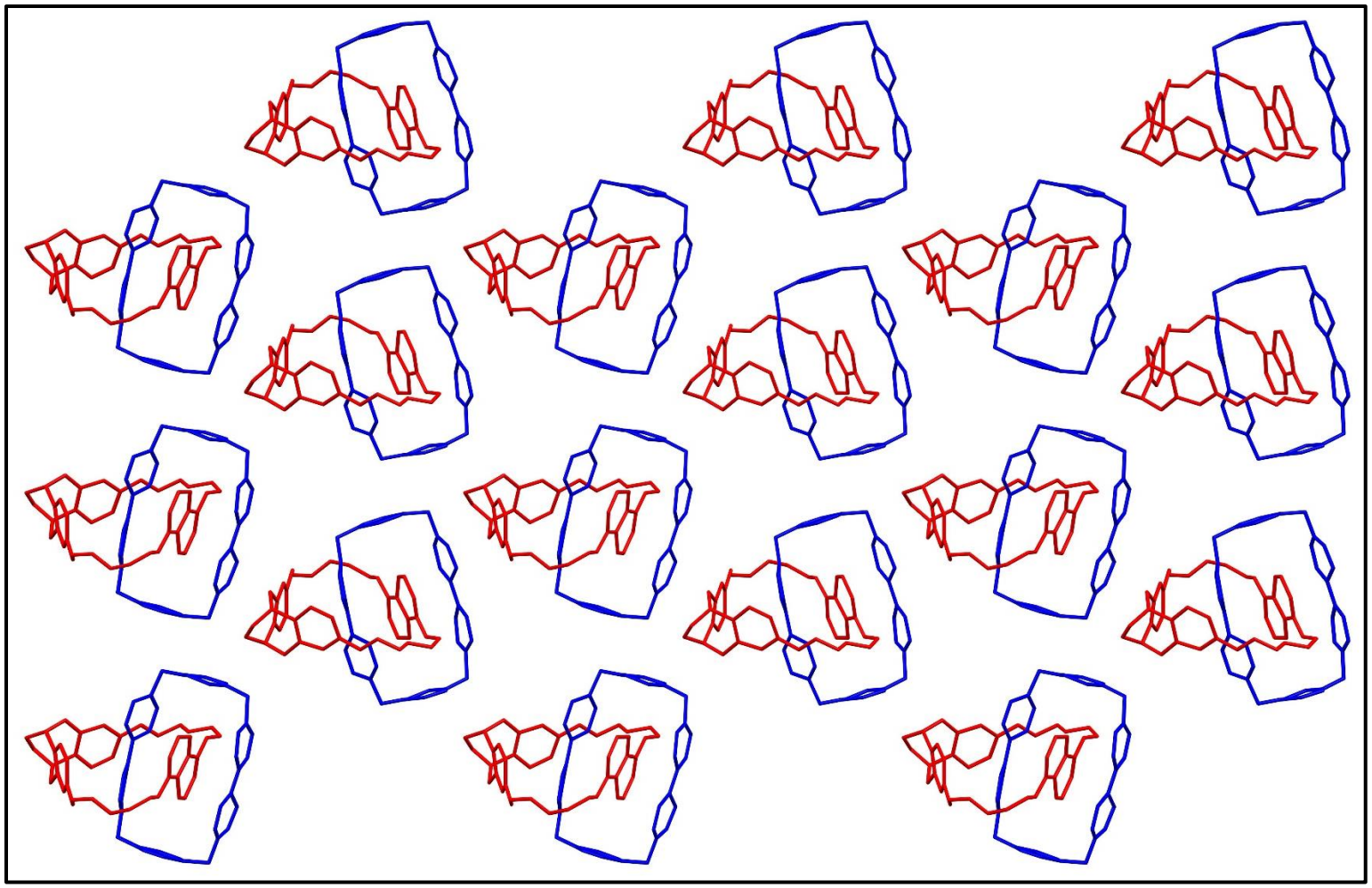

Figure S10. Depth cue presentation of the packing order of enantiopure catenane **(–)-(*S*,*S*)-7•4PF$_6$** viewed along *c*-cell axis solved by single-crystal X-ray diffraction excluding protons, overlaid molecules and PF_6^- counter ions for clarity. CCDC deposition number 2127780, Space Group: $P2_1$, Cell: *a* 14.1 *b* 25.2 *c* 24.5 Å, α 90 β 92 γ 90°, Temperature: 250 K, Crystallized from MeCN; Chiral donor rings are shown in red and the acceptor rings in blue

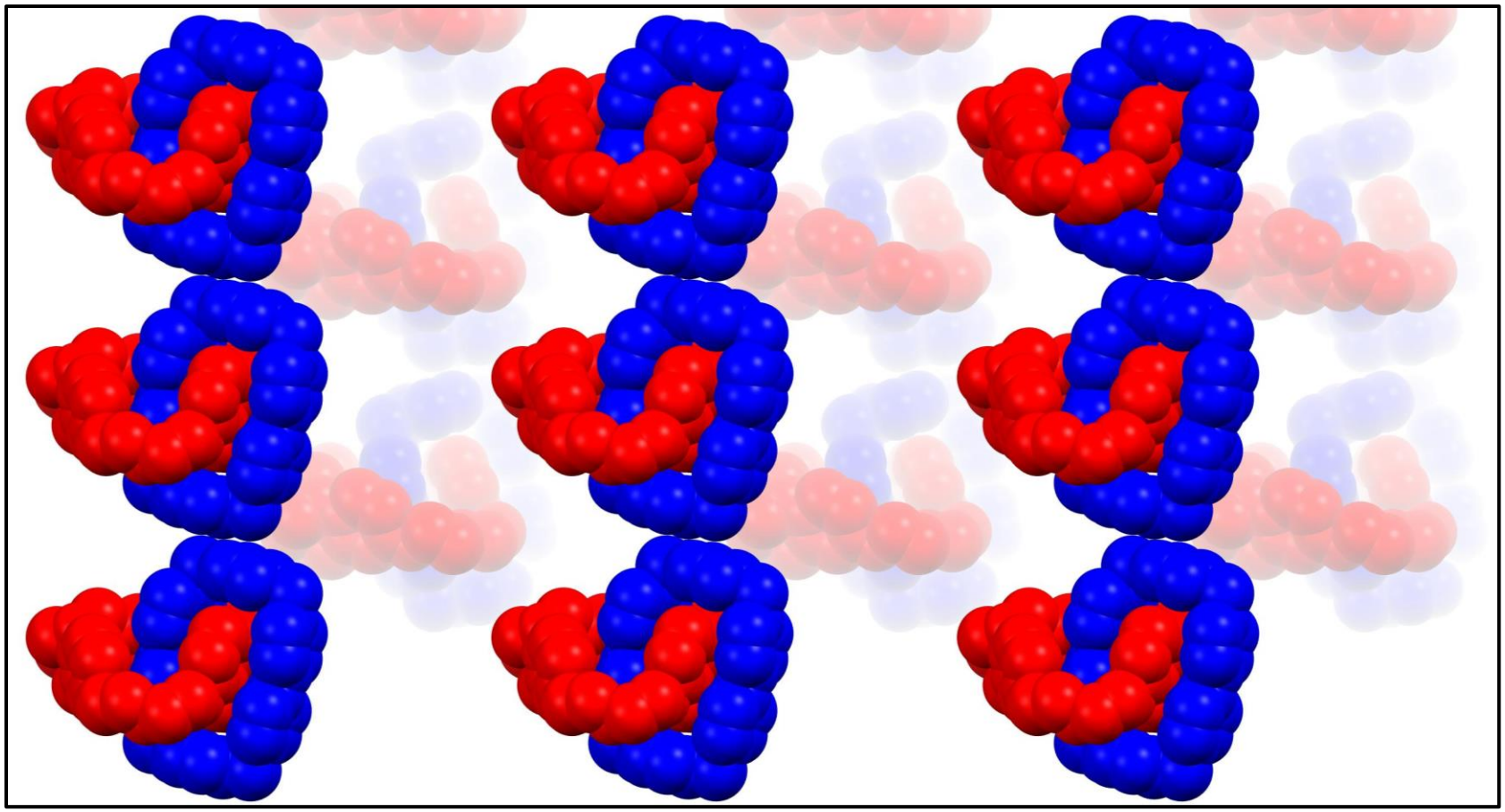

Figure S11. Depth cue spacefill presentation of the packing order of enantiopure catenane **(–)-(*S*,*S*)-7•4PF$_6$** viewed along *c*-cell axis solved by single-crystal X-ray diffraction excluding protons, overlaid molecules and PF_6^- counter ions for clarity. CCDC deposition number 2127780, Space Group: $P2_1$, Cell: *a* 14.1 *b* 25.2 *c* 24.5 Å, α 90 β 92 γ 90°, Temperature: 250 K, Crystallized from MeCN; Chiral donor rings are shown in red and the acceptor rings in blue

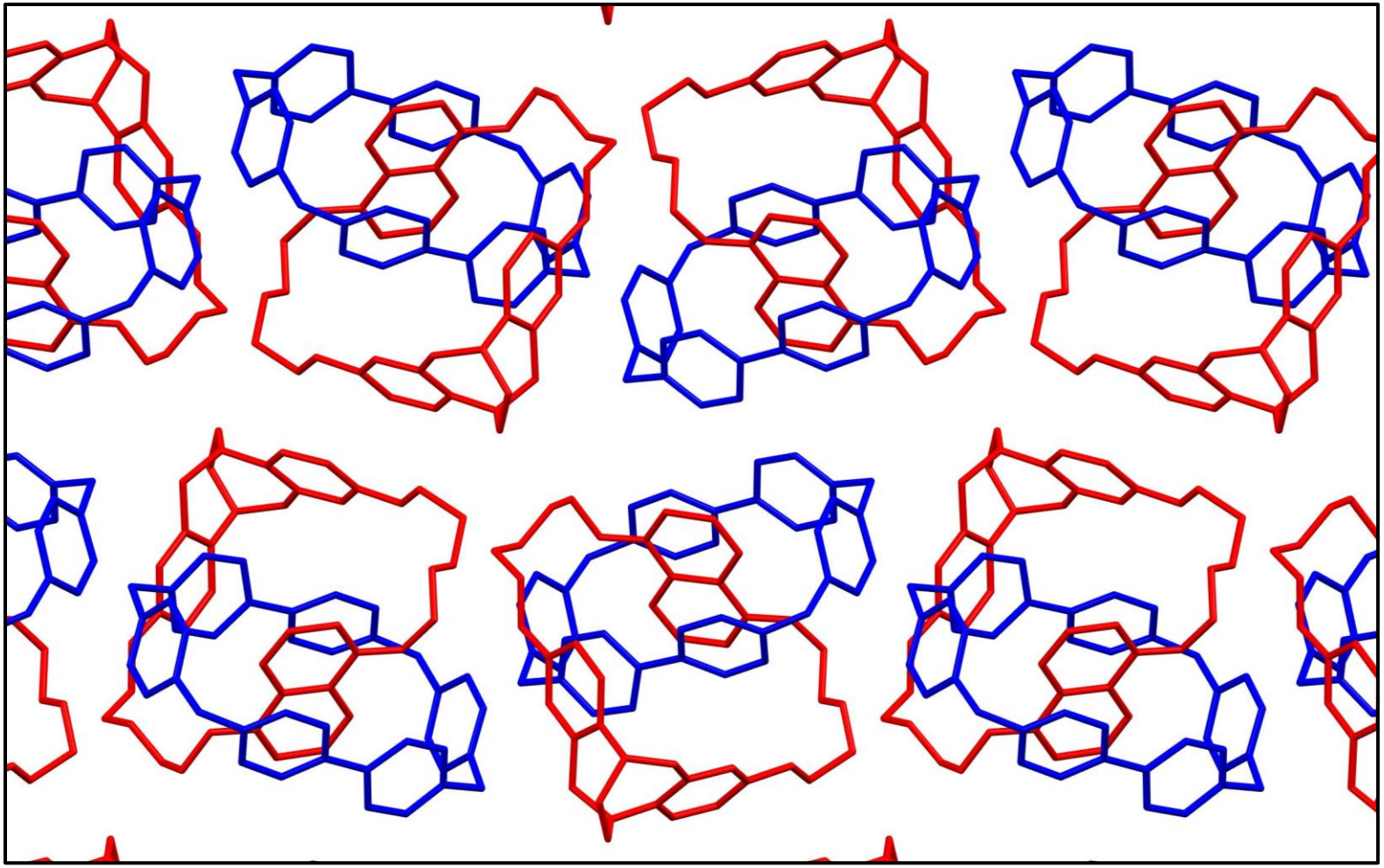

Figure S12. A glimpse of the packing order of racemic catenane **7•4PF$_6$** viewed along *a*-cell axis solved by single-crystal X-ray diffraction excluding protons and PF_6^- counter ions for clarity. CCDC deposition number 2131821, Space Group: $P2_1/c$, Cell: *a* 13.9 *b* 22.2 *c* 23.4 Å, α 90 β 94 γ 90°, Temperature: 100 K, Crystallized from MeCN; Chiral donor rings are shown in red and the acceptor rings in blue

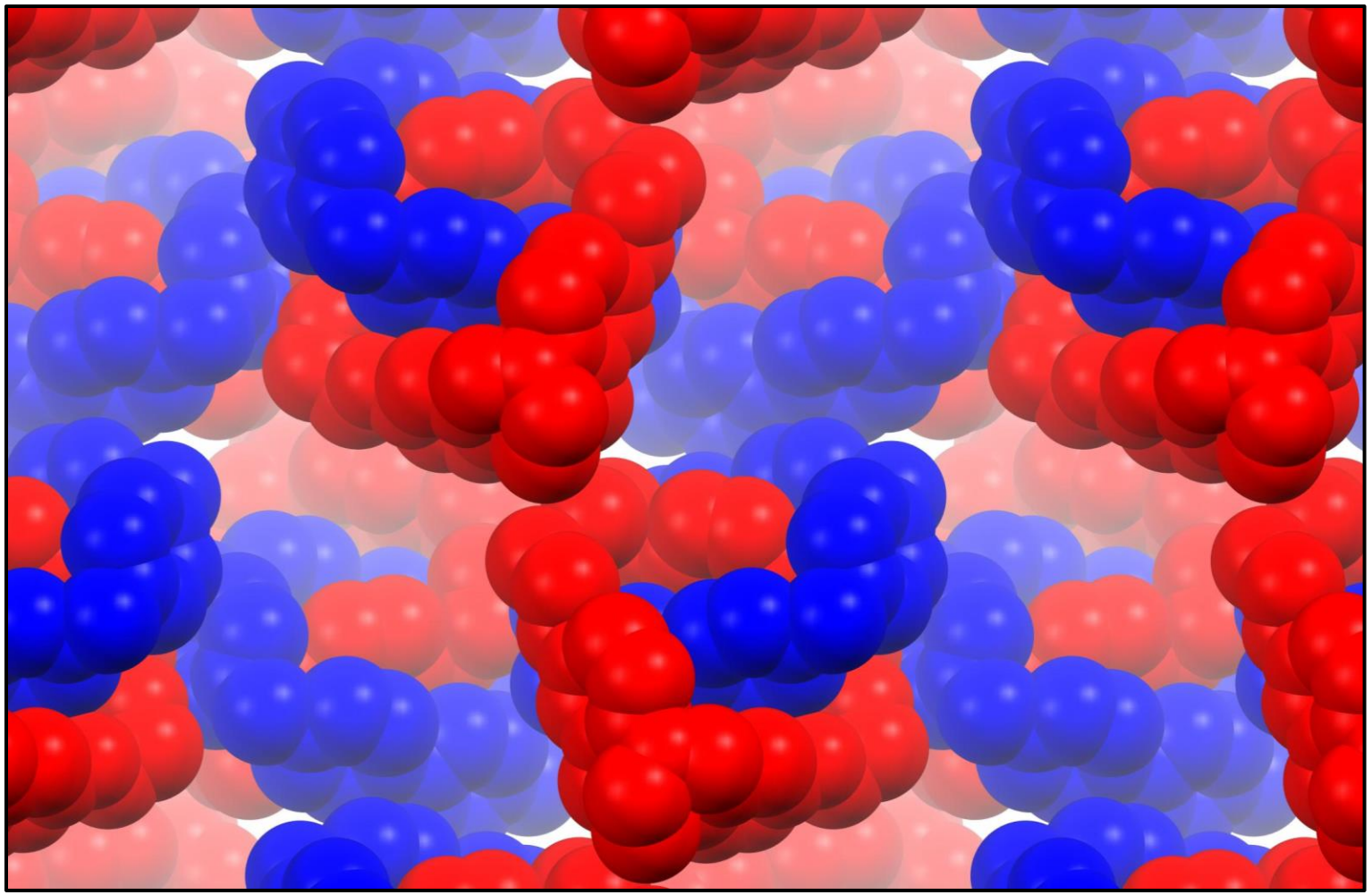

Figure S13. Depth cue spacefill presentation of the packing order of racemic catenane **7•4PF$_6$** viewed along *a*-cell axis solved by single-crystal X-ray diffraction excluding protons and PF_6^- counter ions for clarity. CCDC deposition number 2131821, Space Group: $P2_1/c$, Cell: *a* 13.9 *b* 22.2 *c* 23.4 Å, α 90 β 94 γ 90°, Temperature: 100 K, Crystallized from MeCN; Chiral donor rings are shown in red and the acceptor rings in blue

■ Section C. NMR Spectroscopy and Chiral Discrimination

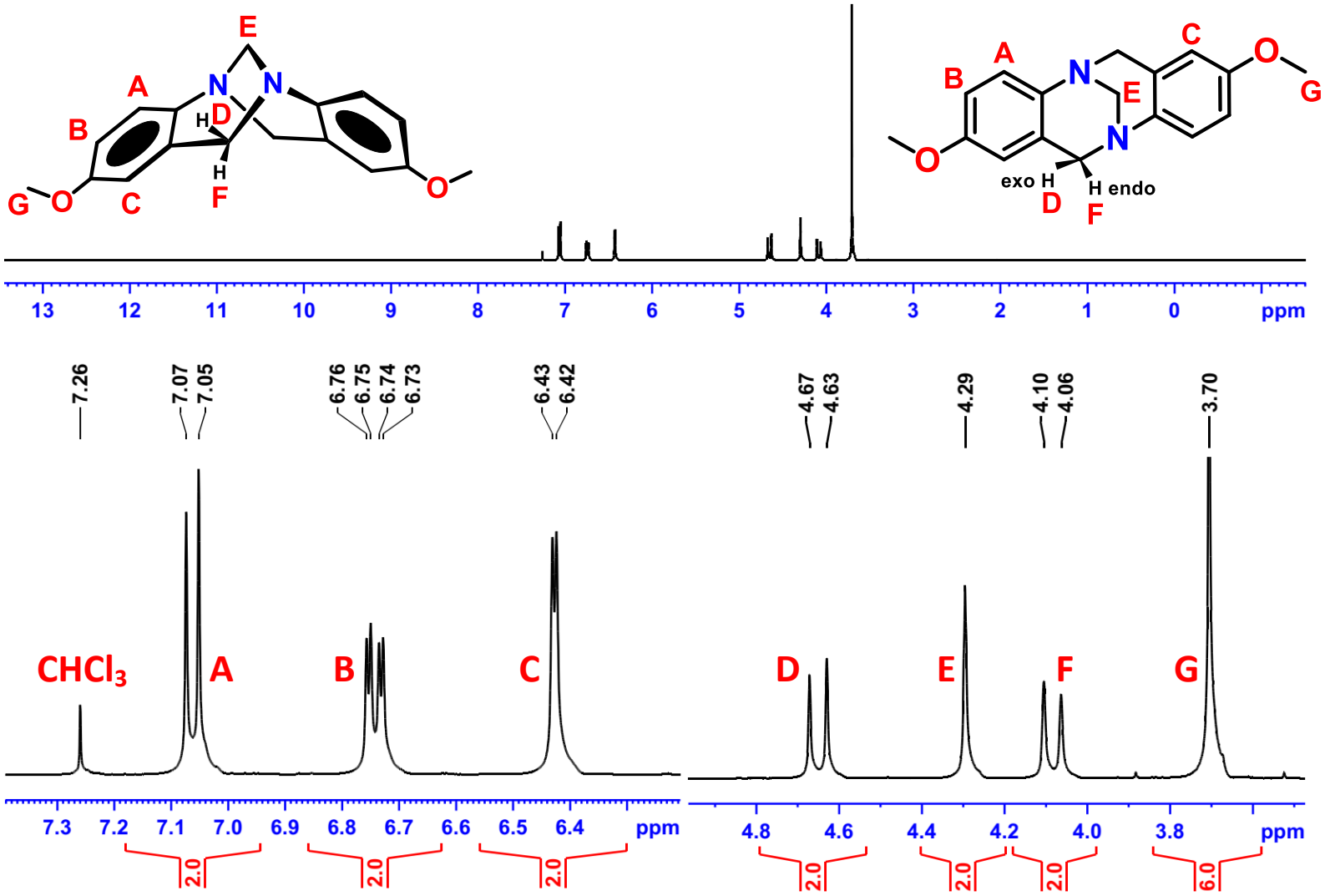

Figure S14. ^{1}H NMR spectrum of racemic Tröger's base analog **1** (500 MHz, $CDCl_3$, 298 K)

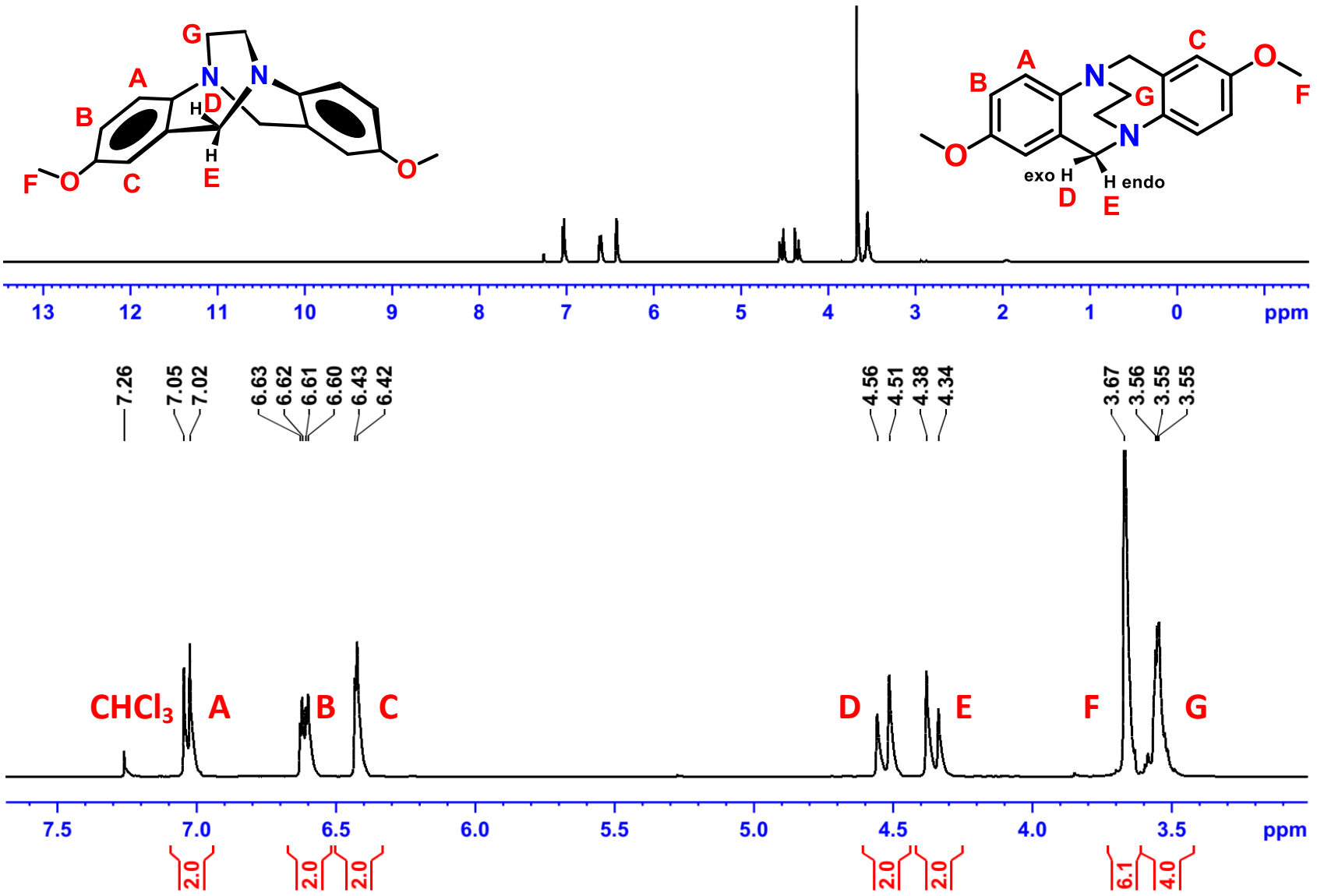

Figure S15. ^{1}H NMR spectrum of racemic Tröger's base analog **2** (500 MHz, $CDCl_3$, 298 K)

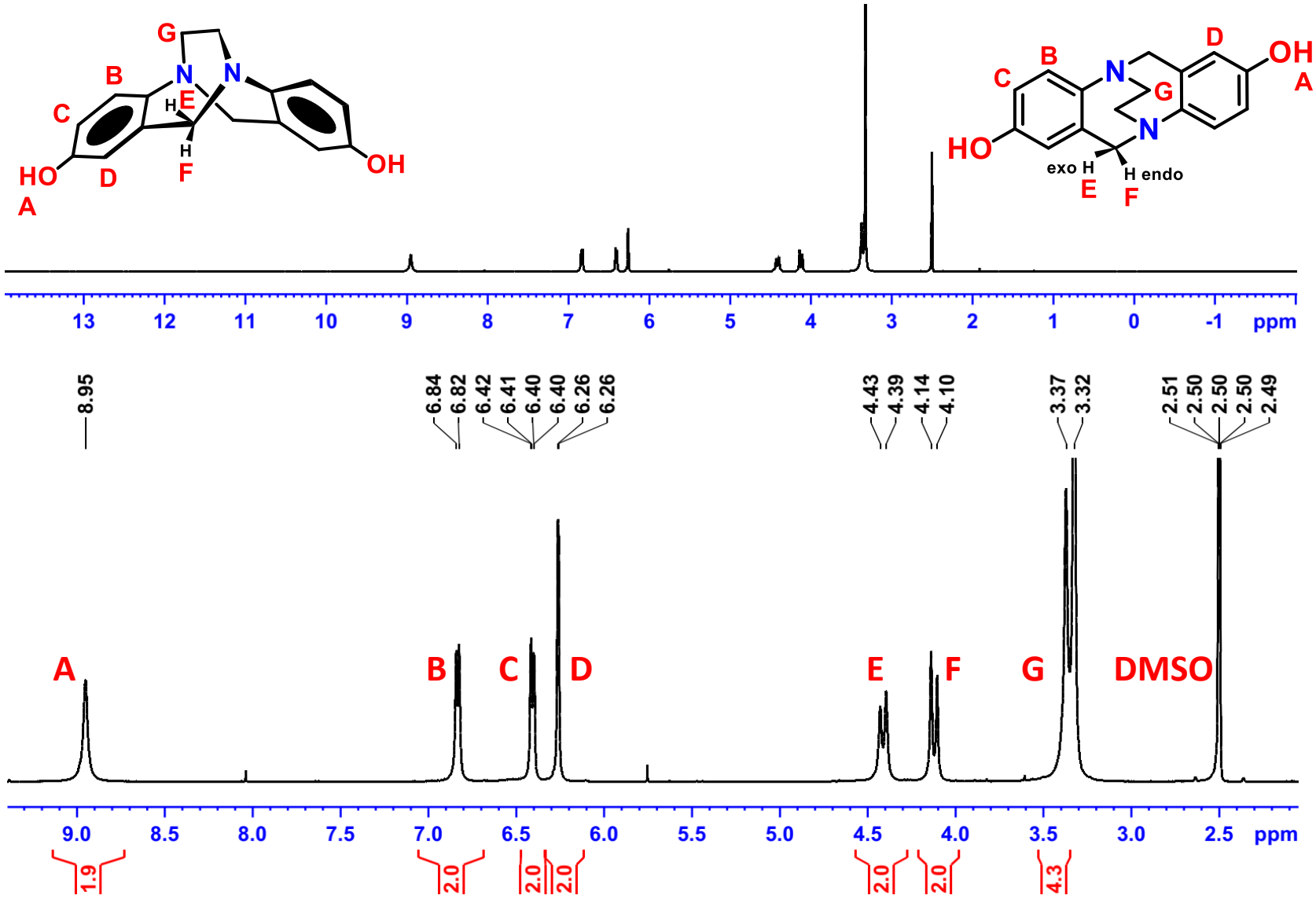

Figure S16. ^{1}H NMR spectrum of Tröger's base analog **3** (500 MHz, CD_3SOCD_3, 298 K)

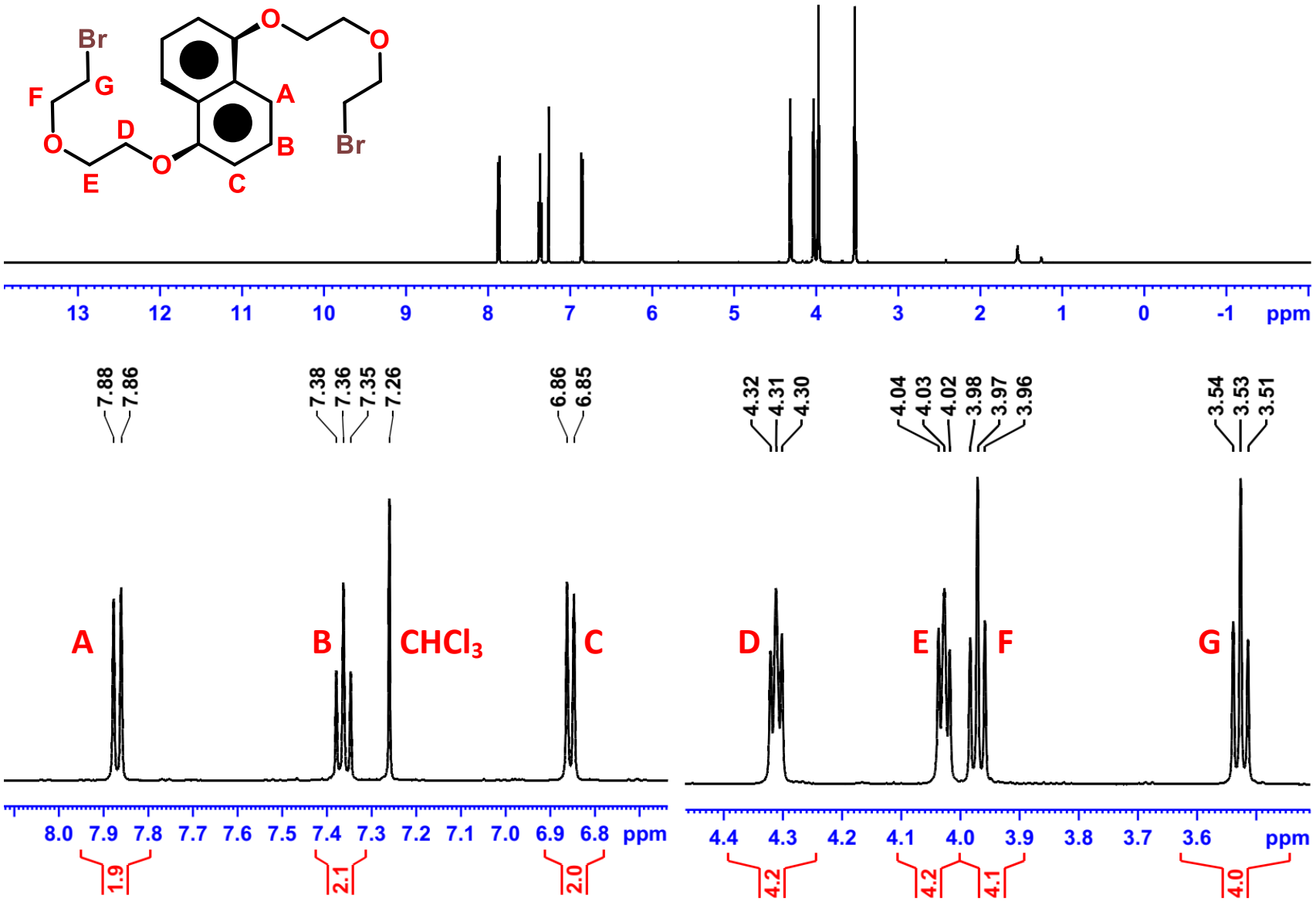

Figure S17. ^{1}H NMR spectrum of linker compound **4** (600 MHz, $CDCl_3$, 298 K)

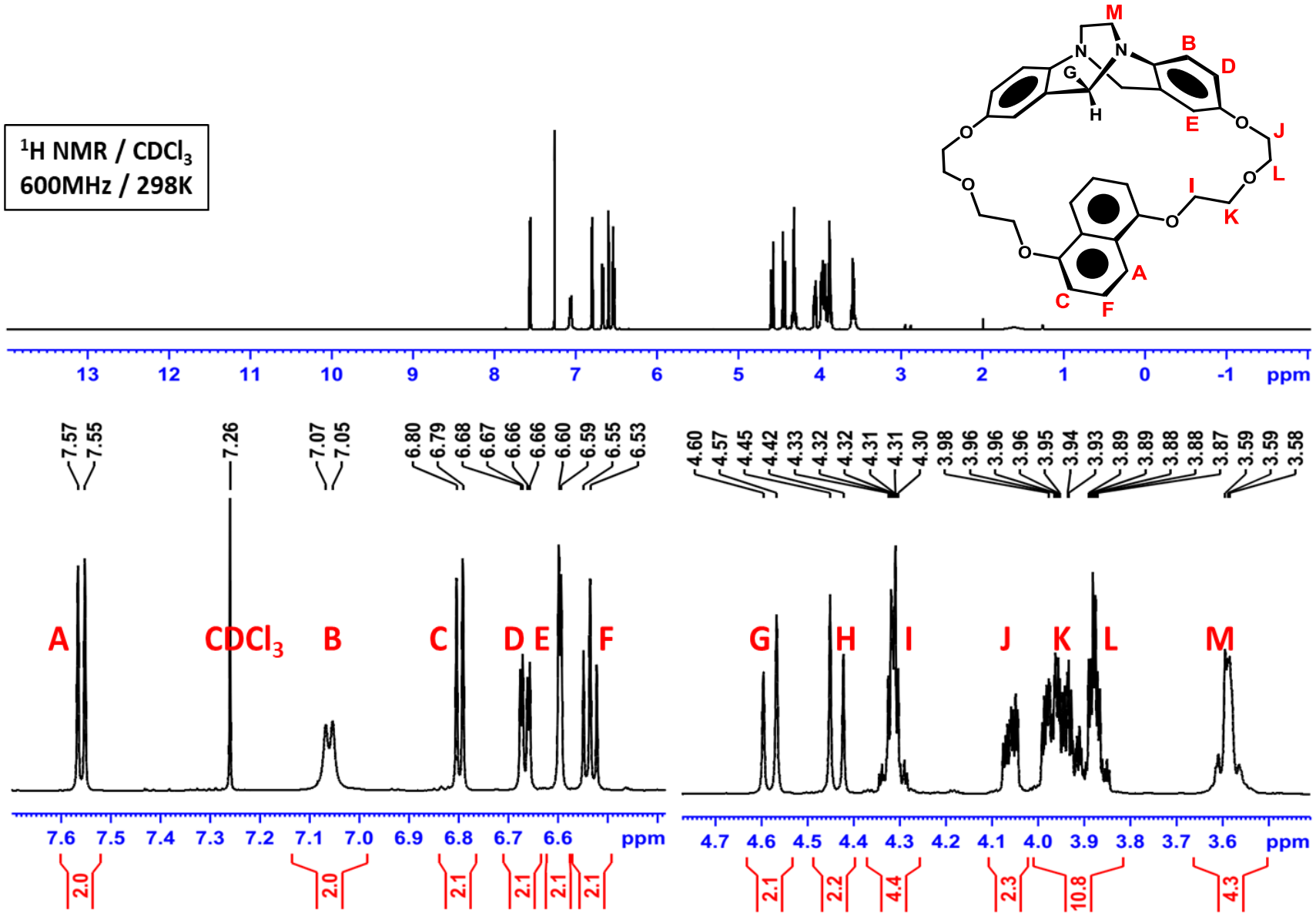

Figure S18. ^{1}H NMR spectrum of macrocycle **5** (600 MHz, $CDCl_3$, 298 K)

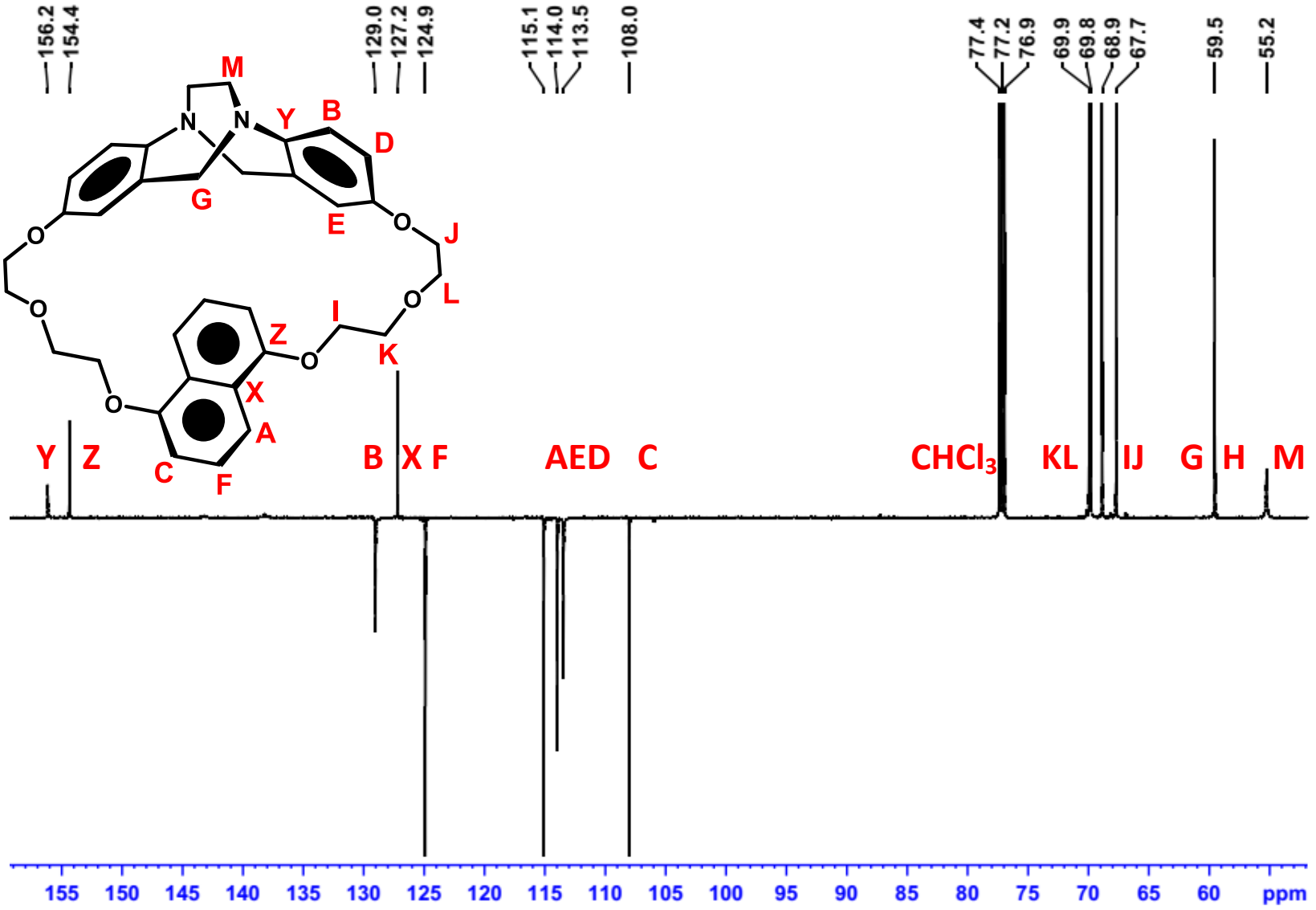

Figure S19. DEPT135 NMR spectrum of macrocycle **5** (150 MHz, $CDCl_3$, 298 K)

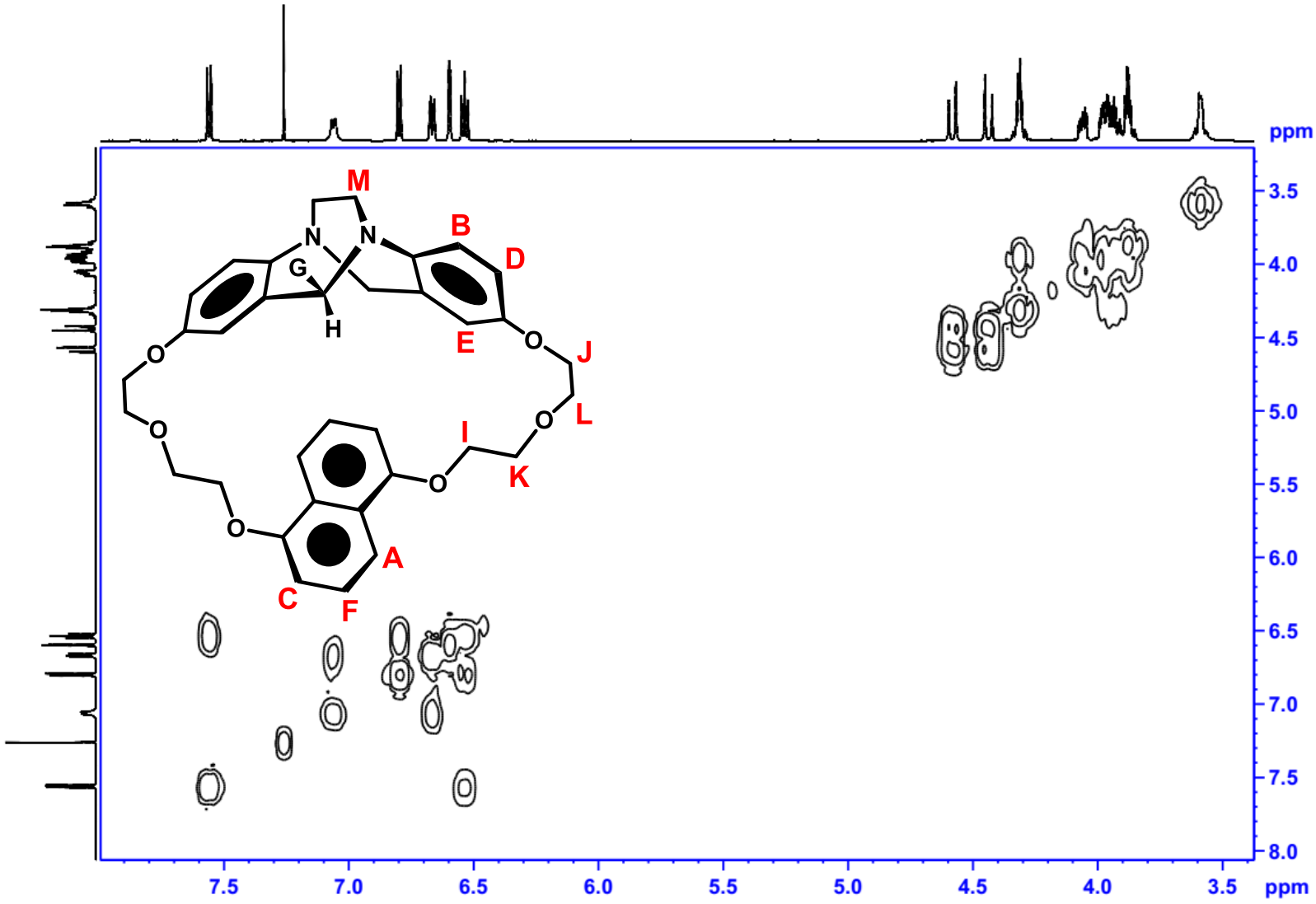

Figure S20. COSY NMR spectrum of macrocycle **5** (600 MHz, $CDCl_3$, 298 K)

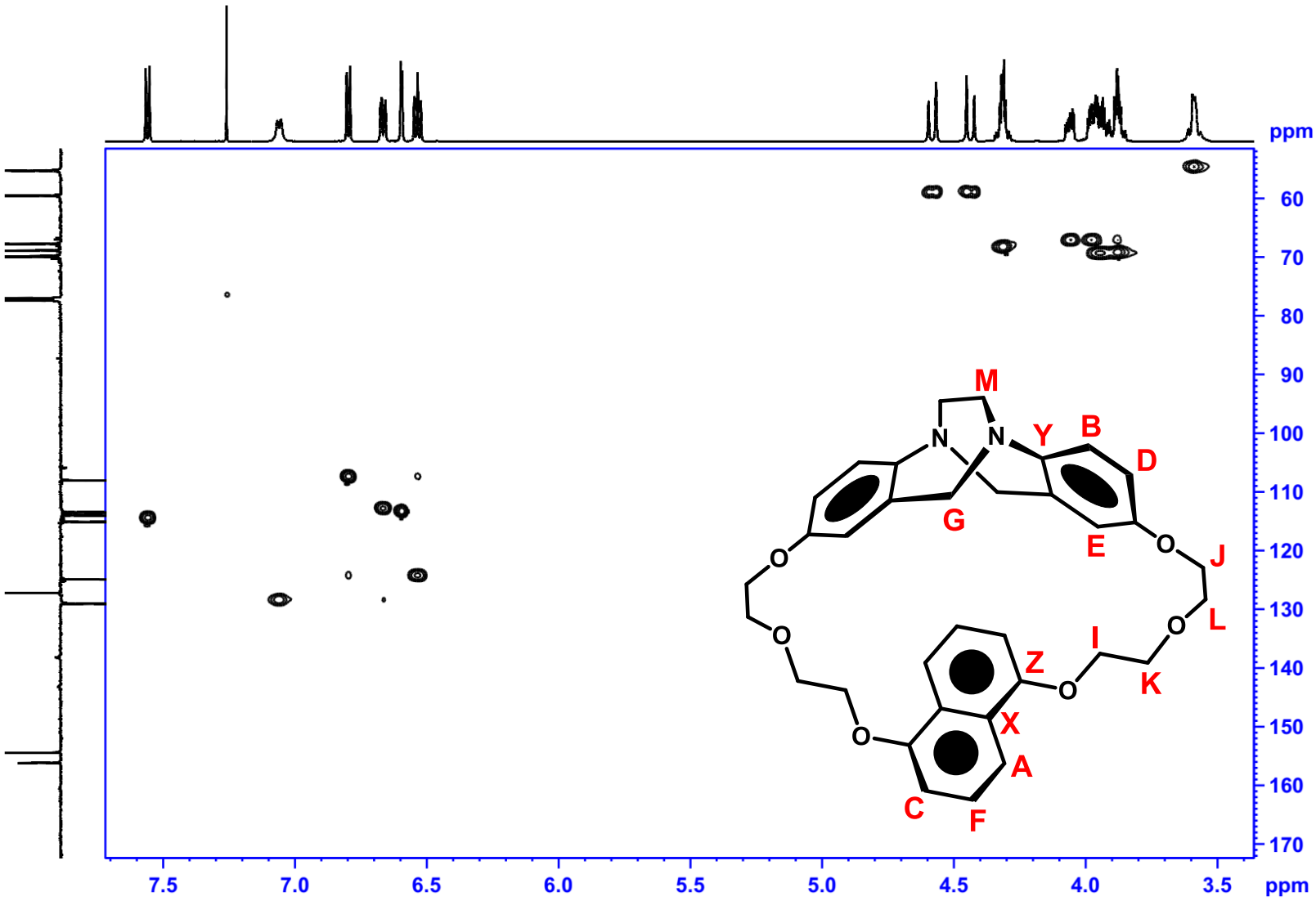

Figure S21. HSQC NMR spectrum of macrocycle **5** (600 MHz, $CDCl_3$, 298 K)

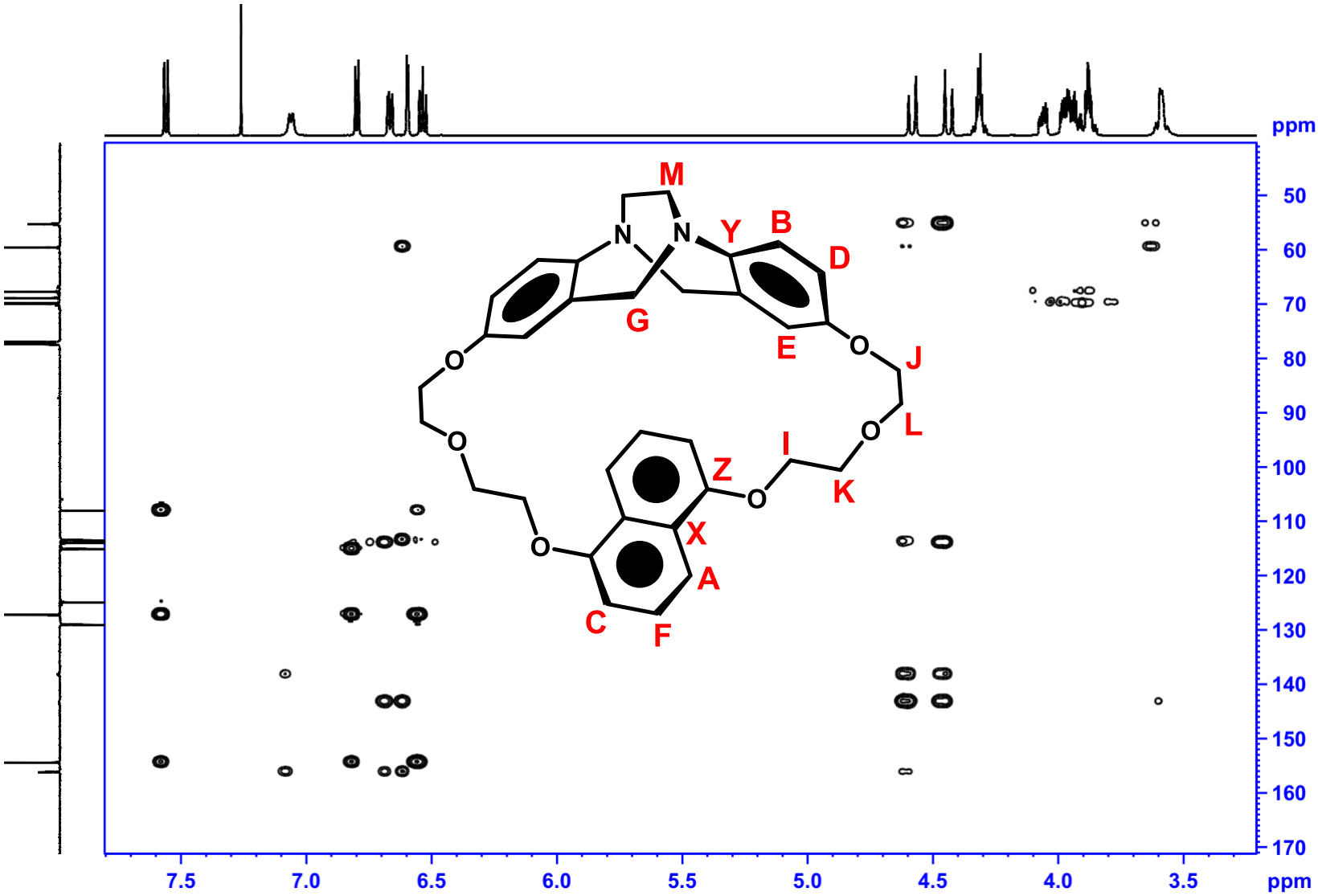

Figure S22. HMBC NMR spectrum of macrocycle **5** (600 MHz, $CDCl_3$, 298 K)

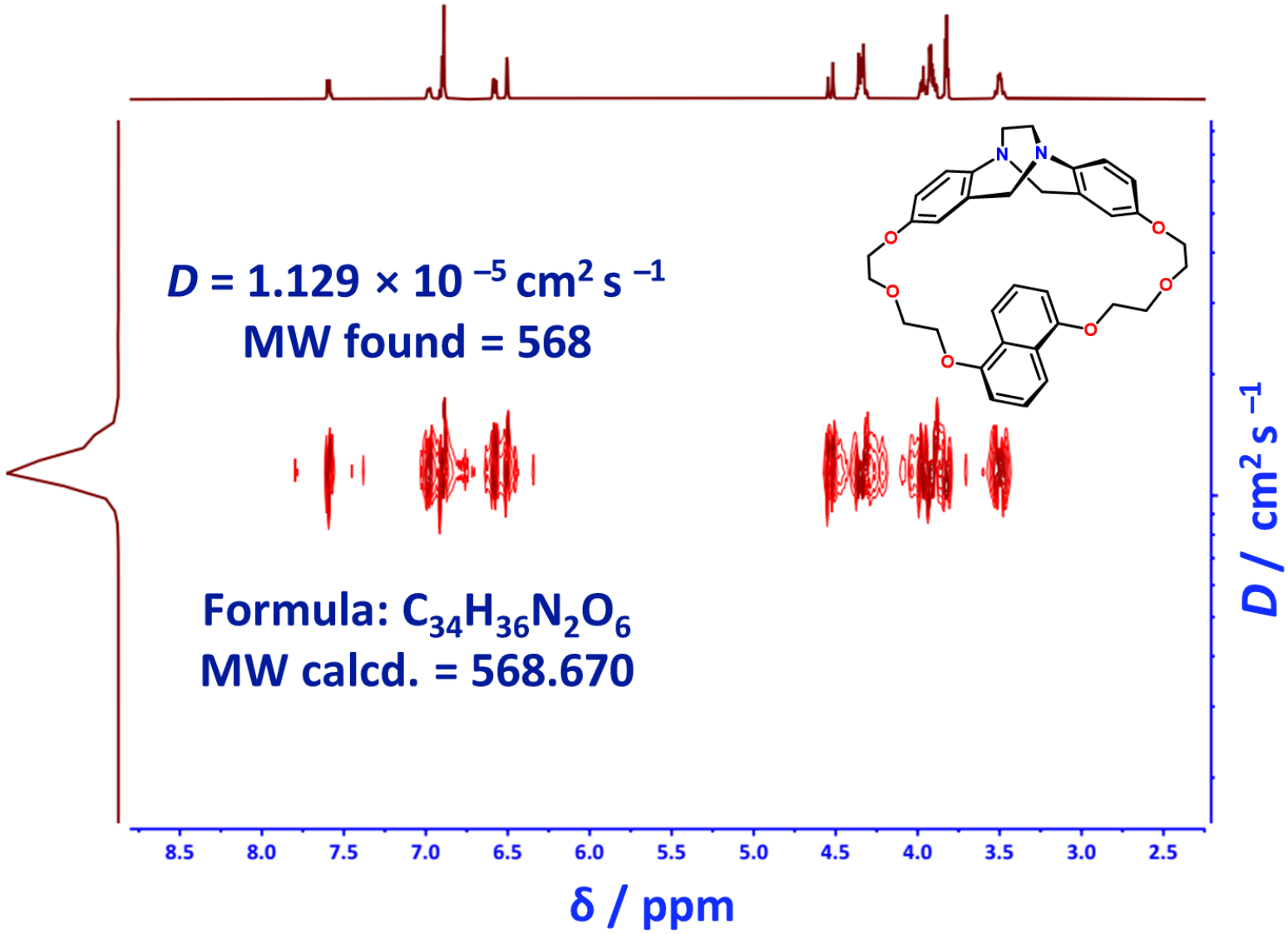

Figure S23. DOSY NMR spectrum of macrocycle **5** (600 MHz, $CDCl_3$ – CD_3CN 1:9 *v/v*, 298 K)

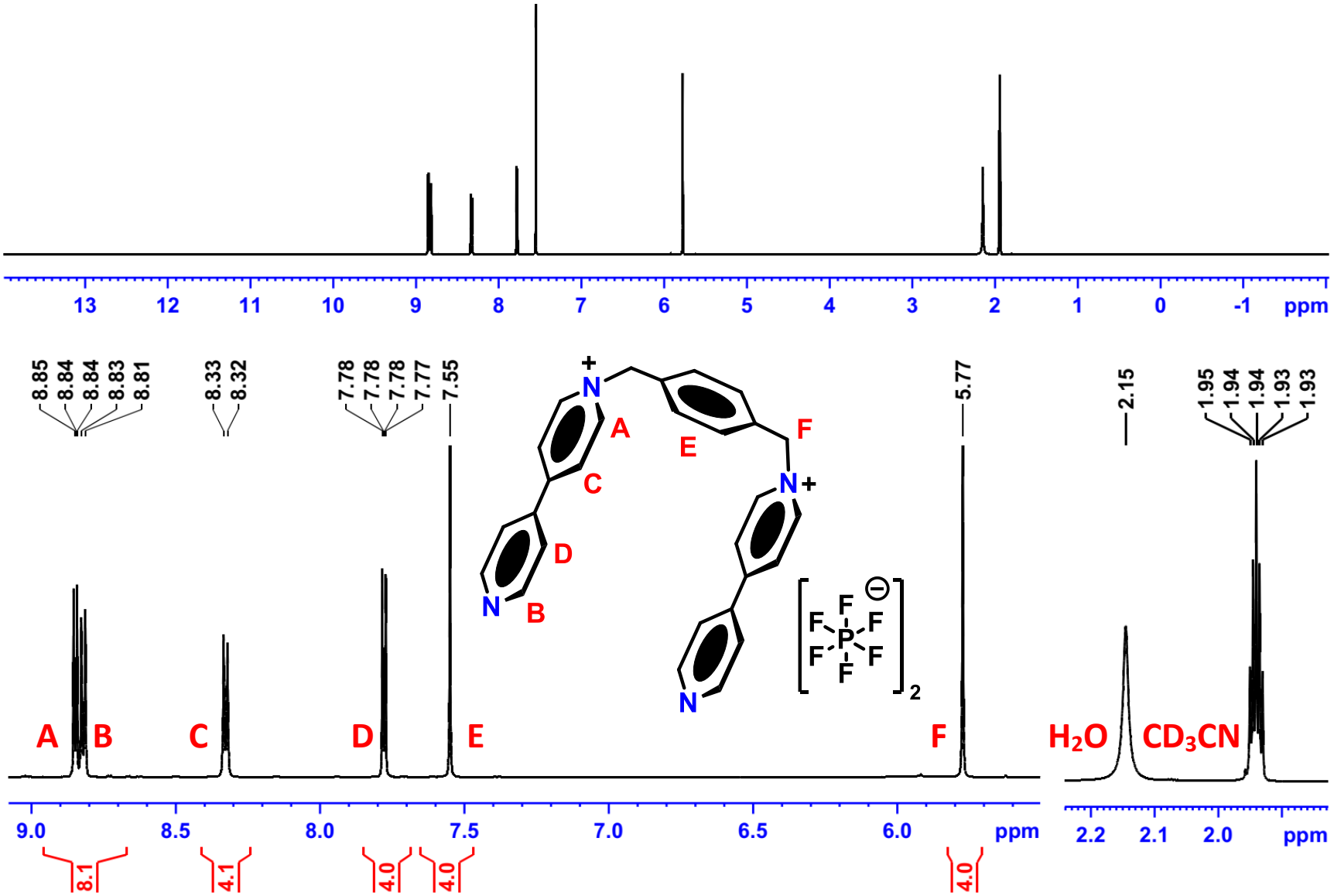

Figure S24. ^{1}H NMR spectra of compound **6** (600 MHz, CD_3CN, 298 K)

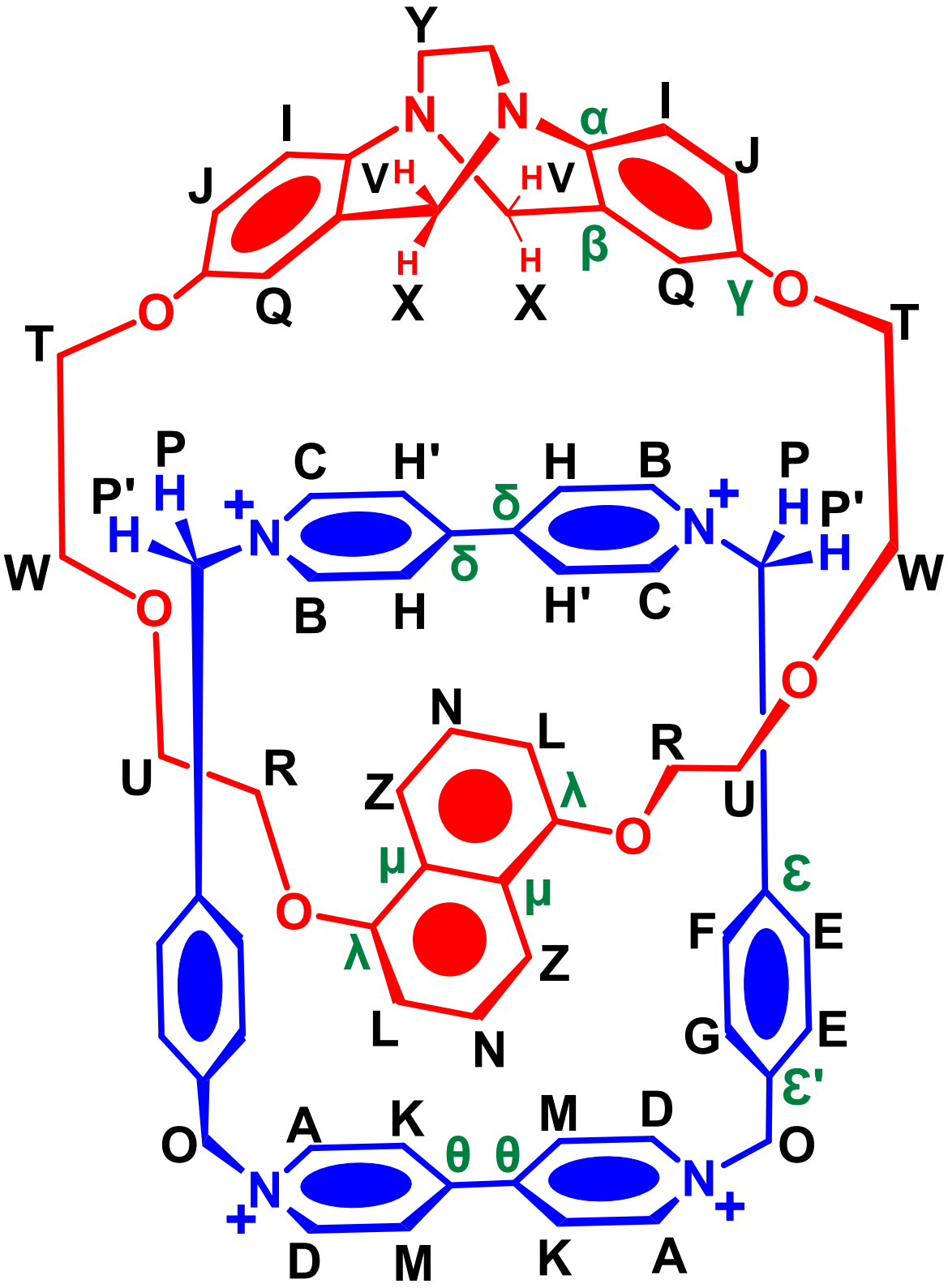

Figure S25. Structure of catenane **7** with atoms labeled for the NMR assignments

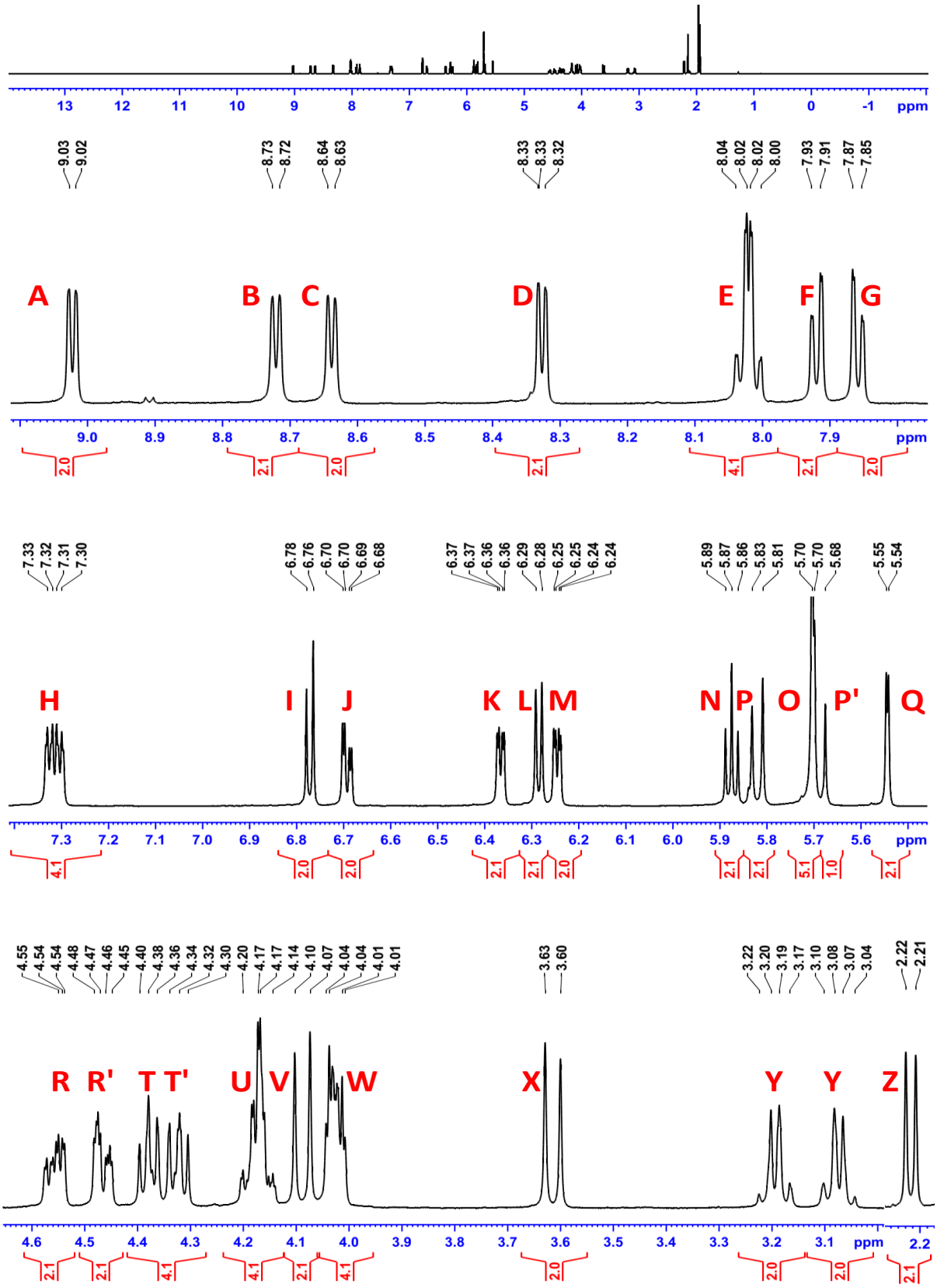

Figure S26. ^{1}H NMR spectrum of catenane **7·4PF$_6$** (600 MHz, CD_3CN, 298 K)

Table S1. Summary of data obtained from NMR analysis of catenane **7·4PF$_6$**

Peak	^{1}H δ / ppm	*J* / Hz	Splitting	Protons	^{13}C δ / ppm	DEPT135
A	9.02	6.5	d	2	145.0	CH / –
B	8.72	6.5	d	2	144.1	CH / –
C	8.64	6.5	d	2	146.1	CH / –
D	8.33	6.5	d	2	144.2	CH / –
E	8.02	8.2, 1.3	dd	4	131.7	CH / –
F	7.92	8.2, 1.3	dd	2	132.0	CH / –
G	7.86	8.2, 1.3	dd	2	132.5	CH / –
H	7.31	6.5, 2.1	m	4	125.8	CH / –
I	6.77	8.7	d	2	130.4	CH / –
J	6.69	8.7, 2.8	dd	2	110.5	CH / –
K	6.37	6.5, 2.3	dd	2	128.1	CH / –
L	6.28	7.9	d	2	105.9	CH / –
M	6.24	6.5, 2.3	dd	2	124.3	CH / –
N	5.87	8.1	t	2	128.5	CH / –
P	5.82	13.5	d	2	65.7	CH_2 / +
O	5.70	NA	s	4	66.2	CH_2 / +
P'	5.68	13.5	d	2	65.7	CH_2 / +
Q	5.54	2.7	d	2	116.0	CH / –
R	4.53–4.57	NA	m	2	68.7	CH_2 / +
R'	4.44–4.48	NA	m	2	68.7	CH_2 / +
T	4.30–4.39	NA	m	4	71.8	CH_2 / +
U	4.14–4.20	NA	m	4	70.6	CH_2 / +
V	4.08	17.3	d	2	67.4	CH_2 / +
W	4.00–4.04	NA	m	4	71.7	CH_2 / +
X	3.62	17.4	d	2	58.8	CH_2 / +
Y	3.04–3.22	NA	m	4	55.5	CH_2 / +
Z	2.21	8.2	d	2	109.4	CH / –
H_2O	2.14	NA	s	4.6	NA	CH_2 / +
CD_3CN	1.94	2.5	p	5.7	118.2, 1.3	CH_2 / +

Table S2. Summary of data obtained from NMR analysis of catenane **7·4PF$_6$**

Peak	COSY	HSQC	ROESY	NOE	DEPT90
A	K	145.0	O L	K O D E	CH / –
B	H	144.1	P H	C P H E F	CH / –
C	H	146.1	P H	B H P F	CH / –
D	M	144.2	L O A	A O M G	CH / –
E	E	131.7	P O	F G O P A B C Z U R	CH / –
F	G	132.0	P	E G P N C B	CH / –
G	F	132.5	O	F E O N Z D	CH / –
H	C	125.8	H B	C B L Z	CH / –
I	J	130.4	J H X	J Q X	CH / –
J	I	110.5	T W	I T Q W	CH / –
K	A	128.1	L R U	M A	CH / –
L	N	105.9	R U K	A D N R U Z	CH / –
M	D	124.3	L K	K D	CH / –
N	Z	128.5	E	L Z F G	CH / –
P	P	65.7	B C E F	P' E L Z N	CH_2 / +
O	O	66.2	D E	D E F G	CH_2 / +
P'	P'	65.7	B C E F	B C E F	CH_2 / +
Q	J	116.0	X V	X V	CH / –
R	U	68.7	U L	L U B	CH_2 / +
R'	U	68.7	U L	U L E	CH_2 / +
T	W	71.8	W J	W J	CH_2 / +
U	R'	70.6	W P L	L E	CH_2 / +
V	X	67.4	X Y	X Y Q	CH_2 / +
W	T	71.7	T U	T U	CH_2 / +
X	V	58.8	V Q	V Q I	CH_2 / +
Y	Y	55.5	Y V	Y V	CH_2 / +
Z	N	109.4	N	N ABCDFG	CH / –
H_2O	H_2O	NA	H_2O	H_2O	CH_2 / +
CD_3CN	CD_3CN	1.3	CD_3CN	CD_3CN	CH_2 / +

Table S3. Summary of data obtained from NMR analysis of catenane **7·4PF$_6$**

Peak	HMBC	^{13}C δ / ppm	DEPT135
α	X V Q J Y	144.8	C / +
β	I V X	141.4	C / +
γ	I Q	155.6	C / +
δ	B C H	146.1	C /–
ε, ε'	F G P O	137.5, 137.6	C / +
θ	D K M	145.3	C / +
λ	N Z L	125.2	C / +
μ	L N Z	151.8	C / +
σ	H B	126.8	C / +

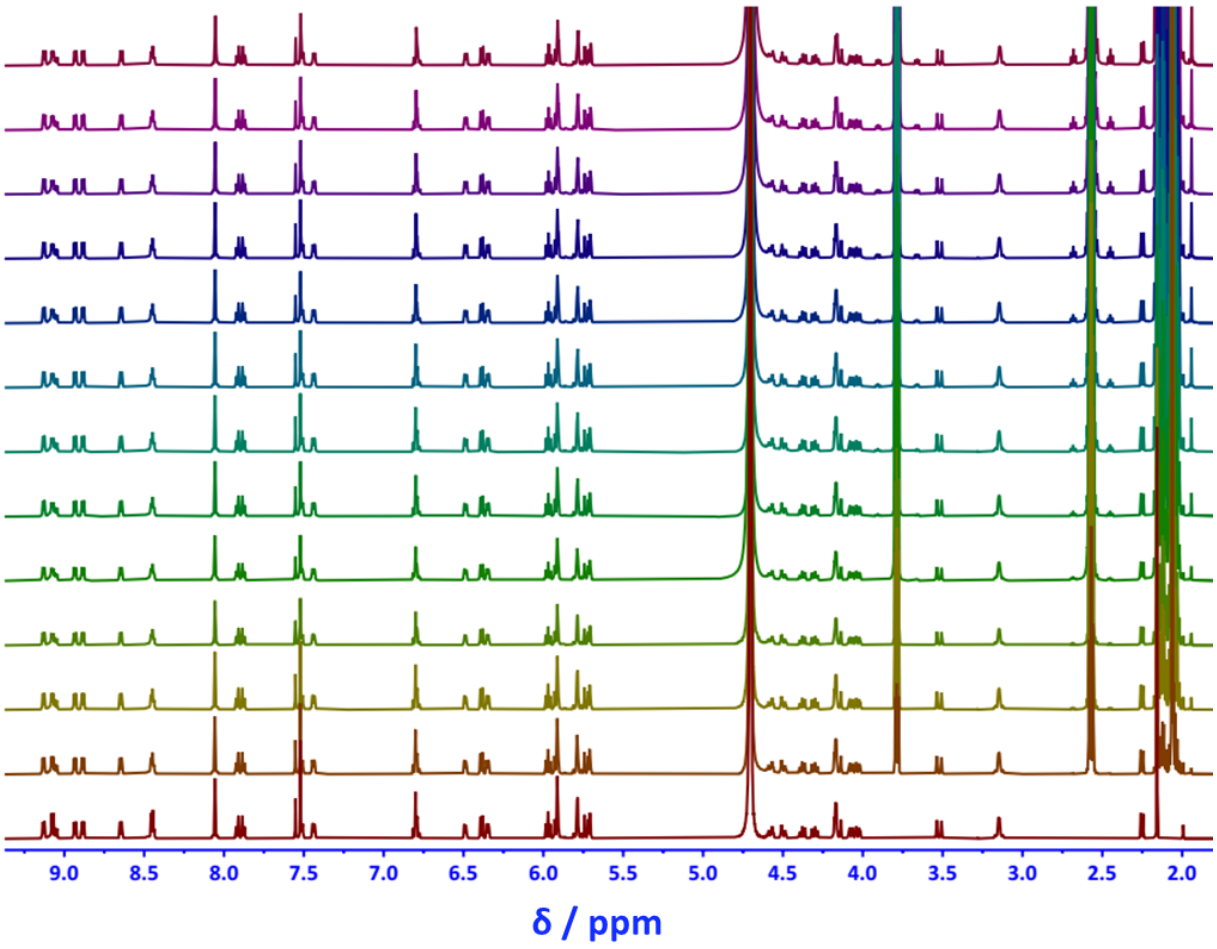

Figure S27. Stacked ^{1}H NMR spectra of racemic catenane **7·4Cl** titrated against (D)-methionine (600 MHz, D_2O, 298 K)

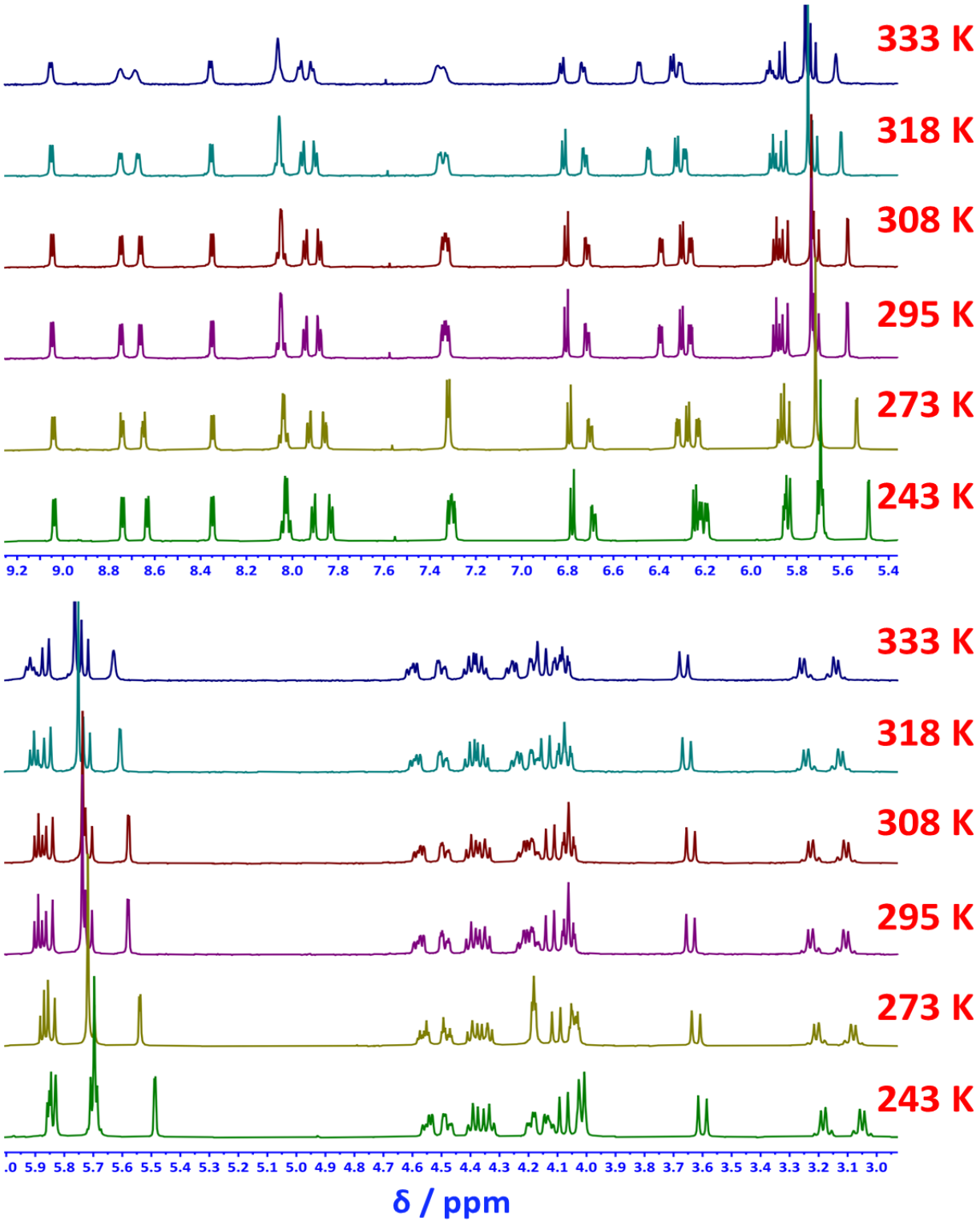

Figure S28. Stacked VT ^{1}H NMR spectra of catenane **7·4PF$_6$** (600 MHz, CD_3CN, 298 K)

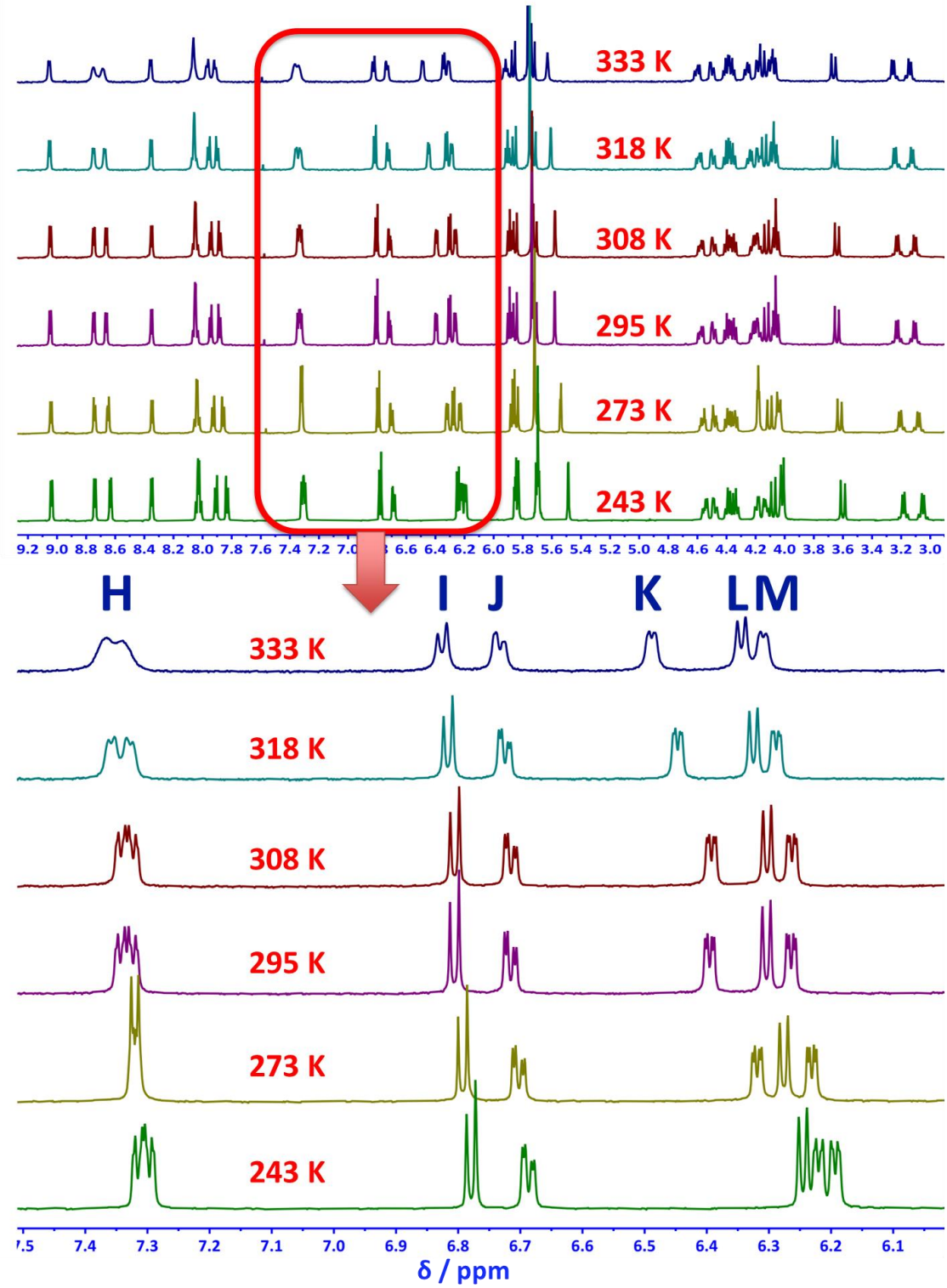

Figure S29. Stacked VT ^{1}H NMR spectra of catenane **7·4PF$_6$**

(600 MHz, CD_3CN, 298 K)

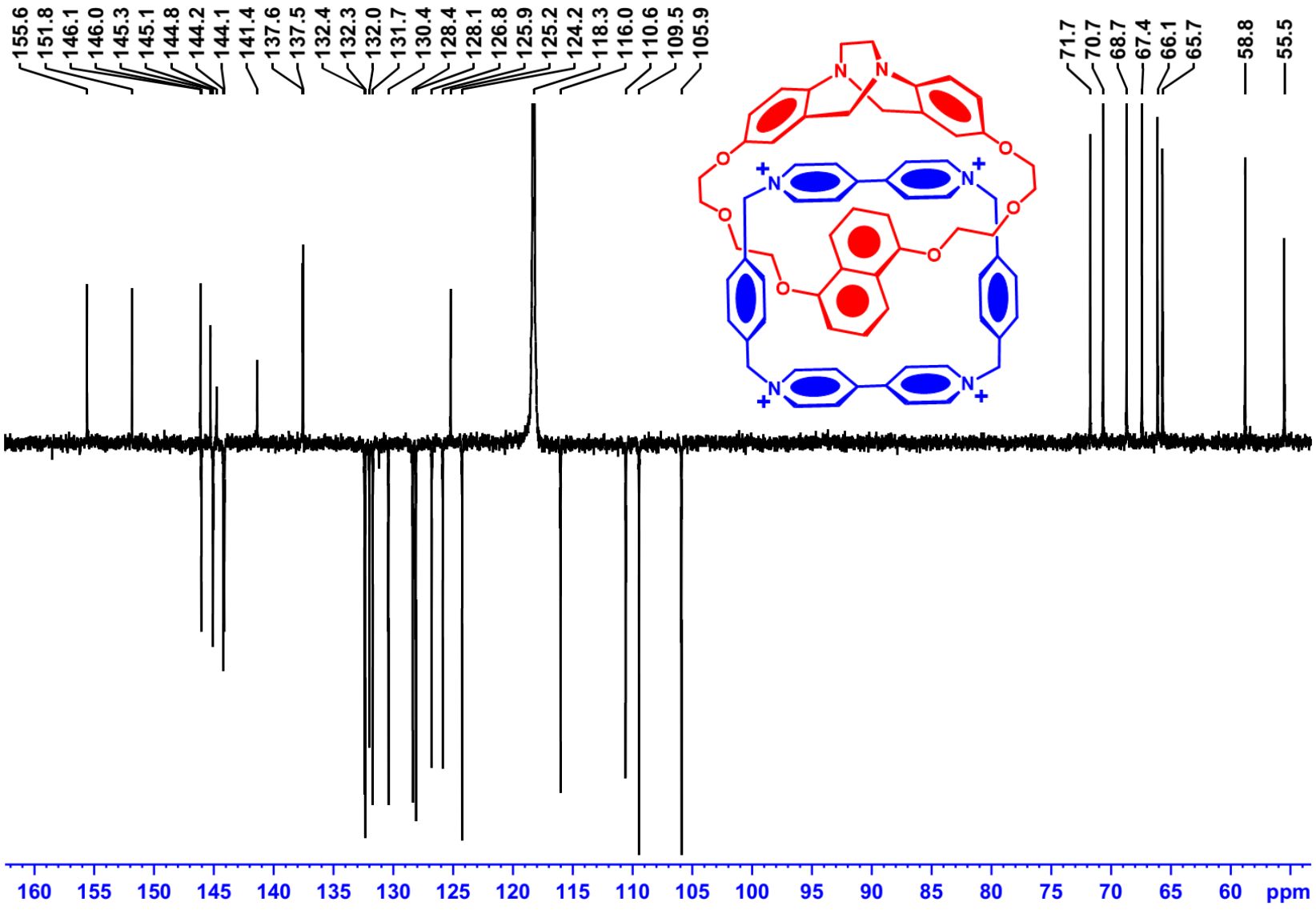

Figure S30. DEPT135 NMR spectrum of catenane **7·4PF$_6$** (150 MHz, CD_3CN, 298 K)

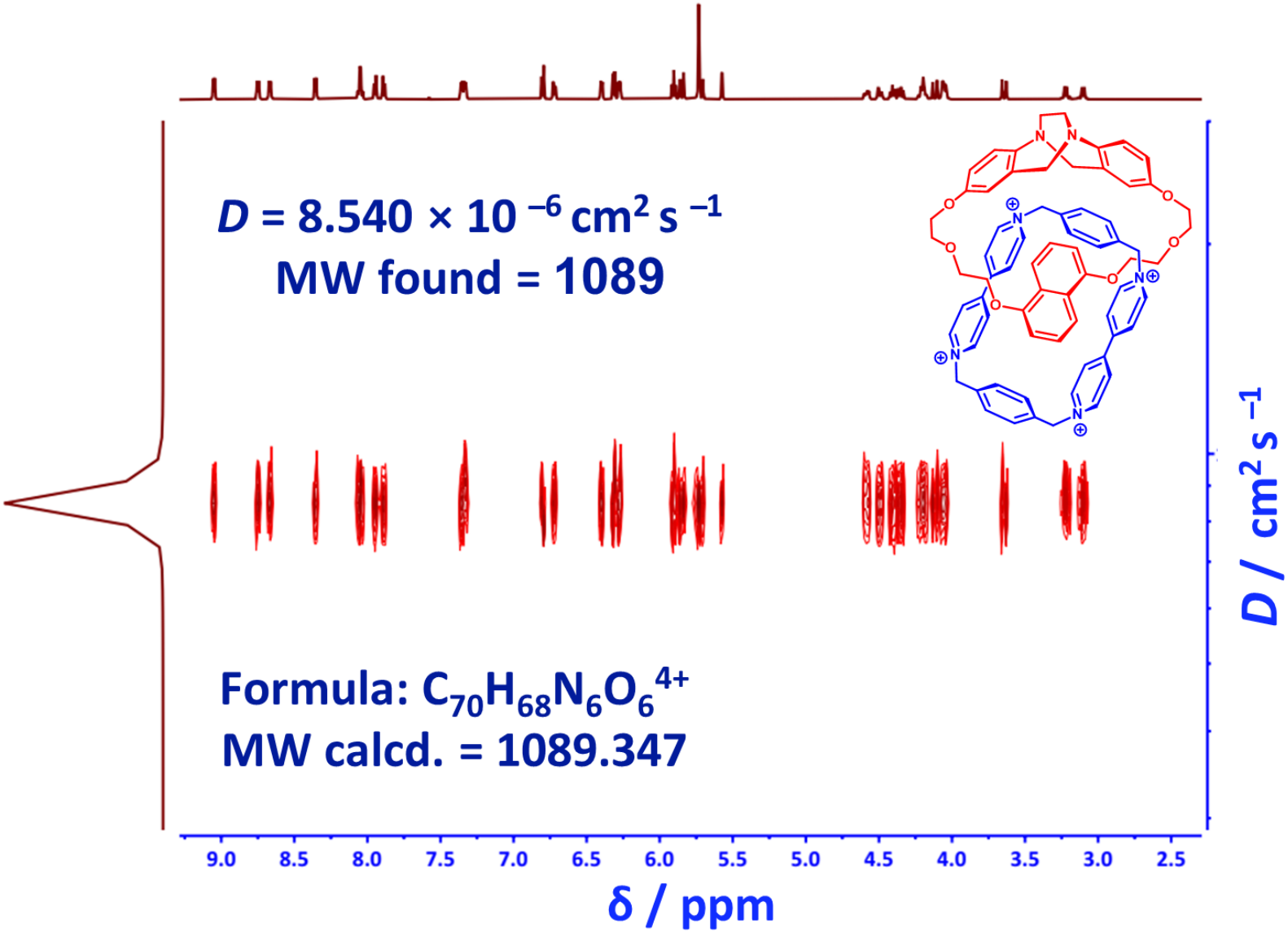

Figure S31. DOSY NMR spectrum of catenane **7·4PF$_6$** (600 MHz, CD_3CN, 298 K)

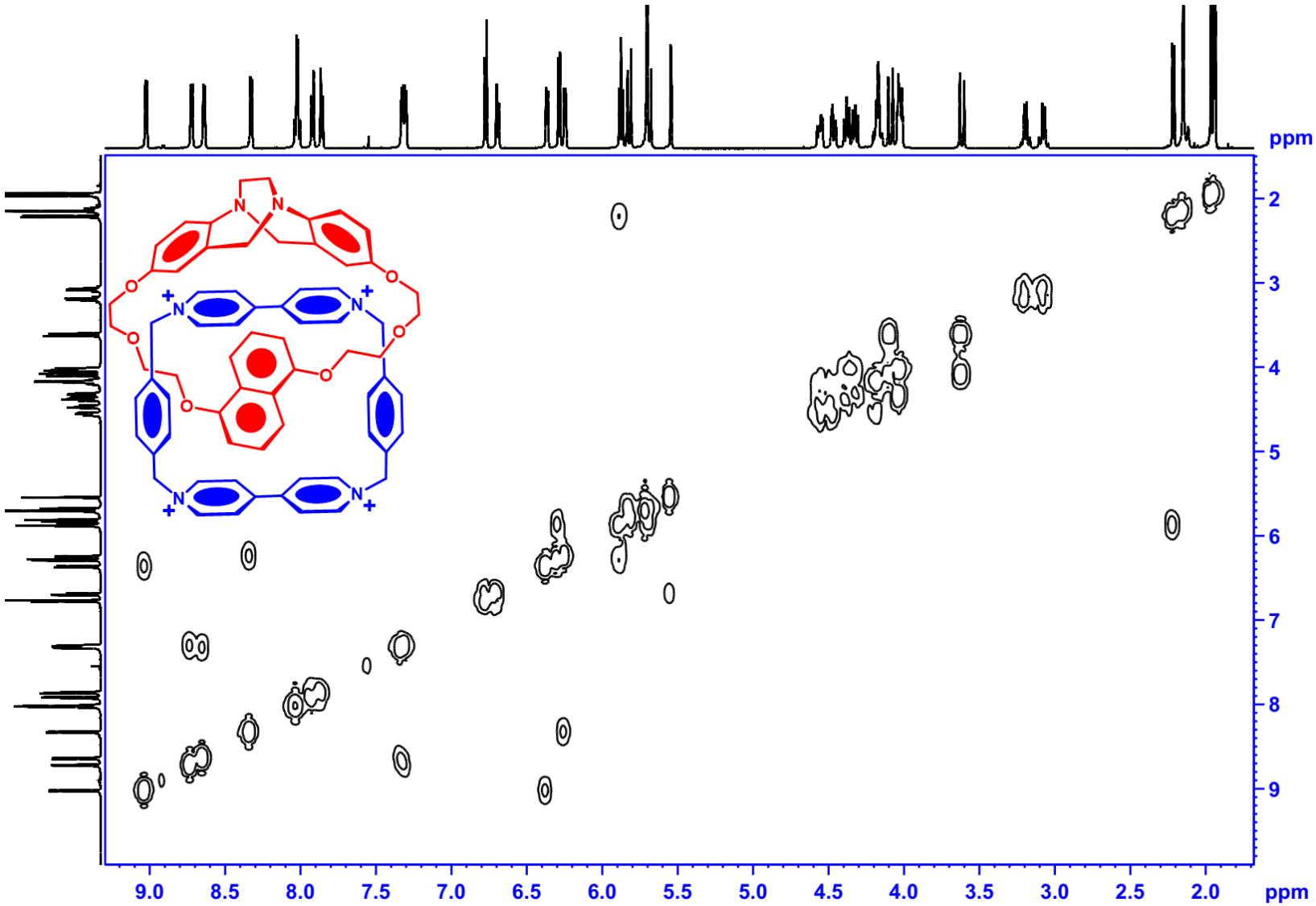

Figure S32. COSY VT-NMR spectrum of catenane **7·4PF$_6$** (600 MHz, CD_3CN, 298 K)

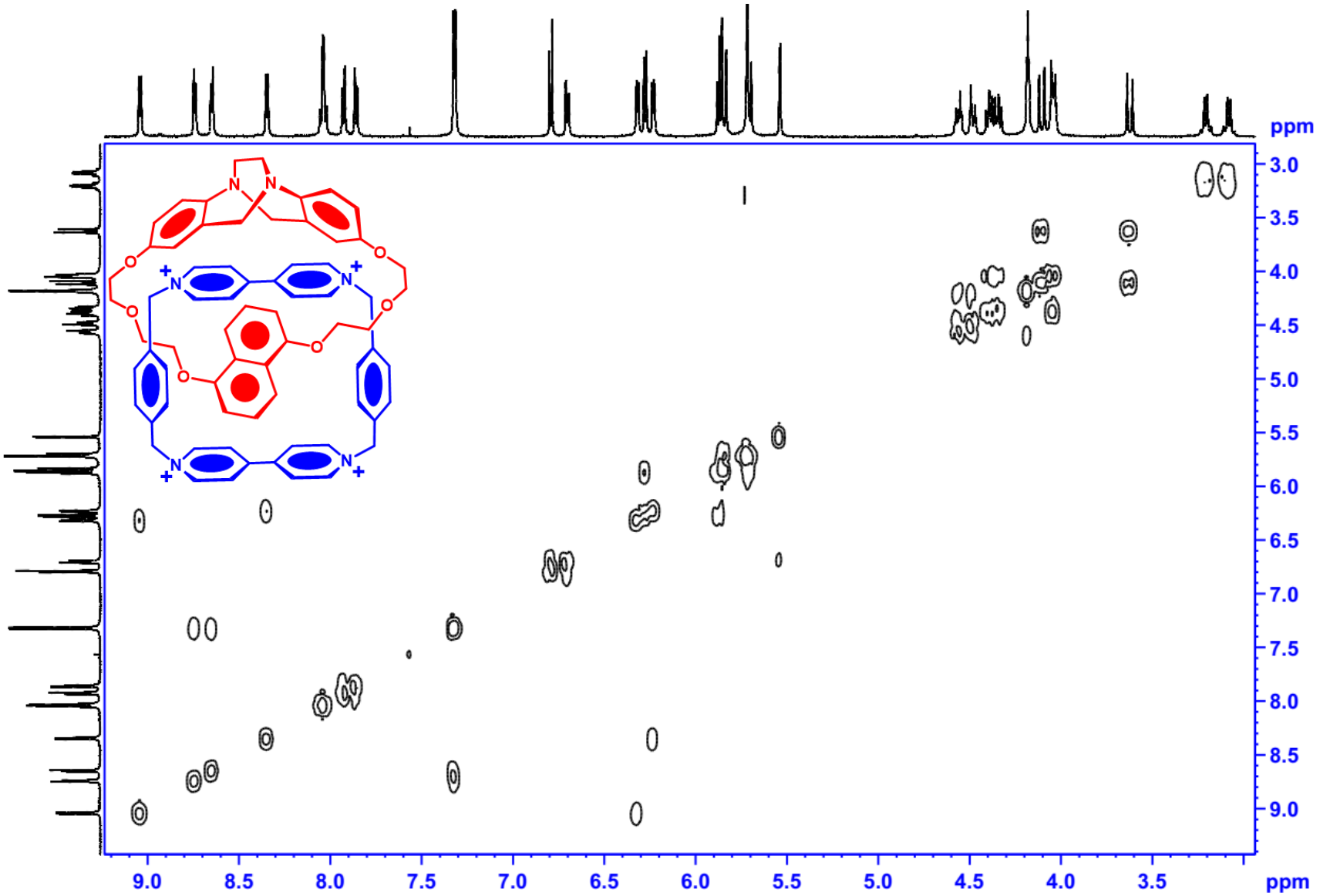

Figure S33. COSY VT-NMR spectrum of catenane **7·4PF$_6$** (600 MHz, CD_3CN, 243 K)

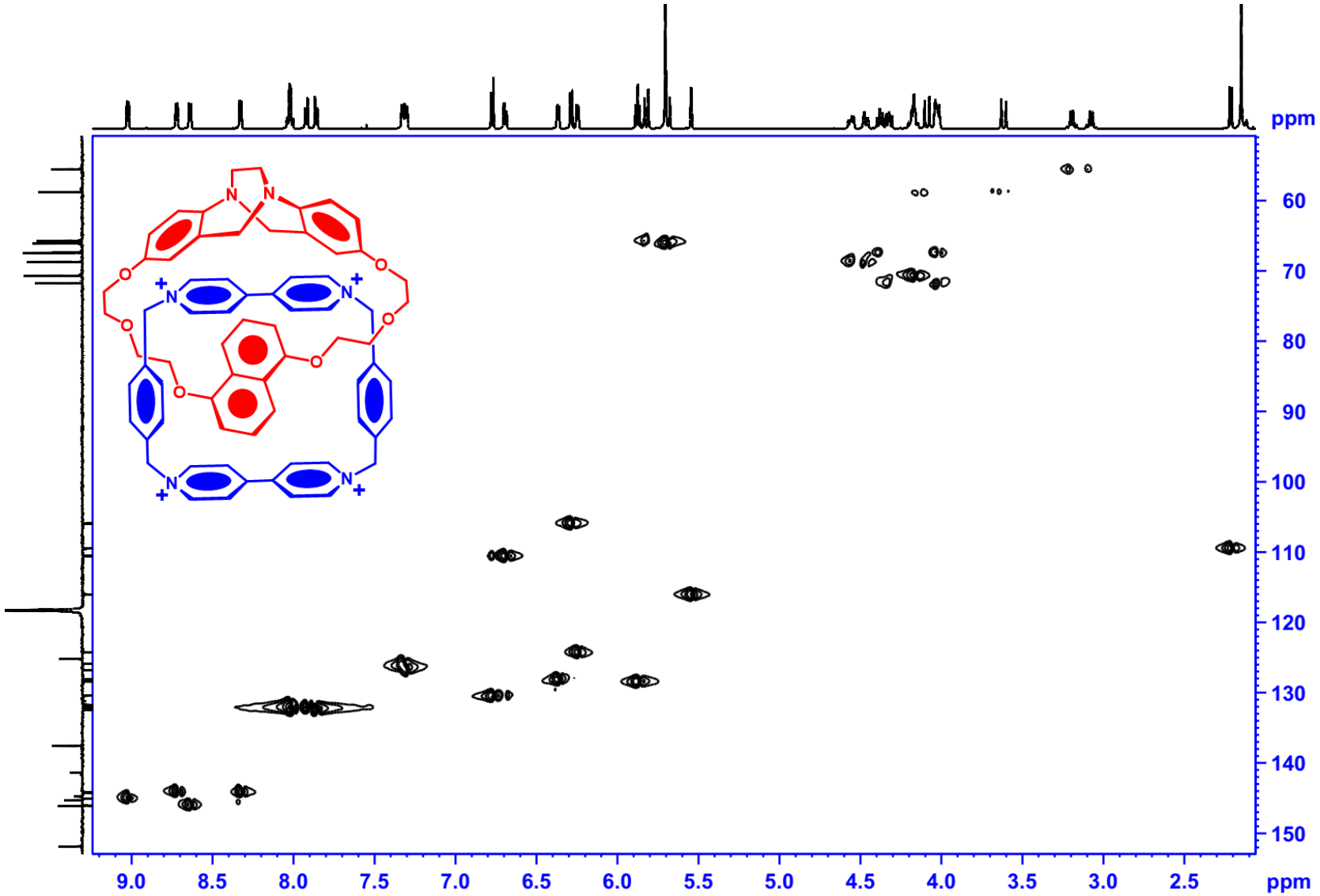

Figure S34. HSQC NMR spectrum of catenane **7·4PF$_6$** (600 MHz, CD_3CN, 298 K)

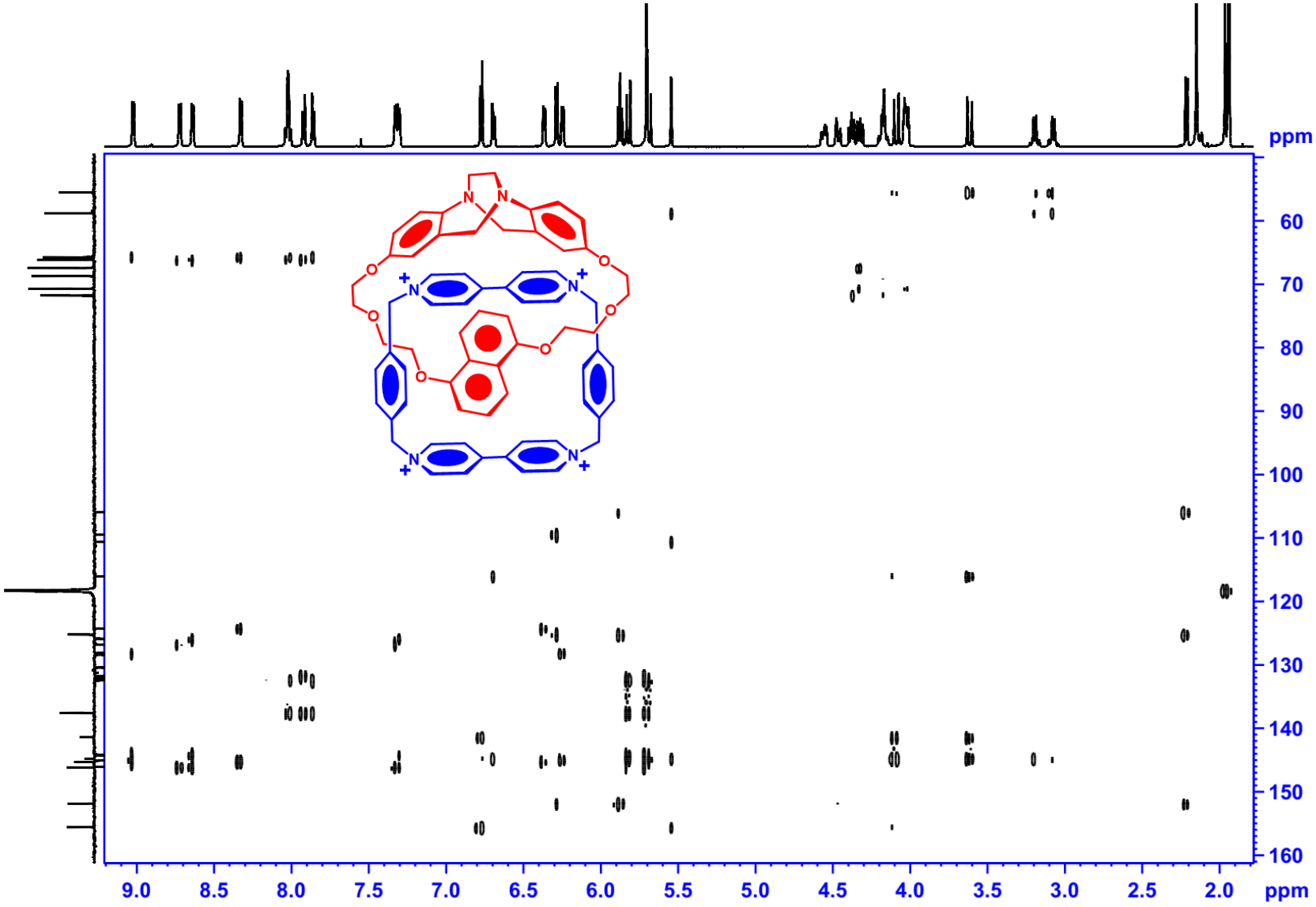

Figure S35. HMBC NMR spectrum of catenane **7·4PF$_6$** (600 MHz, CD_3CN, 298 K)

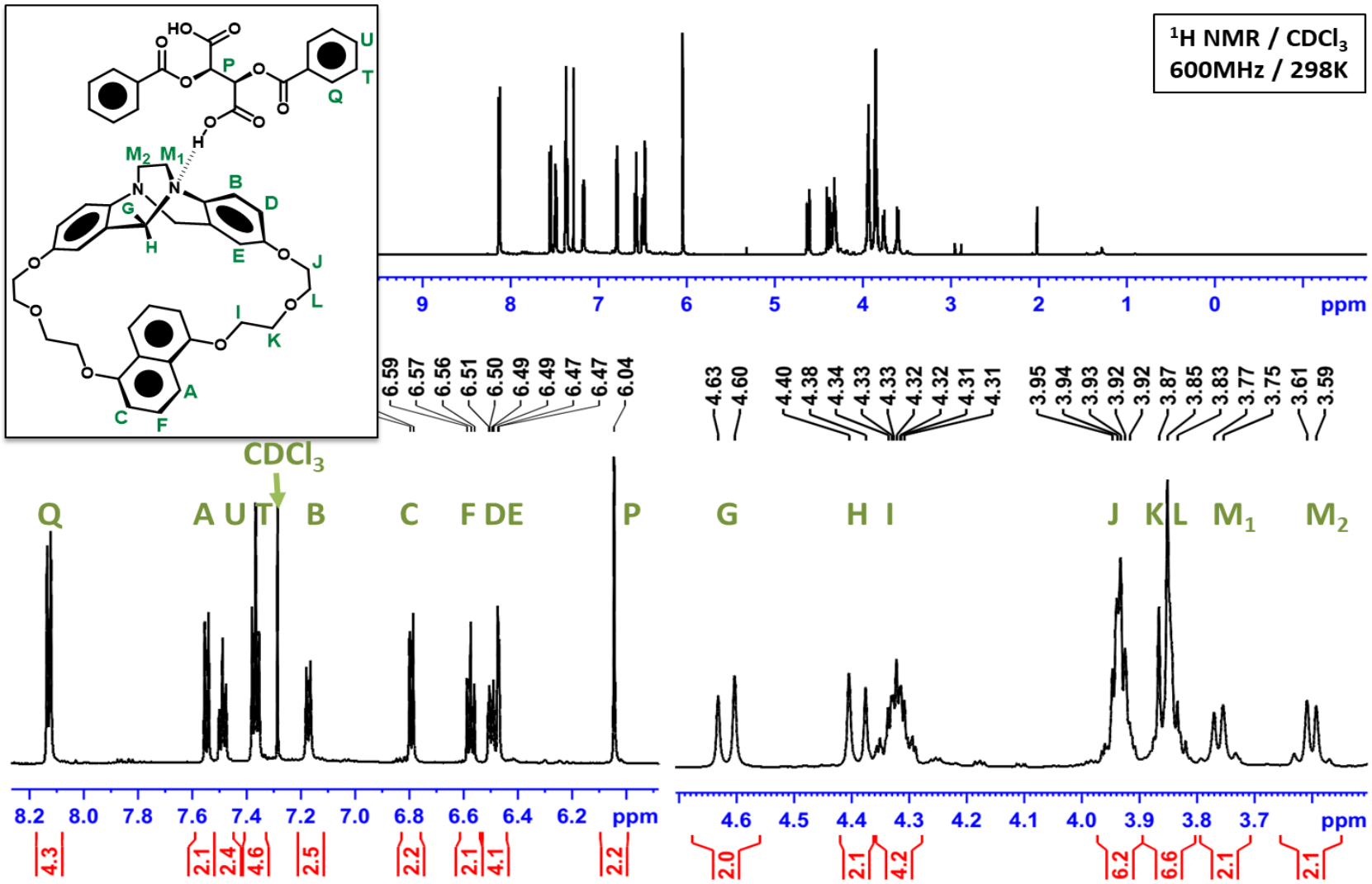

Figure S36. ^{1}H NMR spectrum of macrocycle **(–)-(*S*,*S*)-5** in presence of chiral discriminator (–)-DBTA

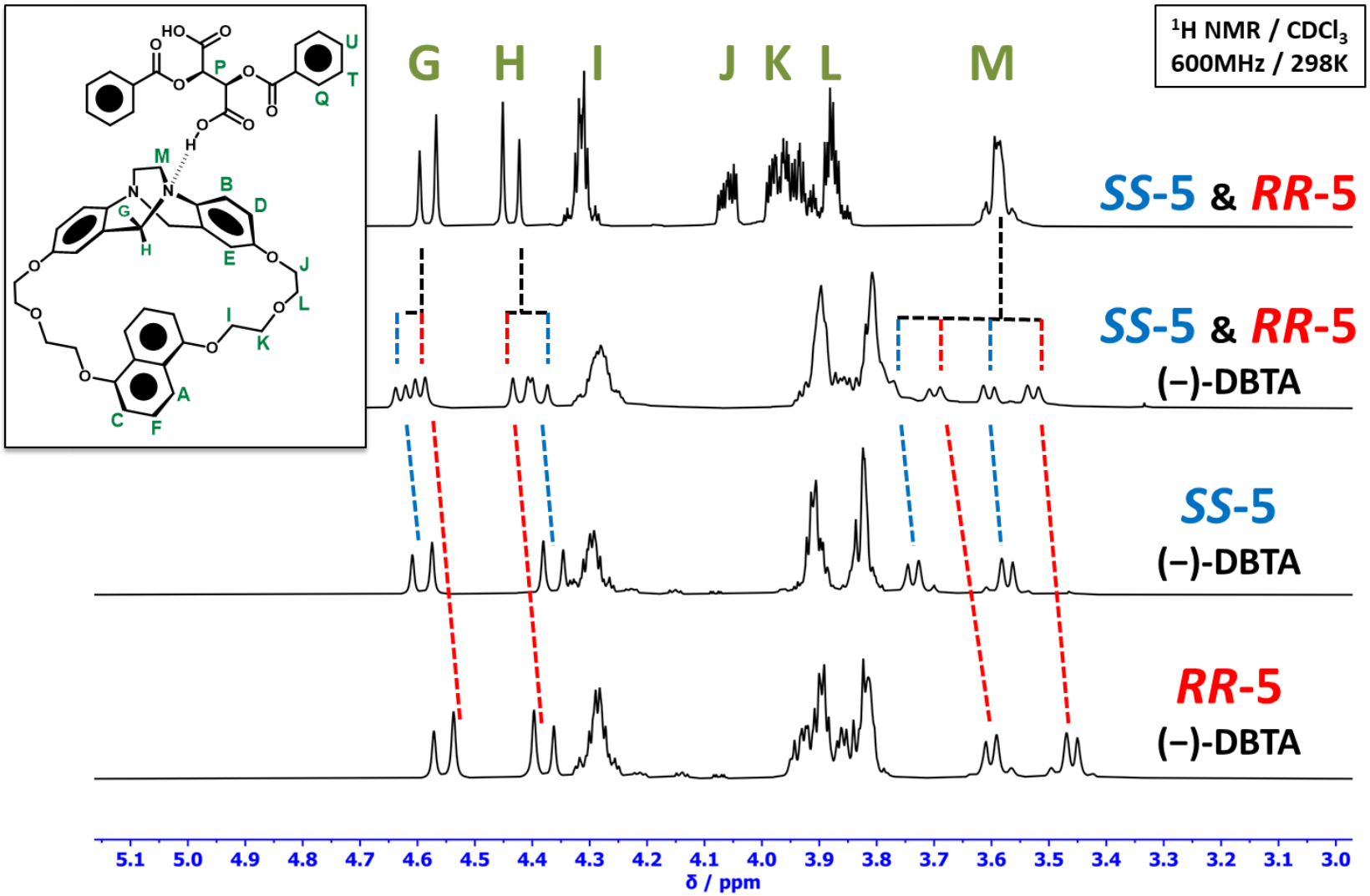

Figure S37. Stacked expanded ^{1}H NMR spectra of racemic and enantiopure forms of chiral macrocycle **5** in the presence of chiral discriminator (–)-DBTA (600 MHz, $CDCl_3$, 298 K)

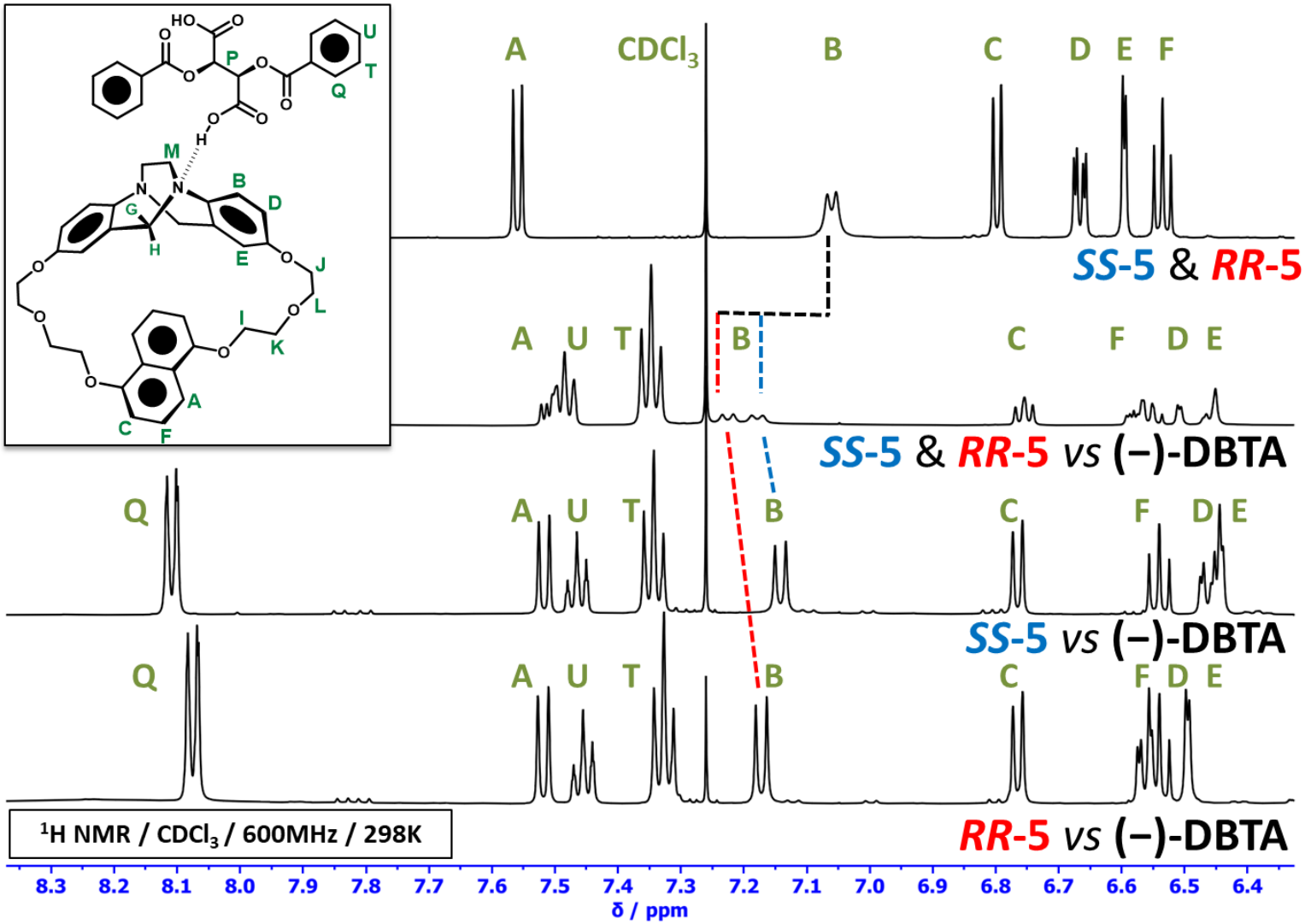

Figure S38. Stacked expanded ^{1}H NMR spectra of racemic and enantiopure forms of chiral macrocycle **5** in the presence of chiral discriminator (–)-DBTA (600 MHz, $CDCl_3$, 298 K)

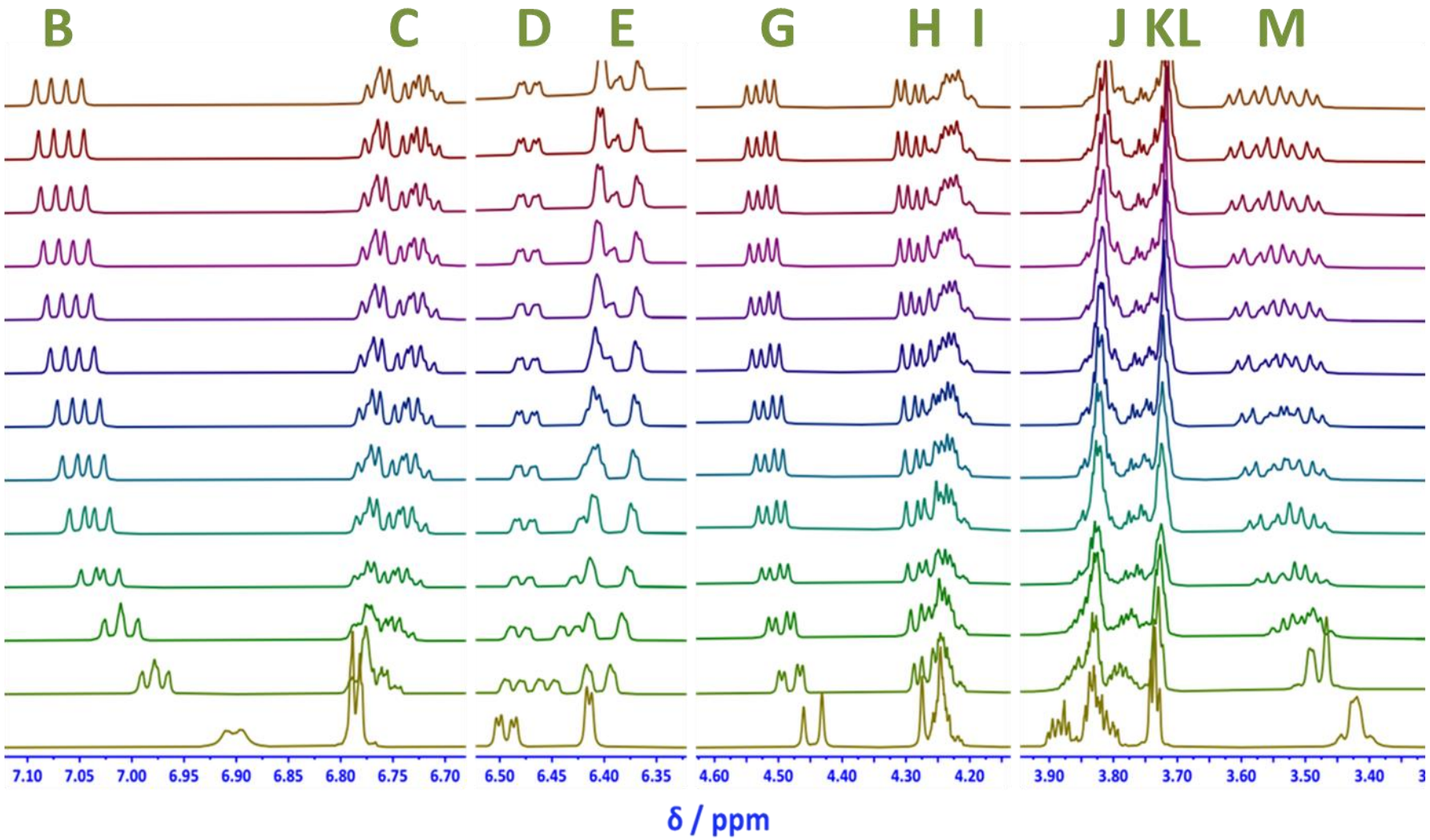

Figure S39. Stacked ^{1}H NMR spectra of racemic macrocycle **5** titrated with chiral discriminator (–)-DBTA (600 MHz, $CDCl_3$–CD_3CN 30% *v/v*, 298 K)

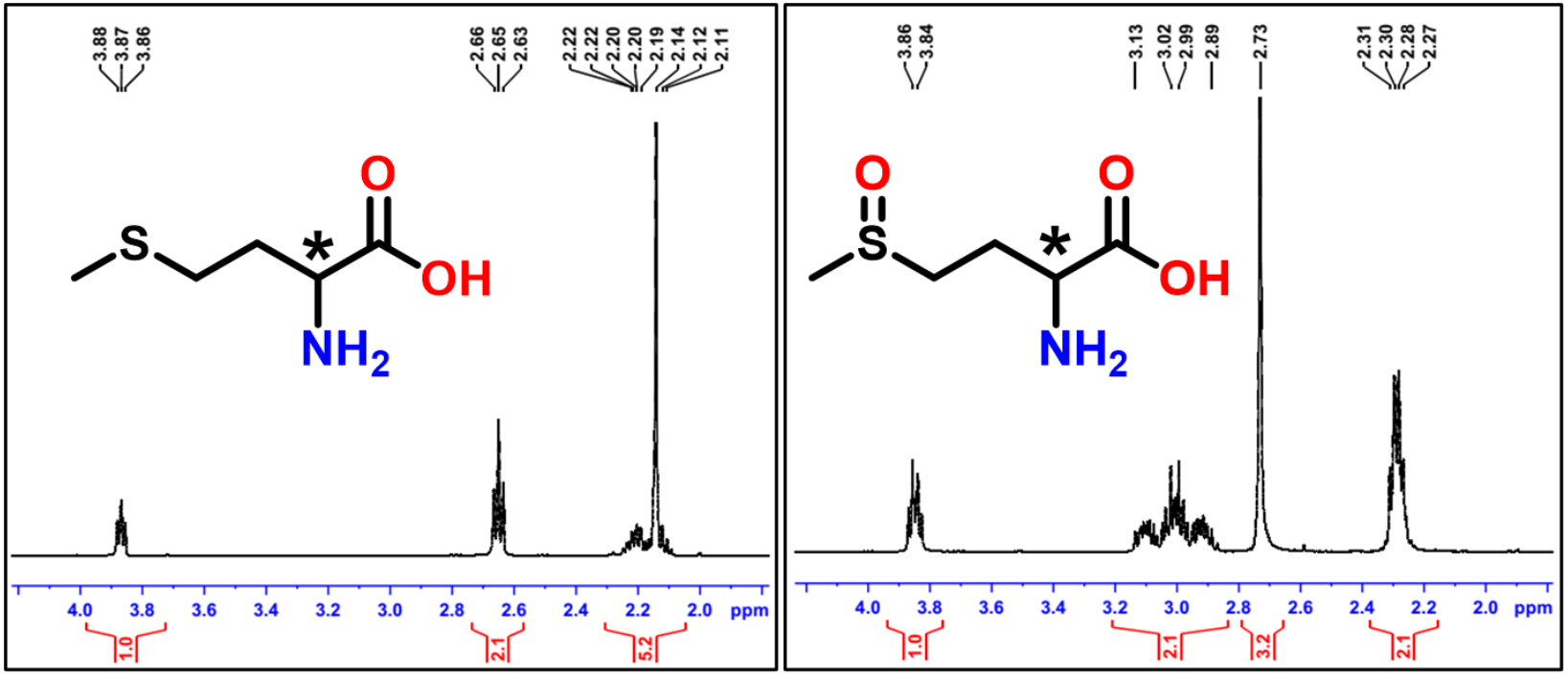

Figure S40. ^{1}H NMR spectra of methionine, and methionine sulfoxide (500 MHz, D_2O, 298 K)

■ Section D. UV-Vis Spectrophotometry and CD Spectroscopy

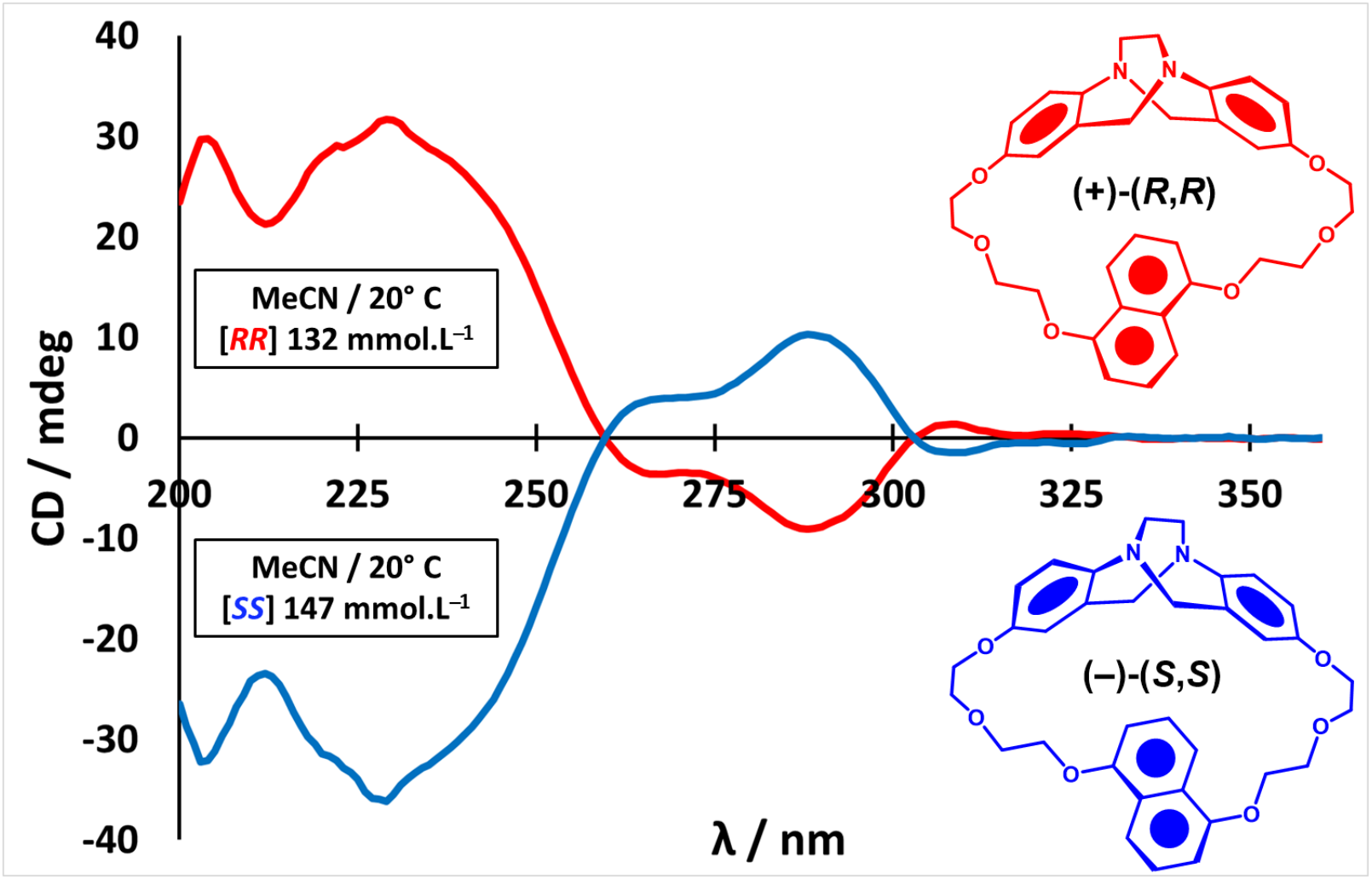

Figure S41. CD spectra of the enantiomers of macrocycle **5** (MeCN, 20° C, d = 10 mm)

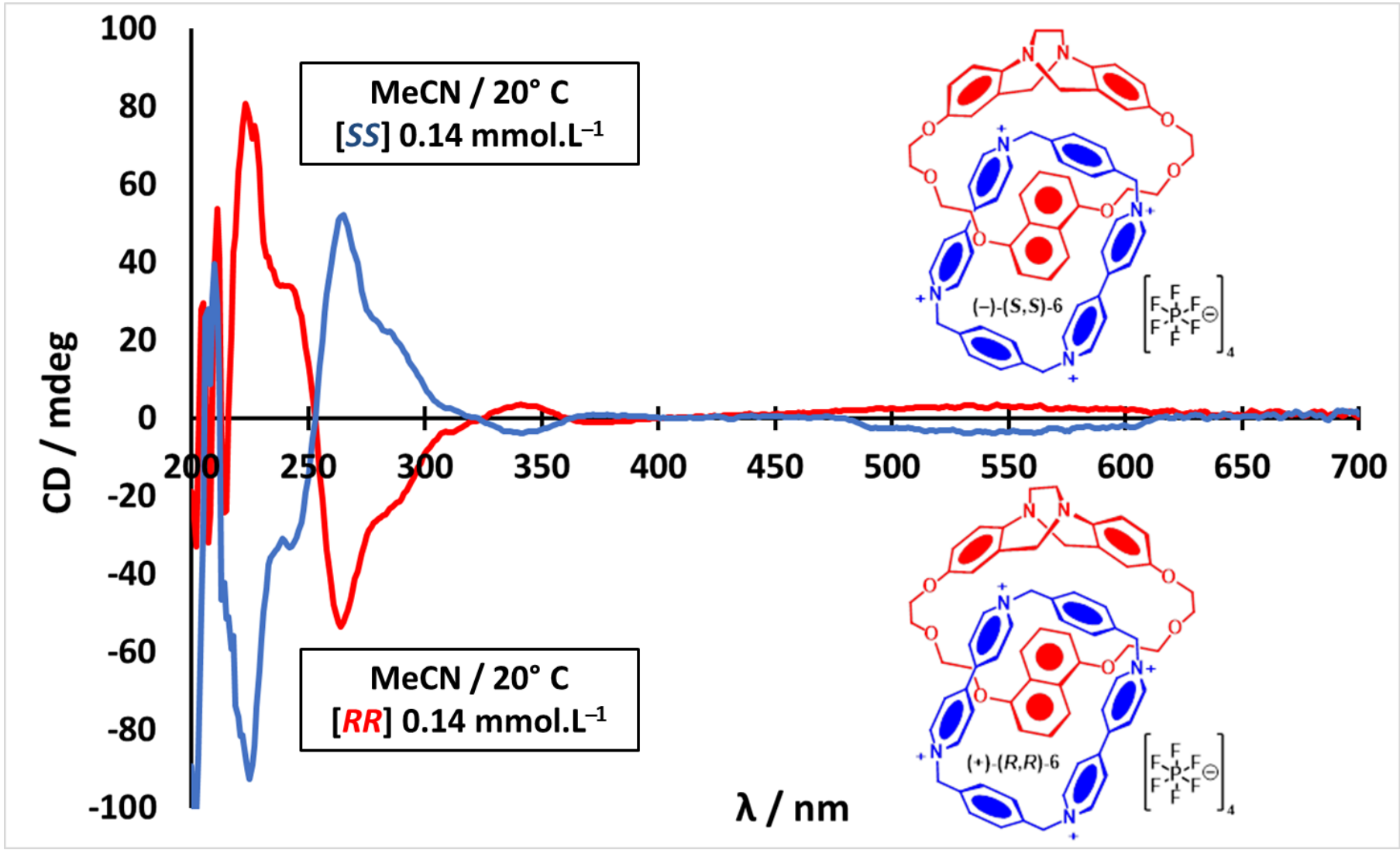

Figure S42. CD spectra of the enantiomers of catenane **7**·4PF_6 (MeCN, 20° C, d = 4 mm, 200 < λ < 700 nm)

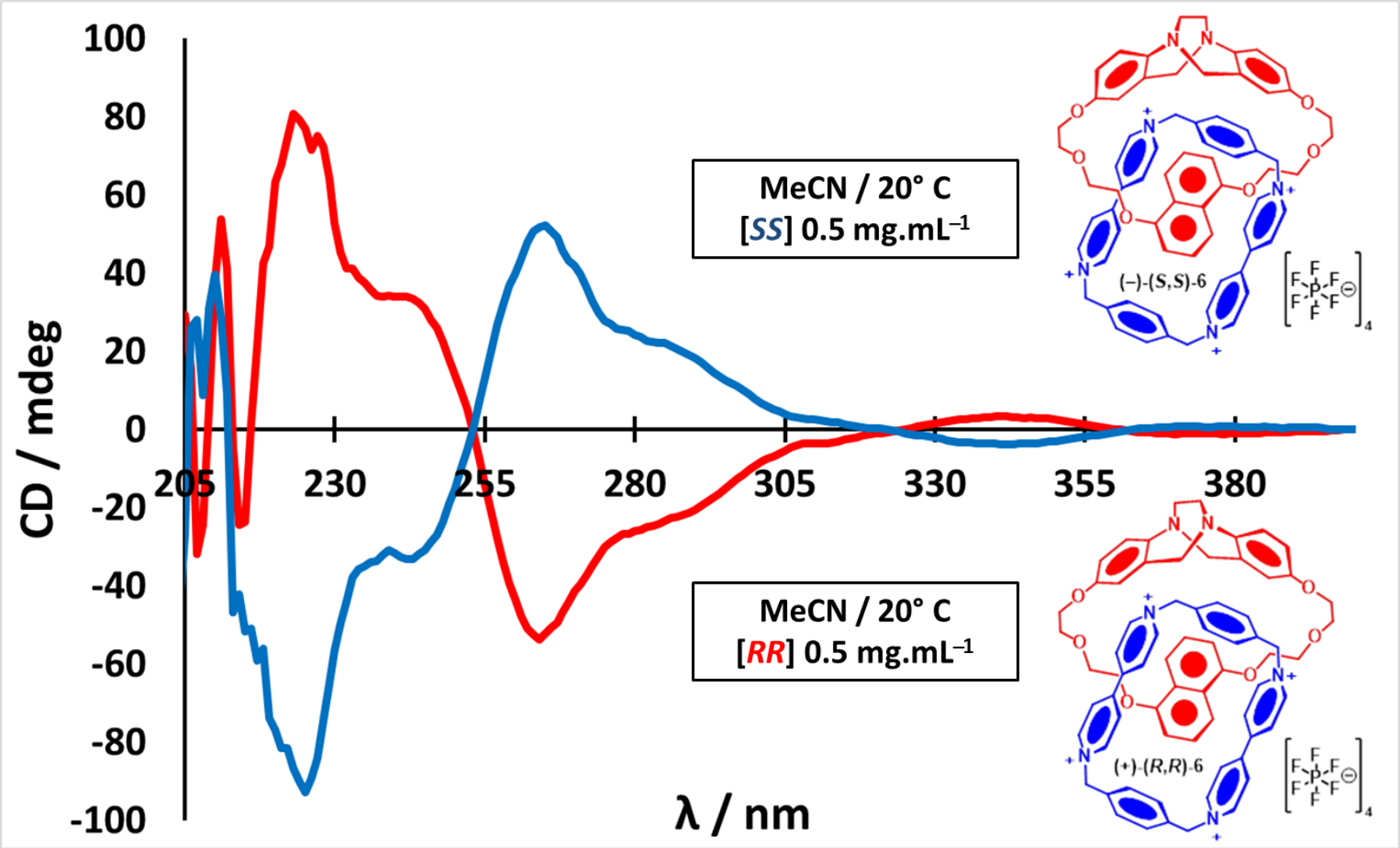

Figure S43. CD spectra of enantiomers of catenane **7**·4PF_6 (MeCN, 20° C, d = 2 mm, 200 < λ < 400 nm)

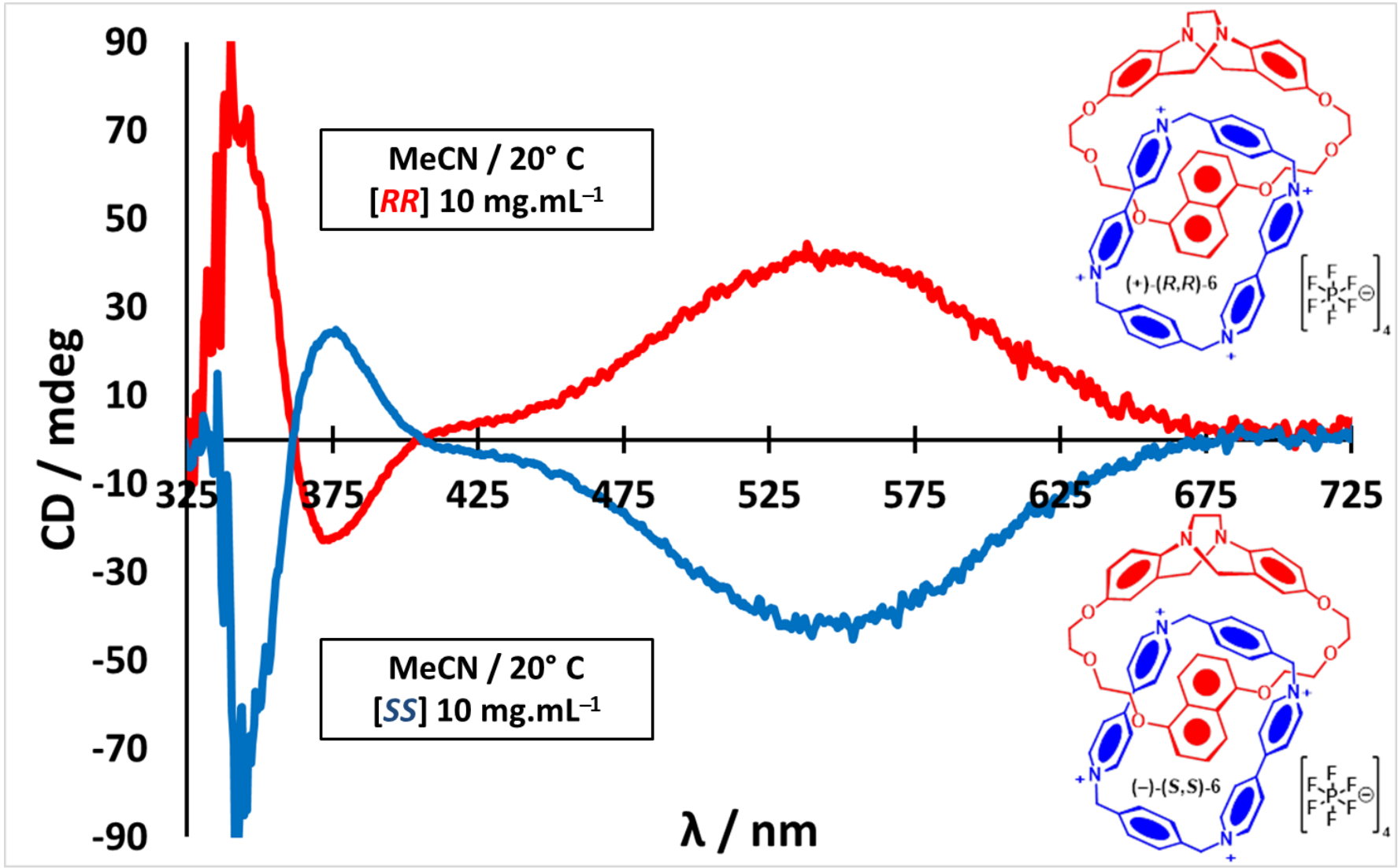

Figure S44. CD spectra of enantiomers of catenane **7**·4PF_6 (MeCN, 20° C, d = 2 mm, 325 < λ < 725 nm)

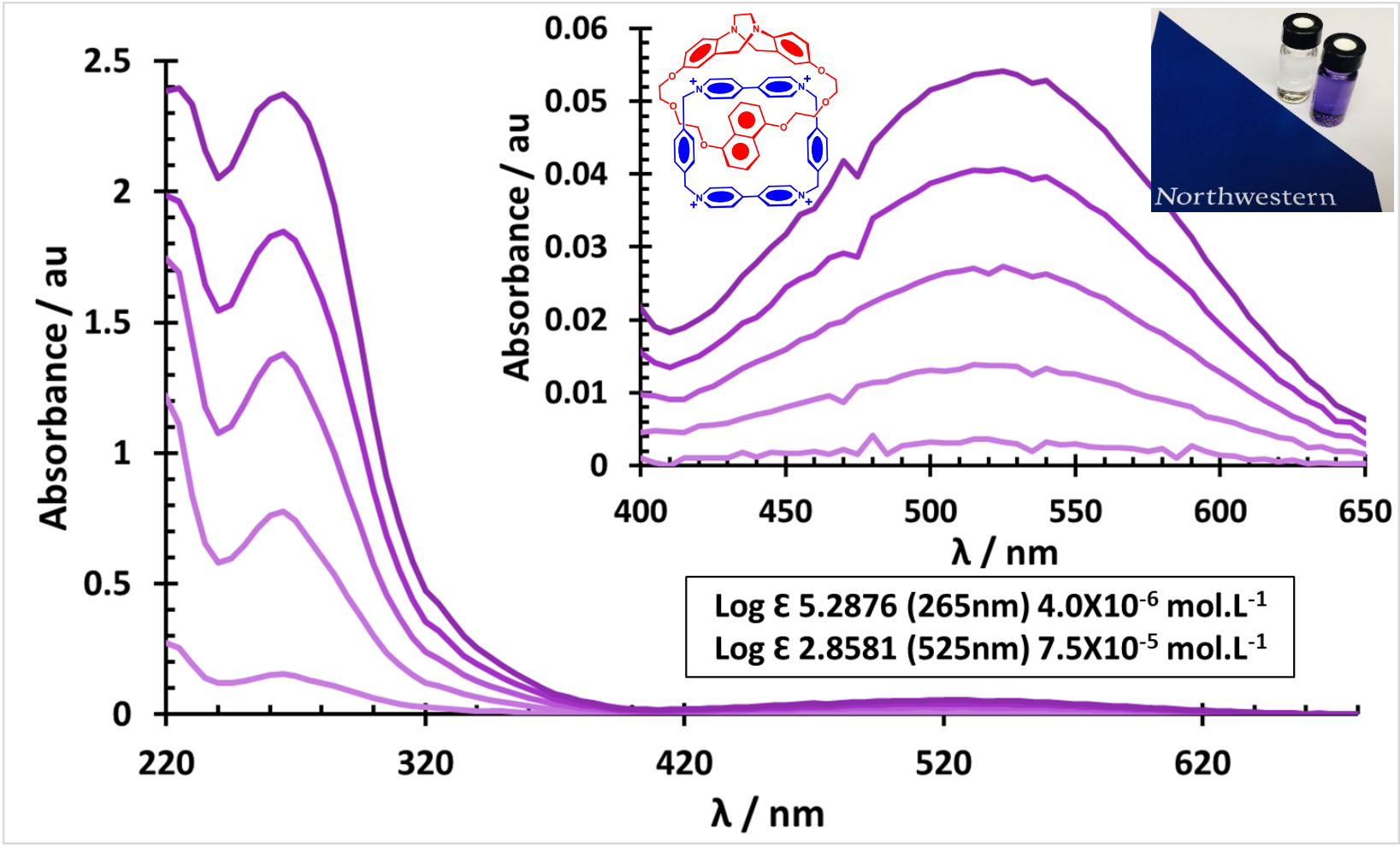

Figure S45. UV/Vis absorption spectra of catenane **7**·4PF_6 (MeCN, 20° C)

Inset: Magnification of the charge-transfer band region ($400 < \lambda < 650$ nm)

■ Section E. High-Resolution Mass Spectroscopy (HR-MS)

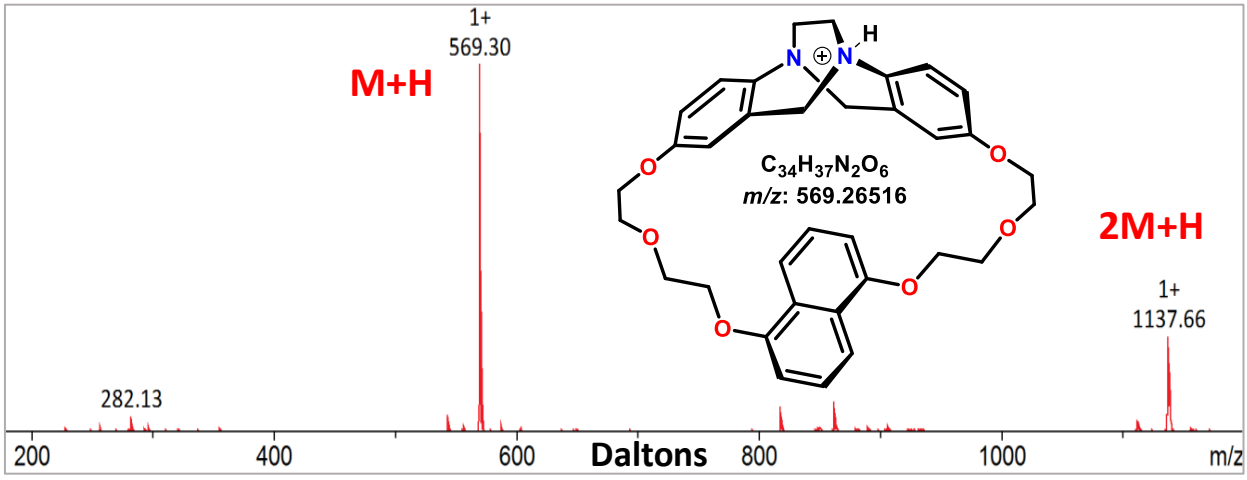

Figure S46. ESI-MS spectrum of macrocycle **5**

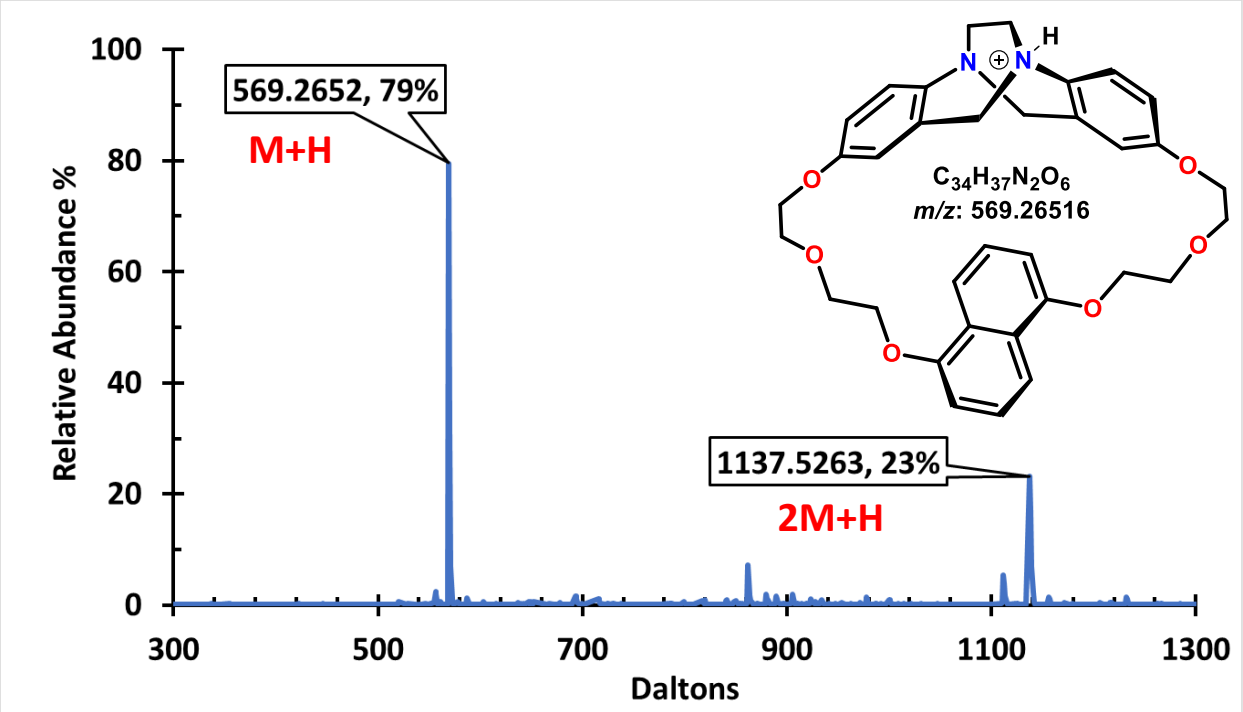

Figure S47. High-resolution ESI-MS spectrum of macrocycle **5**

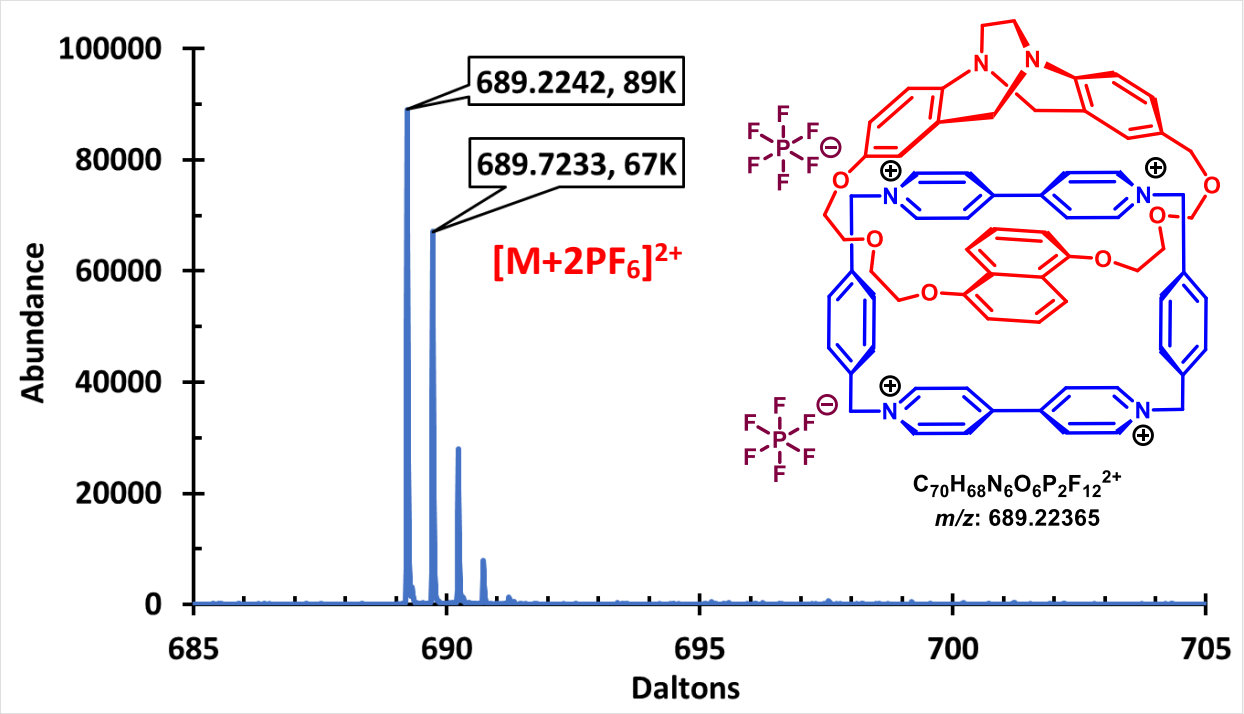

Figure S48. High-resolution ESI-MS spectrum of catenane **7**•4PF_6

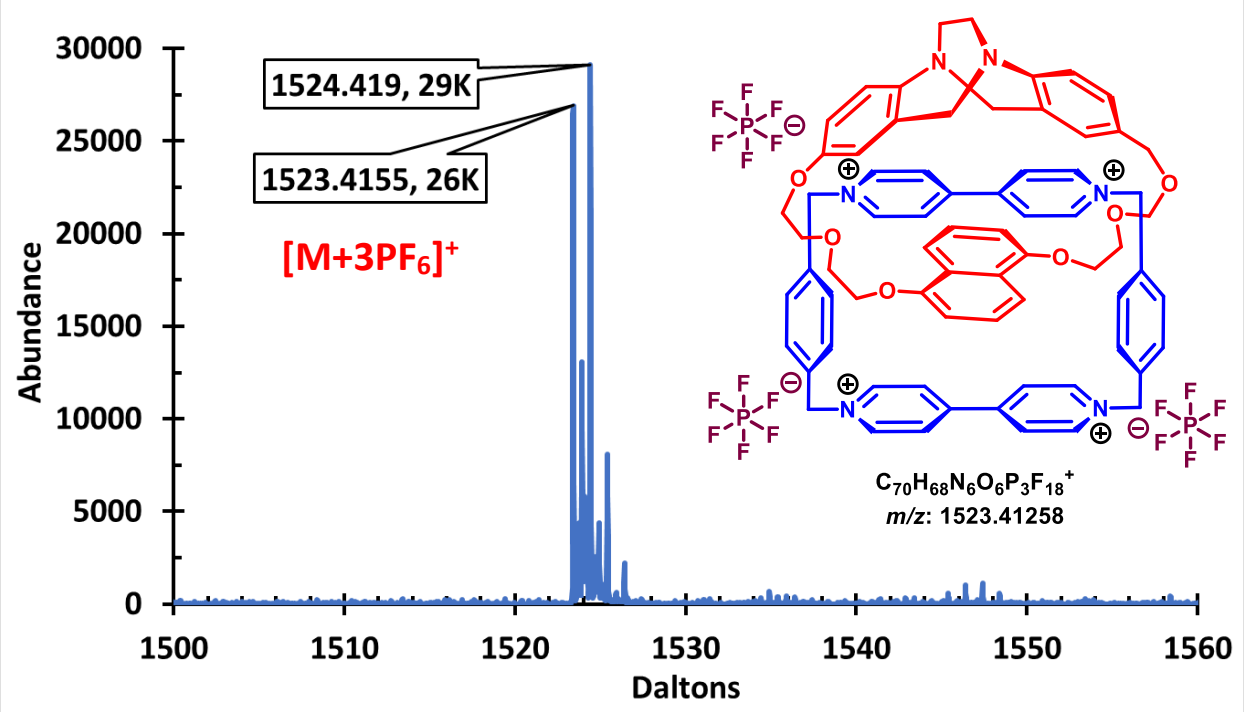

Figure S49. High-resolution ESI-MS spectrum of catenane **7**•4PF_6

■ Section F. Chiral High-Performance Liquid Chromatography (HPLC)

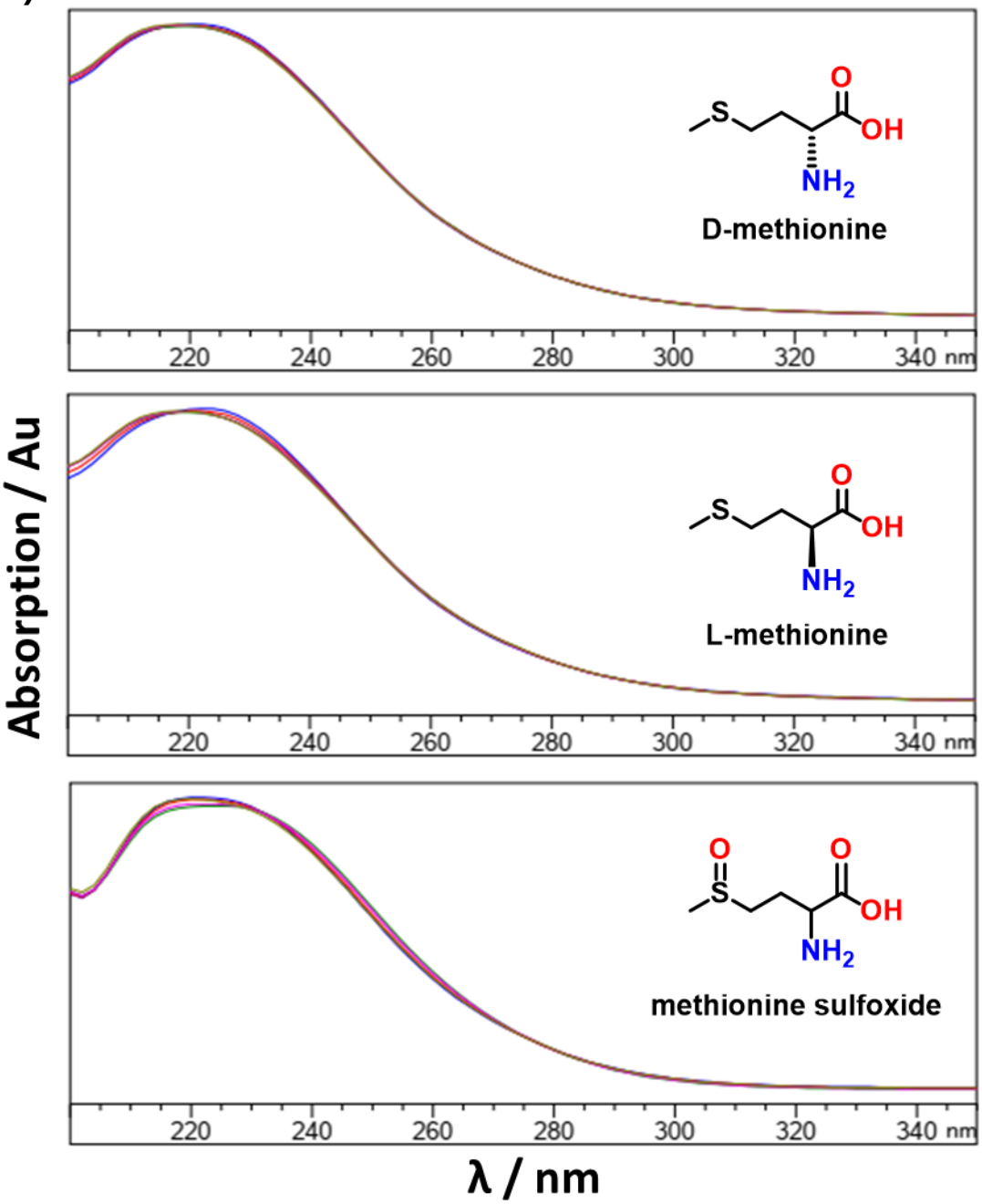

Figure S50. Accumulated UV absorption spectra of D-methionine, L-methionine and methionine sulfoxide elaborating on the inactivity of the species at 338nm[7] and hence setting the multi-channel optical detection for chiral HPLC tests at 235 and 245 nm in this work instead of 338 nm mistakenly used in the literature.

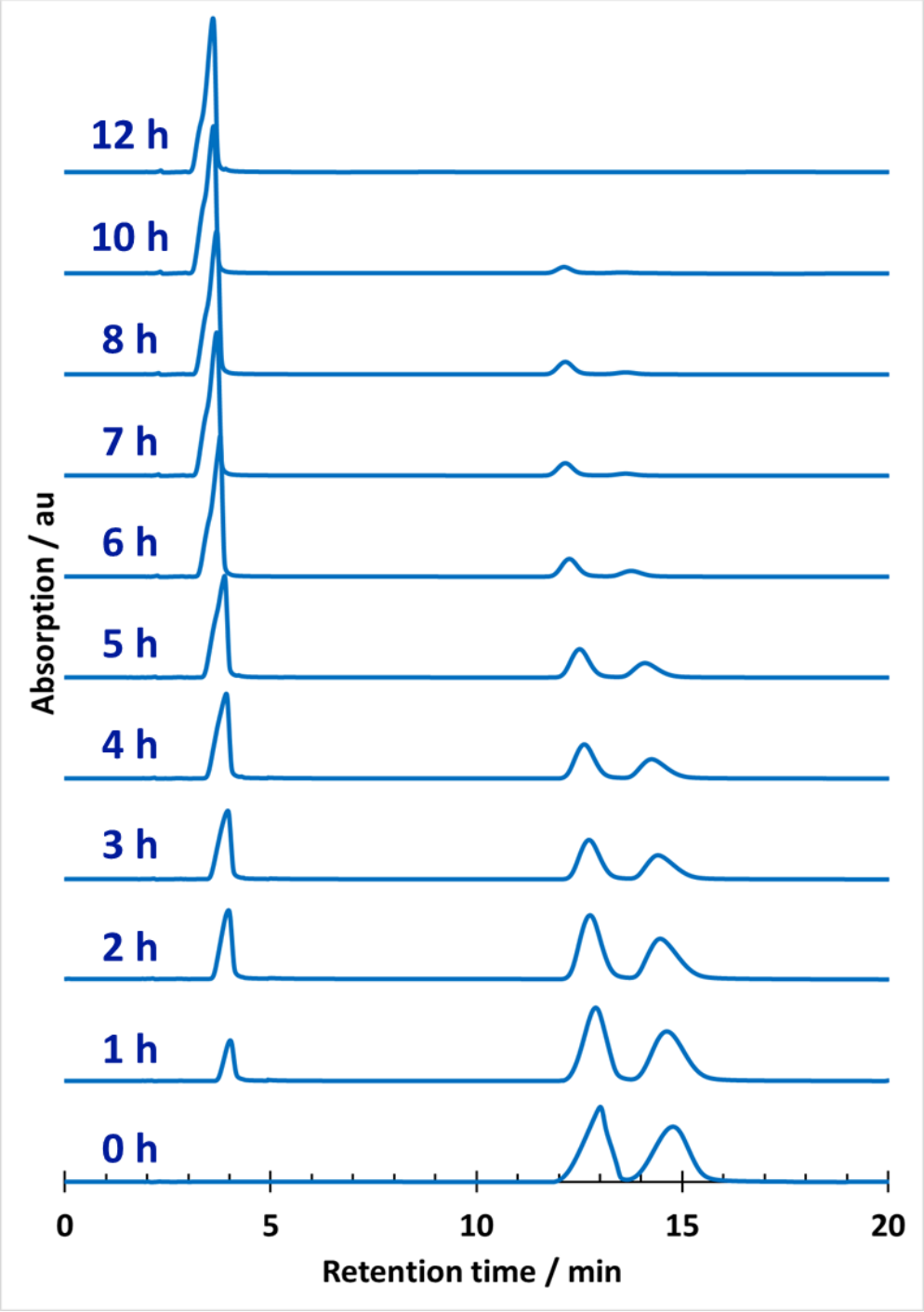

Figure S51. Stacked chiral HPLC traces displaying the enantioselective conversion of DL-methionine using **(–)-(S,S)-7**•4Cl as the chiral photocatalyst. The peaks at around 4, 13 and 15 min are characteristic for methionine sulfoxide, L-methionine and D-methionine, respectively.

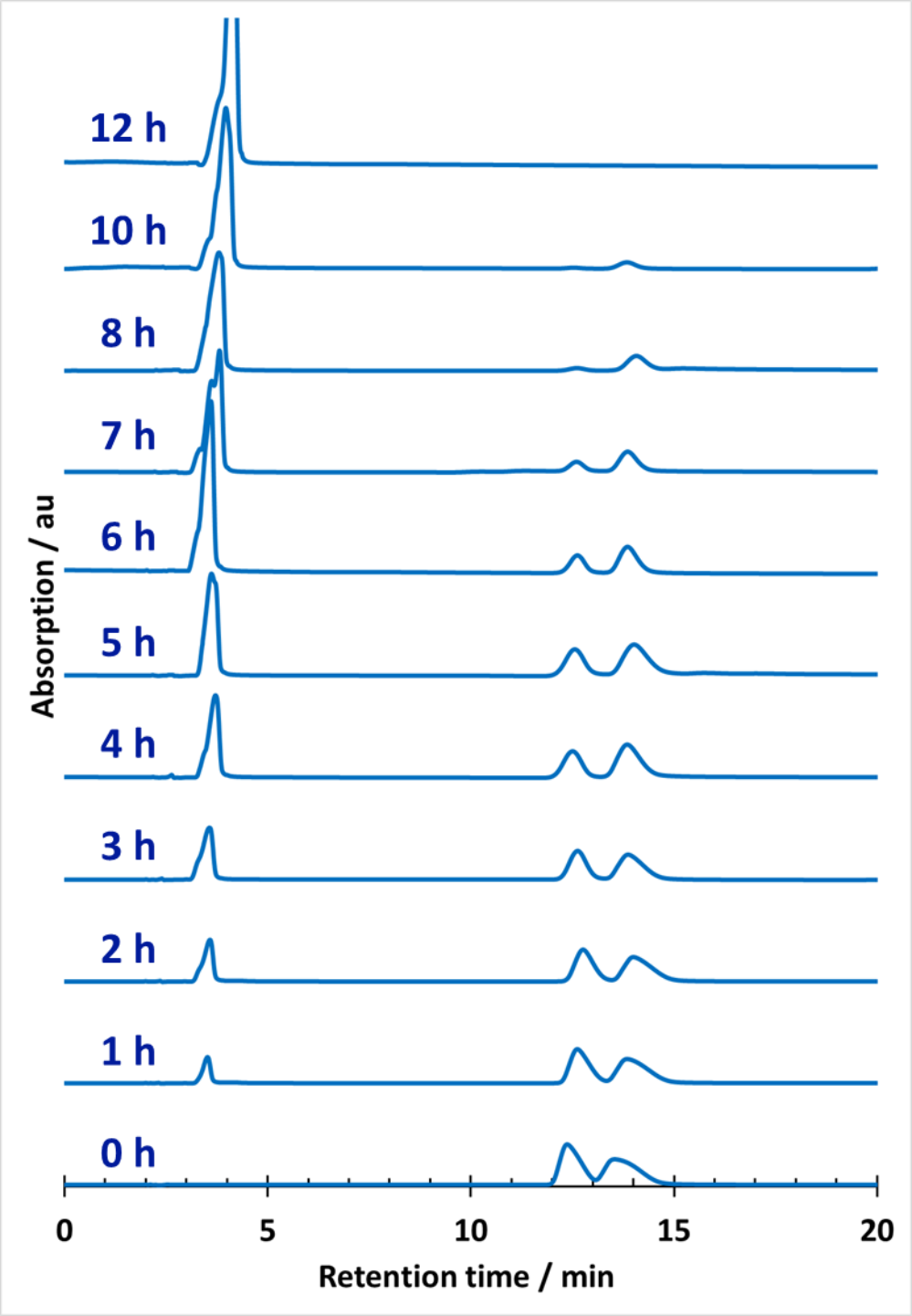

Figure S52. Stacked chiral HPLC traces displaying the enantioselective conversion of DL-methionine using **(+)-(*R*,*R*)-7**•4Cl as the chiral photocatalyst. The peaks at around 4, 13 and 15 min are characteristic for methionine sulfoxide, L-methionine and D-methionine, respectively.

■ References

1 D. Didier, B. Tylleman, N. Lambert, C. M. L. Vande Velde, F. Blockhuys, A. Collas and S. Sergeyev, *Tetrahedron*, 2008, **64**, 6252–6262.

2 Y. Hamada and S. Mukai, *Tetrahedron Asymmetry*, 1996, **7**, 2671–2674.

3 (a) M. Kazem-Rostami, *New J. Chem.*, 2019, **43**, 7751–7755; (b) M. Kazem-Rostami, *Asian J. Nanosci. Mater.*, 2020, **3**, 138–147.

4 (a) Q. M. Malik, S. Ijaz, D. C. Craig and A. C. Try, *Tetrahedron*, 2011, **67**, 5798–5805; (b) M. Kazem-Rostami, *Synlett*, 2017, **28**, 1641–1645.

5 T. Kreher, H. Sonnenschein, B. Costisella and M. Schneider, *J. Chem. Soc., Perkin Trans. 1*, 1997, **22**, 3451–3458.

6 P. R. Ashton, R. A. Bissell, N. Spencer, F. Stoddart and M. S. Tolley, *Synlett*, 1992, **11**, 914–918.

7 Y. Jiao, L. Đorđević, H. Mao, R. M. Young, T. Jaynes, H. Chen, Y. Qiu, K. Cai, L. Zhang, X.-Y. Chen, Y. Feng, M. R. Wasielewski, S. I. Stupp and J. F. Stoddart, *J. Am. Chem. Soc.*, 2021, **143**, 8000–8010.